THERMOBIOMECHANICS OF ARTERIES

A DISSERTATION
SUBMITTED TO THE FACULTY OF THE GRADUATE
SCHOOL AT THE UNIVERSITY OF MINNESOTA
BY

RAMJI T. VENKATASUBRAMANIAN

IN PARTIAL FULFILLMENT OF THE REQUIREMENTS
FOR THE DEGREE OF
DOCTOR OF PHILOSOPHY

JOHN BISCHOF, ADVISER

OCTOBER 2008

ACKNOWLEDGEMENT

To all members of the Bioheat and Mass transfer laboratory for their support during the course of my dissertation. Venkatasubramaniam S. Kalambur, Saravana K. Balasubramanian, Jeung Hwang Choi, Raghav Goel, Neha Shah, Jing Jang, Mithun Shenoi, Mie Hagiwara, Erin Grassl, Sue Clemmings, David Swanlund, Rachana Visaria and Wim Wolkers all have tremendously helped me through their valuable ideas, discussions, criticisms and importantly providing a friendly atmosphere within the group. Thanks to members from other research groups: Jason Perlmutter, Vishard Ragoonanan, Ravi Namani and Eduardo Reategui for useful discussions and collaborative work. Thanks to all my friends in Minneapolis: Neela, Shyam, Coma, Harsha, Arvind, Ramku, Suki, Madhu, Ajitha, Poornima, Senthil, Bhooma, Kodak, Moth, Sarran, Ranga and several others for the support and good times in Minneapolis.

To all faculty members whom I have interacted on various research topics. Thanks to Prof. Victor Barocas and Prof. Alptekin Aksan for useful inputs during the BHMT group and individual meetings. Thanks to Prof. Narendra Simha for his help with indentation experiments and Prof. Traian Dumitrica for useful discussions during the 'Computational Nanomechanics' course. My sincere thanks to Prof. Jonathan Sachs for guiding me through the Molecular Dynamics study.

My adviser, Prof. John C. Bischof, has played the most important role in helping me mature professionally. The individual meetings in his office are probably the best times that I have had during my doctoral study. I have both admired and enjoyed his energy during the brainstorming discussions, constantly motivating nature, passion to confidently venture into new things and his open criticisms. I thank him for all the support and opportunities and sincerely hope that I follow atleast some of practices in future.

Finally, I would like to thank Sukanya, my better half, and my parents for their encouragement and support during the doctoral study. Sukanya has been with me during some of the tough phases and has made me feel confident even during such times. This work is dedicated to Sukanya and my parents.

"THERMOBIOMECHANICS OF ARTERIES"

Ph. D. Thesis by Ramji Venkatasubramanian, dedicated

To,

Sukanya

and

My Parents

for their love, support and encouragement at all times

ABSTRACT

Conventional treatments for arterial diseases, such as balloon angioplasty, often result in restenosis or re-narrowing of the arteries. In the last few years, the clinical importance of thermal therapies for atherosclerosis involving both freezing (cryoplasty) and heating (*in-stent* heating) has increased significantly because of their potential to control or minimize restenosis. An alternative to these therapies includes replacing the diseased artery through preserved arterial grafts which brings with it the need to effectively preserve them. Cryopreservation, i.e. preservation of tissues by freezing to very low temperatures, has therefore become an important problem in medicine. As mechanical properties of arteries play a large role in blood flow, a complete understanding of the biomechanical changes following thermal treatments and the underlying mechanisms is essential for further optimization of these treatments through controlling biomechanical changes. The objective of this dissertation was to quantify the biomechanical changes and investigate the underlying mechanisms post freeze-thaw. In this dissertation, the following specific aims were pursued:

1. Quantification of freeze-thaw induced biomechanical changes in arteries
2. Investigation of underlying mechanisms of thermobiomechanics

SA1 involved quantification of freeze-thaw induced mechanical property changes in arteries using both uniaxial tensile tests and indentation. While uniaxial tensile tests were chosen for relatively easy sample preparation and testing, indentation was performed in order to study a more localized biomechanical response while characterizing the diseased artery response. SA2 involved investigation of the mechanisms underlying the biomechanical changes. This primarily involved understanding the changes to the collagen matrix and SMCs following thermal treatments. Changes to collagen matrix stability were assessed by quantifying the changes to the amide-III band using the FTIR spectroscopy. Changes in SMC function were studied from the response of arteries to norepinephrine and acetylcholine. Finally, MD simulations were performed as a tool to further investigate dehydration induced increase in thermal stability of the collagen matrix due to freeze-thaw at the molecular level.

The important conclusions of this dissertation research are:

1. Freeze-thaw causes significant stiffening of the arteries. While, significant increase in the physiological elastic modulus (and reduction in toe region) was observed in the uniaxial tensile response, the peak and equilibrium modulus measured from indentation increased significantly following freeze-thaw.
2. Freeze-thaw induces significant changes in the collagen matrix and smooth muscle cells (SMCs) that are arguably the most important components of an artery. While dehydration accompanied by increased thermal stability was observed following freeze-thaw in the collagen matrix, it caused complete destruction of SMCs measured through loss in function.
3. At the molecular level, dehydration due to freeze-thaw (or any osmotic treatments) results in formation of new sidechain-backbone hydrogen bonds that are typically absent under hydrated conditions. These newly formed intra-protein hydrogen bonds in the absence of water molecules increase the thermal stability of the tropocollagen molecule.

TABLE OF CONTENTS

LIST OF TABLES

LIST OF FIGURES

PERMISSIONS

Dear Sir,

With reference to your request (copy herewith) to reprint material on which Springer Science and Business Media controls the copyright, our permission is granted, free of charge, for the use indicated in your enquiry.

This permission
- allows you non-exclusive reproduction rights throughout the World.
- permission includes use in an electronic form, provided that content is
  * password protected;
  * at intranet;
- excludes use in any other electronic form. Should you have a specific project in mind, please reapply for permission.
- requires a full credit (Springer/Kluwer Academic Publishers book/journal title, volume, year of publication, page, chapter/article title, name(s) of author(s), figure number(s), original copyright notice) to the publication in which the material was originally published, by adding: with kind permission of Springer Science and Business Media.

The material can only be used for the purpose of defending your dissertation, and with a maximum of 100 extra copies in paper.
Permission free of charge on this occasion does not prejudice any rights we might have to charge for reproduction of our copyrighted material in the future.

Best wishes,
Nel van der Werf (Ms)
Rights and Permissions/Springer
Van Godewijckstraat 30 | P.O. Box 17
3300 AA Dordrecht | The Netherlands
tel +31 (0) 78 6576 298
fax +31 (0)78 65 76-300
Nel.vanderwerf @springer.com
www.springer.com

-----Original Message-----
From: ramji@me.umn.edu [mailto:ramji@me.umn.edu]
Sent: woensdag 22 oktober 2008 20:38
To: Permissions Europe/NL
Subject: Permission for Dissertation Usage

Dear ABME Editor,

I'm, Ramji Venkatasubramanian, finishing up my PhD at the University of Minnesota, Minneapolis. I have authored couple of publications in the Annals of Biomedical Engineering:

1. Venkatasubramanian, R.T., Grassl, E.D., Barocas, V.H., Lafontaine, D. and Bischof, J.C., Effects of freezing and cryopreservation on the mechanical properties of arteries. Annals of Biomedical Engineering, 2006. 34(5):823-32.
2. Balasubramanian, S.K. Venkatasubramanian, R.T., Menon, A. and Bischof, J.C., Thermal injury prediction during cryoplasty through in vitro characterization of smooth muscle cell biophysics and viability. Annals of Biomedical Engineering, 2008. 36(1):86-101.

I also have the following manuscript submitted for review in ABME:

1. Venkatasubramanian, R.T., Wolkers,W., Barocas, V.H., Lafontaine, D., Soule, C., Iaizzo, P. and Bischof, J.C.,Freeze-Thaw Induced Biomechanical Changes in Arteries: Role of Collagen Matrix and Smooth Muscle Cells. Annals of Biomedical Engineering (Submitted).

I request permission to use the text and figures from my previous publications as well as manuscript submitted for review in my doctoral dissertation.

Please let me know if I need to send any additional forms to you.

Thank you.
Regards,
Ramji

CONTRIBUTION OF THE AUTHORS AND OTHERS

This dissertation describes the accumulated doctoral research of the author with contributions and guidance from several collaborators. The author worked closely with the adviser, Dr. John. C. Bischof on the design of experiments, data analysis and preparation of each chapter of this thesis and manuscripts for journal submission. The contribution of the author and others are described below:

Chapter 1: This chapter reviews the previous work in the field of 'Thermobiomechanics' or thermally induced biomechanical changes in arteries. The present author prepared and edited the manuscript.

Chapter 2: This chapter describes the uniaxial tensile tests performed to quantify the biomechanical changes in arteries due to freeze-thaw. The present author performed all the biomechanical experiments and data analysis. The histological analysis was carried out in collaboration with Dr. James Coad of the Department of Pathology at West Virginia University. The present author also created and edited the manuscript for publication. The results from this chapter were published in the following citation:

i. Venkatasubramanian, R.T., Grassl, E.D., Barocas, V. H., Lafontaine, D. and Bischof, J.C. (2006) "Effect of freezing and cryopreservation on the mechanical properties of arteries." *Annals of Biomedical Engineering* **34**(5): p823-832.

Chapter 3: This chapter describes the indentation tests performed to quantify the biomechanical changes in arteries due to freeze-thaw. The present author performed all the biomechanical experiments, data analysis, created and edited the manuscript for publication. The results from this chapter have been submitted as the following citation that is presently in review at the time of dissertation submission:

i. Venkatasubramanian, R.T., Simha, N.H., Tatsutani, K. and Bischof, J.C.

(2008) “Effect of cryoplasty on mechanical properties of human and porcine arteries using indentation.” *Cryobiology* (In review at the time of dissertation submission).

Chapter 4: This chapter describes the studies performed to investigate the freeze-thaw effect on the arterial components (collagen, smooth muscle cells or SMCs) and subsequently the components’ contribution to the overall artery biomechanics. The present author performed all the experiments and the data analysis. The histological analysis was carried out in collaboration with Dr. Schmechel of the Department of Lab Medicine and Pathology at University of Minnesota. Experiments on functional assessment of Smooth muscle cells were performed in collaboration with Dr. Paul Iaizzo of the Department of Surgery at the University of Minnesota. The results from this chapter have been submitted as the following citation that is presently in review at the time of dissertation submission:

i. Venkatasubramanian, R.T., Wolkers, W., Barocas, V.H., Lafontaine, D., Soule, C., Iaizzo, P., and Bischof, J.C. (2008) “Freeze-thaw induced biomechanical changes in arteries: Role of collagen matrix and smooth muscle cells.” *Annals of Biomedical Engineering* (In review at the time of dissertation submission).

Chapter 5: This chapter describes the molecular dynamics simulations performed on a single tropocollagen molecule to study the thermal stability and the molecular level changes induced by dehydration. The present author performed all the simulations in collaboration with Dr. Jonathan Sachs and Jason Perlmutter from the Department of Biomedical Engineering at the University of Minnesota. The present author also created and edited the manuscript for publication. This chapter is being prepared for the following citation:

i. Venkatasubramanian, R.T., Perlmutter, J., Sachs, J. and Bischof, J.C. (2008) “Nanoscale unfolding of a single tropocollagen molecule.” *Cellular and Molecular Bioengineering* (In preparation at the time of dissertation

submission).

Chapter 6: The present author summarized all the data and created and edited this chapter of the dissertation.

APPENDIX A: This chapter describes the thermal model of cryoplasty in arteries to predict the temperature distribution. The results from this chapter, along with results from experiments performed by Saravana K Balasubramanian from the Department of Mechanical Engineering at the University of Minnesota that characterize SMC injury in different *in vitro* model systems were used to predict thermal injury during cryoplasty. This work was published in the following citation:

i. Balasubramanian, S.K., Venkatasubramanian, R.T., Menon, A. and Bischof, J.C. (2008) "Thermal injury prediction during cryoplasty through *in vitro* characterization of smooth muscle cell biophysics and viability." *Annals of Biomedical Engineering* **36**(1): p. 86-101.

1 THERMOBIOMECHANICS OF ARTERIES: A REVIEW

This chapter reviews the previous work in the field of 'Thermobiomechanics' or thermally induced biomechanical changes in arteries. The present author prepared and edited the manuscript.

Abstract

This review article presents an overview of an evolving field in thermobiomechanics or thermally induced biomechanical property changes of arteries. Current treatments for atherosclerosis, their drawbacks as well as some potential thermal treatments aimed to overcome some of the drawbacks in the conventional treatments are reviewed. As arterial biomechanics plays an important role in hemodynamics, there a need to understand the biomechanical implications of thermal treatments which requires quantification of changes in overall artery biomechanics as well as molecular and/or cellular component changes in arteries. Some important experimental (biomechanical tests, CD, FTIR, and DSC) and computational (MD) tools useful in the quantification of the different changes (cellular, molecular and tissue level) are reviewed. Additionally, previous studies on understanding the thermally induced biomechanical and component changes have also been reviewed. Finally, the scope for future research leading to studies in this dissertation is discussed.

1.1 INTRODUCTION

1.1.1 Atherosclerosis, restenosis and current treatments

Atherosclerosis is an inflammatory disease characterized by plaque formation, proliferation of the smooth muscle cells and therefore narrowing of the arteries. The plaque essentially is a build up of fatty acid deposits on the inside wall of arteries. The formation of plaque results in hardening and narrowing of the arteries thereby disrupting normal blood flow in the vessel. The plaque formed usually ruptures and results in thrombosis or a fibrinous clot which could eventually lead to other cardiovascular diseases [1]. Atherosclerosis in peripheral arteries such as femoral or popliteal arteries is referred to as peripheral arterial disease (PAD), where as atherosclerosis in coronary arteries which carry blood to the heart is termed coronary arterial disease (CAD). While CAD mostly is characterized by chest pain, PAD results in leg pain as the blood flow to the heart or legs, respectively, is impeded due to narrowed or completely blocked arteries.

Atherosclerosis is a major health care problem in the United States that is characterized by plaque formation, proliferation of the smooth muscle cells and narrowing of the arteries. Angioplasty and by-pass surgeries have been commonly used to treat atherosclerosis. In angioplasty, a balloon-tipped catheter is inserted into the diseased artery and the balloon is then inflated to widen the passageway for blood[2]. In case of bypass surgeries, arteries from elsewhere in the patient's body are grafted to bypass the diseased artery[2]. Additionally, stents have been used to prevent re-narrowing of arteries. A stent is a hollow mesh that is inserted to hold the artery at the physiologically favorable particular diameter thereby avoiding any narrowing due to plaque formation[3]. In 1999 alone, there were more than 400,000 coronary angioplasties performed in the US to treat atherosclerosis, with 30-40% of these resulting in re-stenosis[4, 5]. Restenosis is a major drawback that often occurs following balloon angioplasty or use of stents[6]. Restenosis involves re-narrowing of arteries over time which can result in complications similar to atherosclerosis. During balloon angioplasty, the matrix fibers are overstretched to which the arteries respond through elastic recoil followed by thrombus formation and smooth muscle cell activation. This activation leads to smooth muscle cell (SMC) proliferation and extracellular matrix (ECM) remodeling

that ultimately results in restenosis [7]. These drawbacks have motivated interests in other treatments such as heating and freezing for control of restenosis.

1.1.2 Thermal treatments for arterial disease

Thermal treatments have contributed significantly to biomedicine and have shown potential in the treatment of cancer [8-10]. Recently, research is being carried out looking at the potential of thermal approaches in the treatment of cardiovascular disease [5, 11-17], especially diseases pertaining to blood vessels.

Thermal Treatments	Name	Description	Studies
Freeze-thaw	Cryoplasty	Radial freezing of artery to -10 to -20°C using liquid nitrous oxide. Used to treat atherosclerosis and restenosis in peripheral arteries such as femoral, iliac, popliteal, etc.	Kataoka et. al. 2002 Laird et. al. 2005 Joye 2005
	Cryopreservation	Preservation technique used to store native/artificial vascular grafts. Involves freezing up to -80°C in the presence of cryoprotective agent (CPA)	Pegg. et. al. 1994 Song et. al. 2000 Grassl et. al. 2003
Heating	In-stent heating (Ultrasound, Electromagnetic heating, Laser)	Potential treatment to prevent in-stent restenosis through heating of steel stents using electromagnetic, laser or ultrasound.	Floren et. al. 2004 Karaca et. al. 2003 Mudra et. al. 2002

Table 1.1 Thermal treatments used for atherosclerosis and restenosis

Like cancer, atherosclerosis and restenosis involve rapid proliferation of cells. Motivated by their use for treating cancer, thermal treatments are being looked into for treating atherosclerosis and restenosis. Table 1.1 describes different potential *in vivo* thermal treatments for arterial diseases that involve either freezing or heating. Cryoplasty is a recently developed approach used in the treatment of peripheral arterial disease that involves freezing of the artery [18, 19]. This approach has shown promise in reducing restenosis post treatment [15] and involves opening of narrowed arteries using liquid nitrous oxide to simultaneously inflate and cool the dilatation balloon. The diseased arteries are frozen to a balloon temperature of -10° to -20°C for about 40-60 seconds [20]. Efforts are now focused on optimizing cryoplasty by varying treatment parameters. Appendix A

(Chapter 7) discusses temperature prediction in arteries during cryoplasty using a thermal model which could be potentially useful in such optimization.

One possible advantage of freezing over heating (in this case burn) is the maintenance of the extracellular matrix (ECM) structure as previously shown in skin [21]. This is important because the ECM is believed to play a critical role in determining the mechanical properties of several soft tissues[22-25] including arteries. It is therefore believed that cryoplasty would cause minimal or no change to the structure of the ECM. However, future sections in the review will focus on the crudeness of this assumption which forms an important motivation for continued work in this area.

Like freezing, heating too has shown potential to improve the efficacy of atherosclerotic treatment. In a study involving noninvasive in-stent inductive heating in an electromagnetic field, in-stent restenosis was more effectively prevented[13]. Laser and ultrasound have also been used for heating in the treatment of in-stent restenosis[14, 16]. However, these approaches have the disadvantage of leaving the stent inside the body post treatment which may further lead to complications. Also, placing stents in certain arteries like popliteal arteries is difficult due to their physiological locations which preclude bending.

As an alternative to direct *in vivo* therapies, the diseased artery can also be replaced using cryopreserved allografts[26-28] or perhaps in the future by engineered arterial vessels which will also likely require cryopreservation[29, 30]. Cryopreservation involves freezing of the arteries in the presence of certain chemicals, called cryoprotective agents (or CPA) that maintain the cellular and mechanical integrity of the tissues. Upon thawing the vessel can be used, however the determination of the proper CPA and cooling protocol for optimal cryopreservation, i.e. maintaining the cellular and mechanical integrity, is still an area of ongoing work.

1.2. THERMOBIOMECHANICS: DEFINITION AND IMPORTANCE

Temperature can change the cellular and mechanical integrity of arteries thereby altering their biomechanical properties. Understanding these changes therefore is important for optimization of thermal treatments. Thermobiomechanics refers to these changes as shown in Table 1.2. Sections 2.1 and 2.2 briefly review the importance of biomechanics

in artery function. The biomechanical properties of the artery primarily contribute to the following functions: a) smooth muscle cell (SMC) growth and functioning, and b) hemodynamics. Studies indicate that both abnormal smooth muscle growth[1] and disorderly blood flow [31] are precursors to pathological condition and can ultimately result in atherosclerosis.

1.2.1 Biomechanical effects on cell growth and functioning

The mechanical properties of the arteries play an important role in the smooth muscle cell (SMC) growth and function. SMCs are primarily responsible for the maintenance of the complex ECM structure through production of collagen, elastin and proteoglycans. Stegemann et. al. [32] present a detailed review on how the mechanical and biochemical stimulation of the ECM affect the SMC function and therefore their phenotype. Briefly, the mechanical signals are transmitted by the ECM to the cell via integrin receptors thereby affecting the functioning at the cellular level. The SMCs in the artery are continuously subjected to cyclic tensile stresses as a result of the pulsatile pressure waveform. It has been shown that the growth and functioning of SMCs in producing ECM proteins [33] and various other growth factors [34] is affected by cyclic stress (or strain). A change in mechanical properties of the artery due to thermal treatments will therefore alter the stress pattern required for the normal functioning of SMCs. Abnormal stimulation of the growth factors (resulting in SMC proliferation) or abnormal production of ECM proteins is a characteristic feature during atherosclerosis or restenosis [1, 7, 35].

1.2.2 Biomechanical effects on hemodynamics

The biomechanical properties of the artery wall play an important role in hemodynamics [36]. In a theoretical study, Cox compared the pulsatile blood flow in a viscoelastic tube with a flow in an elastic tube and found that the effect of viscoelasticity is not severe [37]. Therefore, for simplicity, the artery is usually assumed to behave like a thin-walled cylindrical elastic tube to understand the complex pulsatile blood flow. The wave equation for the pulsatile blood flow in elastic arteries is given by the Moens-Korteweg relation (Eqn. 1.1) under the assumptions that the flow is pulsatile and that arteries are thin cylindrical tubes with elastic walls [38].

$$c = \sqrt{\frac{Eh}{2\rho a}} \tag{1.1}$$

Here, c is the wave speed of the blood flow. E, h, a and ρ are the elastic modulus, thickness, internal radius of the artery and density of the blood respectively. While the elastic assumption of the artery is a reasonable first approximation, it should be stressed that the artery is infact viscoelastic in nature. Incorporating the viscoelastic nature of the artery wall coupled with the blood being a non-Newtonian fluid makes the hemodynamics problem much more complex [39]. Fortunately, recent advancements in computational capabilities have enabled researchers to begin to solve this fluid-solid coupling thereby improving predictive models of hemodynamics [36].

Changes in mechanical properties of the arteries post thermal treatments may result in a local change in blood flow. This condition can be compared to inserting a vascular graft with different mechanical properties than that of the native vessel [40]. The change in the wave speed results in changes in impedance (Z) to the blood flow (given by Eqn. 1.2) and therefore alters the wave transmission and reflection [38].

$$Z = \frac{P}{Q} = \frac{\rho c}{A} \tag{1.2}$$

where P, Q and A are the oscillatory pressure, flow rate and cross-sectional area respectively. ρ and c are the density and wave speed of the blood respectively. As c changes due to biomechanical property changes (Eqn. 1.1), Eqn. 1.2 suggests that impedance will also change. This in turn will lead to impedance mismatch with adjacent vessel sections which creates potential sites for development of recirculation zones. Studies indicate that atherosclerotic plaques are prone to develop in physiological regions where such recirculation zones are predicted[31, 41]. As the mechanical properties of the artery wall directly influence the blood flow inside the artery, changes in these properties may potentially lead to chronic blood flow disorders and ultimately reoccurrence of arterial disease as shown in Fig. 1.1. Thus, quantification and understanding of the underlying mechanisms of the biomechanical changes is critical in the optimization of all thermal treatments.

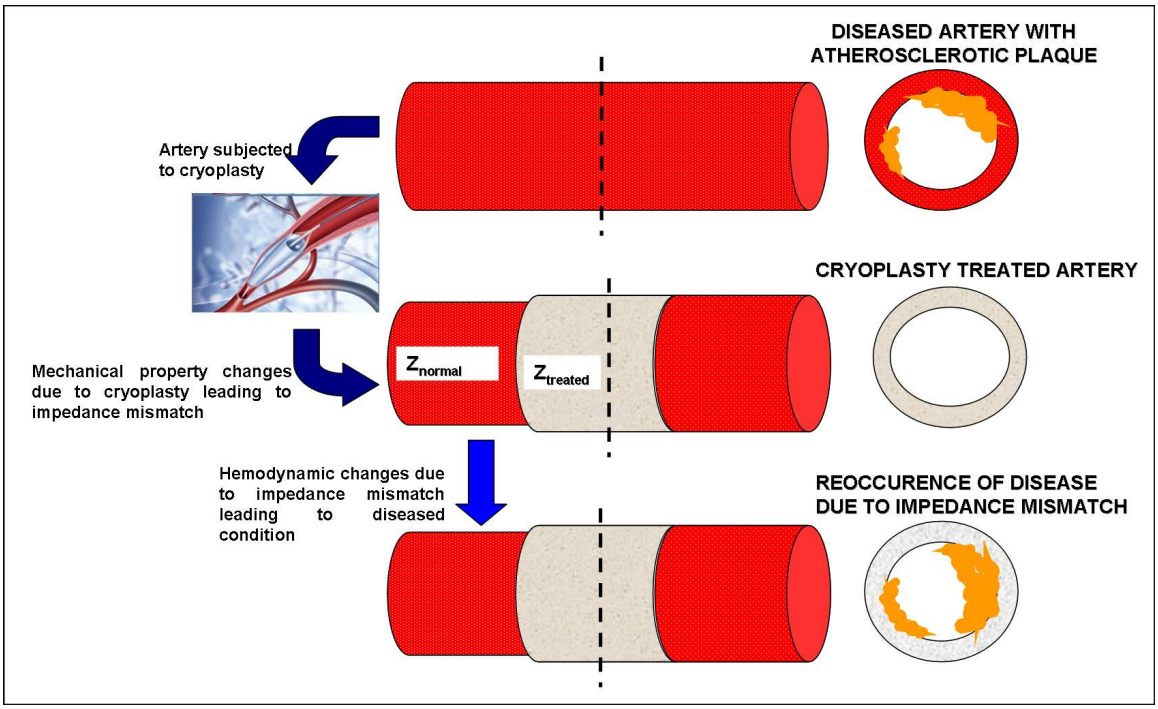

Figure 1.1 Impedance mismatch in artery post cryoplasty and possible reoccurrence of arterial disease.

1.3. QUANTIFICATION OF THERMALLY INDUCED BIOMECHANICAL CHANGES

As artery biomechanics plays an important role in cellular growth/functioning and hemodynamics, quantification of the biomechanical changes in arteries is extremely important. In this section, measurement techniques (see Table 1.3) used to study artery biomechanics, both in-vitro [42-53] and in-vivo, have been reviewed [54, 55]. Additionally, a review on different studies involving measurement of thermally induced biomechanical changes in arteries has been presented (see Table 1.2).

IMPORTANCE OF ARTERY THERMOBIOMECHANICS	
Cell growth and functioning	Bargava et. al. 2003, Cunningham and Gotlieb 2005, Durante et. al. 2000, Ross 1999, Stegemann et. al. 2005, Wilson et. al. 1993
Hemodynamics	Humphrey and Taylor 2008, Nerem 2000, Taylor et. al. 1998
QUANTIFICATION OF THERMALLY INDUCED BIOMECHANICAL CHANGES	
Freeze-thaw	Adham et. al. 1996, Blondel et. al. 2000, Pukacki et. al. 2000, Litwin et. al. 1973, Rosset et. al. 1996, Wang et. al. 2005
Heating	Kang et. al. 1995
QUANTIFICATION OF THERMALLY INDUCED COMPONENT CHANGES	
Freeze-thaw	Collagen Hydration/Stability: Miles et. al. 2005, Miller 2006, Neidert et. al. 2004, Cell viability: Balasubramanian et. al. 2008, Grassl et. al. 2005
Heating	Collagen Hydration/Stability: Wright and Humphrey 2002 (Review) Cell viability: Orihara et. al. 2002

Table 1.2 Thermobiomechanics of arteries: an overview of previous work

1.3.1 Biomechanical measurements in arteries

Arteries, like many other soft tissues, exhibit a complex mechanical response that is both non-linear and viscoelastic [56, 57]. While several hyperelastic models have been proposed to characterize the non-linear behavior (refer to [58, 59] for a review), the viscoelastic nature of soft tissues is commonly characterized using a typical stress-relaxation or creep test. Several different techniques to measure the material properties of arteries, both *in vitro* and *in vivo* have been proposed.

Uniaxial tensile testing (see Fig. 1.2) has been used *in vitro* to characterize the mechanical properties of different soft tissues including arteries [42-47]. An exponential model (equation 1.3) is often used to explain the non-linear uniaxial response of soft tissues [60] :

$$\frac{dP}{d\lambda} = C_1 P + C_2 \tag{1.3}$$

where P is the Eulerian tensile stress, λ the stretch ratio and C_1 and C_2 are the material parameters. Uniaxial testing does not measure the tissue anisotropy. Alternatively, biaxial or multiaxial tests could be used as they include anisotropic effects [53], but some of these tests are difficult to perform and their results more difficult to interpret.

Measurements \ Attributes		Resolution	Global vs. Local response	Physiological loading	Anisotropy	Sample Preparation	Residual Stress
In vitro	Uniaxial	Mm	Gross Average	NA	NA	Easy	Yes
	Biaxial	cm	Gross Average	NA	Yes	Difficult	No (Artery cut open)
	Indentation	Multiscale	Gross & Localized	NA	NA	Easy	No (Artery cut open)
	Inflation test	cm	Gross Average	Yes Radial and Axial	Yes	Moderate	Yes
In vivo	OCT	mm	Localized	Yes	Yes	NA	Yes
	Ultrasound	mm	Localized	Yes	Yes	NA	Yes

Table 1.3 Biomechanical measurements in arteries

In vitro pressure-diameter inflation tests (see Fig. 1.3) have been used to study the properties of arteries under physiological conditions [48, 49]. The non-linear pressure-diameter response of arteries has been modeled by Hayashi as [49] (see equation 1.4).

$$\ln\left(\frac{P}{P_s}\right) = \beta\left(\frac{D}{D_S} - 1\right) \tag{1.4}$$

where P_s is the standard pressure and D_s is the corresponding inner diameter of the artery, while β is the stiffness parameter. If both changes in radial (diameter) and axial (length or artery section) directions can be measured, inflation tests can be sensitive to anisotropy as well.

Indentation testing (see Fig. 3.1) is another commonly used *in vitro* test to measure the localized mechanical properties of soft tissues like articular cartilage [50, 51]. Indentation studies using arteries are limited [52] as physiologically, the arteries are subjected more to loads in tension than compression as in indentation. Indentation offers

the ability to measure the local variation in the mechanical properties, for e.g. spatial variation in elastic modulus E (r_{artery}, θ, z). The spatial resolution depends on the size of the indenter tip used. Studying local variation in mechanical properties can be very important in understanding the diseased response (i.e. properties of a diseased wall or plaque). Finite element simulation of the indentation is usually used to extract different material parameters of the respective hyperelastic model used [61]. While localized mechanical properties can be extracted from indentation, it is very important to correlate the mechanical properties (such as E) measured using indentation to other tension tests such as inflation or uniaxial as arteries are loaded in tension under *in vivo* conditions before being used in models to study hemodynamics.

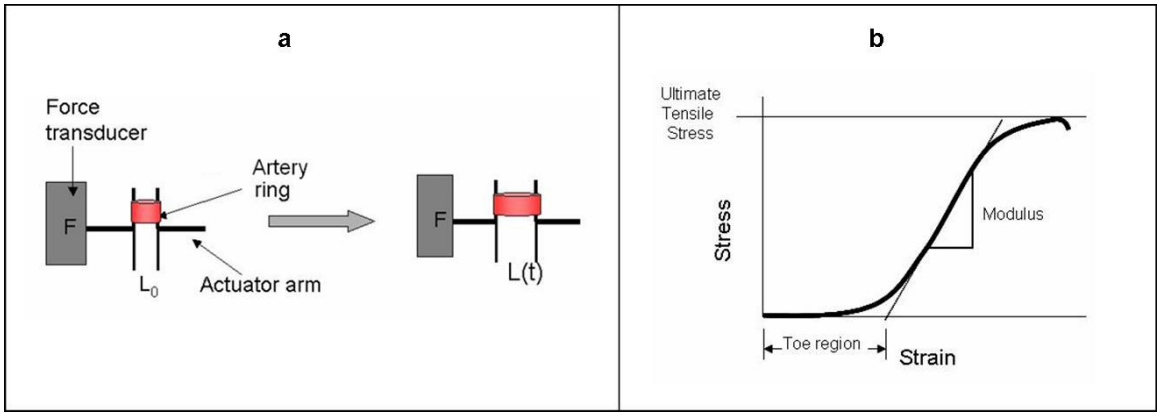

Figure 1.2 Uniaxial Tensile testing in artery rings: a) measurement set up and b) typical stress-strain curve.

Among the *in vivo* techniques, optical coherence tomography (OCT) and ultrasound elastography are used in the measurement of localized (i.e. spatial variations in) mechanical properties [54, 55]. Typically, these methods allow measurement of strains by measuring local displacements and assuming that the loading condition of the artery is constant in all the cases, relative changes to the mechanical properties are extracted. Such *in vivo* measurements offer the potential to be used as tools for guiding interventional procedures (balloon dilatation, ablation) and detection of plaque vulnerability [54]. Thus, each of the listed techniques in Table 1.3 have certain advantages in measuring the mechanical response of arteries under different conditions (e.g. normal vs. diseased;

global vs. local measurement, *in vivo* vs. *in vitro*). However, it is important to realize that while the mechanical responses from different tests may correlate, caution must be exercised in directly comparing a parameter extracted from one test to another.

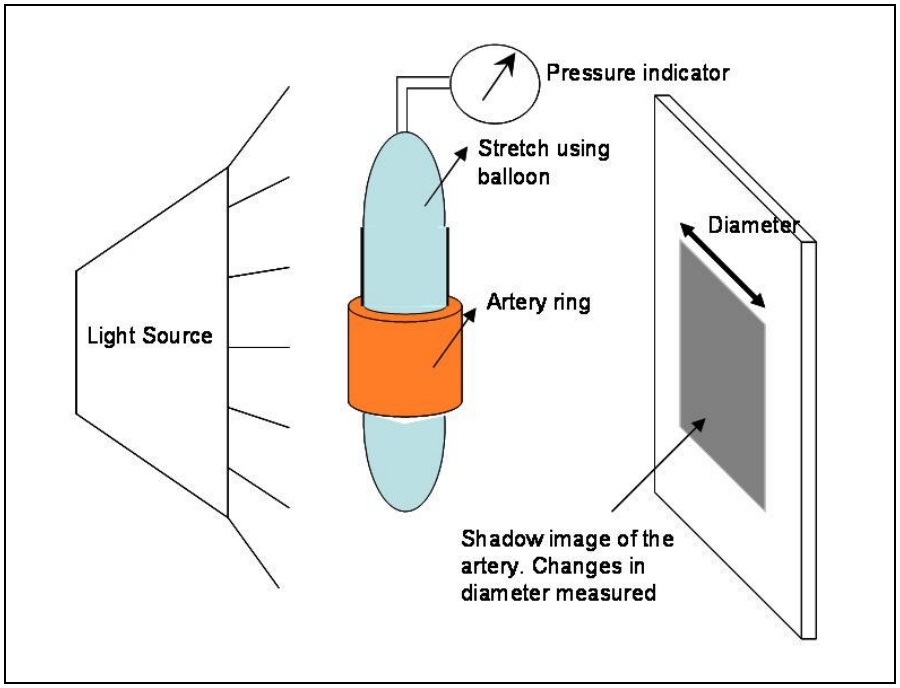

Figure 1.3 Pressure-diameter inflation testing in artery rings

1.3.2 Biomechanical property changes due to thermal treatments

Changes due to freeze-thaw

Several studies on effect of freezing on the mechanical properties of connective tissues such as tendon, ligament and cartilage [62-66] as well as arteries [42, 67-71] exist (Table 1.2). Most of these studies on arteries were performed in the presence of cryoprotective agents [42, 67-71]. Among these studies, the results are mixed depending on the particular artery and test used. For example, in a pulsed flow loop experiment, Rosset et al. [70] saw a change in the response of cryopreserved human common carotid artery (CCA) after freezing, but did not see a change in cryopreserved superficial femoral artery (SFA). Also, Pukacki et al. [69] measured the compliance and elastic modulus of DMSO cryopreserved iliofemoral arteries and compared them with fresh samples. They saw no changes in cryopreserved

arteries. However, Blondel et al. saw a difference in the measured strains and stresses, but not in the calculated elastic moduli or compliance values of cryopreserved SFA subjected to inflation tests[67]. In another study, Adham et al. [42] performed uniaxial tests on cryopreserved thoracic aortas and they observed a decrease in the high stress modulus, but it was not statistically significant. While studies quantifying the freeze-thaw induced biomechanical changes to improve cryopreservation exist, no study looking at the biomechanical effects of cryoplasty on arteries has been performed.

Changes due to heating

The effect of heating on the biomechanics of tissues is dependant on the temperature range and the time of exposure. Kang et al. observed that there was no significant difference in the multiaxial passive behavior when bovine coronary arteries were exposed to a temperature range of 21^{o}C-55^{o}C for 20 mins [72]. However, the arterial specimens exhibited circumferential stiffening after 20-40 mins of exposure. Further, they also observed that mechanical changes post 90s of exposure to 70^{o}C and 80^{o}C were significantly different. Stiffening of the specimens was observed due to shrinkage when the arterial segments were exposed to high temperatures. Baek et al. [73] heated bovine epicardium at 75^{o}C for 15mins and observed that the thermally treated tissues showed significant stiffening when compared to native tissues. However, Chae et al. [74] showed that the storage moduli of the nasal septal cartilages decreased when heated up to a temperature of 70^{o}C although most cardiovascular tissues exhibited stiffening on heating above the denaturation temperature (55^{o}C-60^{o}C). This suggests that the structural organization of ECM in tissues plays a key role in determining the biomechanics of soft tissues as reviewed by Silver et al. [75]. These studies suggest that changes to ECM organization possibly play an important role in the biomechanical changes during heating. Additionally, cell death could also play an important role.

1.4 MECHANISMS UNDERLYING THERMOBIOMECHANICAL CHANGES

An understanding of the mechanisms underlying thermobiomechanical changes requires measurement of the component changes due to the thermal treatments. This is because the overall biomechanical response of an artery at the tissue level is governed by its

structural components. Structurally, artery wall is composed of the extracellular matrix (ECM) and different types of cells distributed into three layers: intima, media and adventitia. In most arteries, collagen is the most important structural protein of the ECM, which also contains elastin, glucosaminoglycans, etc [76]. Among the cells, smooth muscle cells (SMCs) are the predominant cell type in the artery; mostly found in the media or middle layer [76, 77]. However, depending on the artery type (muscular or elastic), its structural composition varies. For instance, in a muscular artery type such as femoral artery, collagen matrix and smooth muscle cells (SMCs) form the important structural components of the artery [76, 77]. On the other hand, an elastic artery such as the aorta has a high elastin content and is low in SMC content [76, 77]. In addition to these components, water accounts for a high weight proportion (~ 70%) of most soft tissues including arteries [78]. During thermal treatments, changes to the arterial components and/or their hydration ultimately cause the observed biomechanical changes. In order to establish the mechanisms underlying these biomechanical changes, in addition to measurement of the biomechanical changes, it is important to understand the changes to the components and then connect them to the biomechanical changes through component based mechanical models (see Table 1.2 for an overview). In this section, different measurement techniques that can quantify the molecular and cellular component changes are reviewed.

1.4.1 Measurement of matrix hydration/stability

ECM, or the extra-cellular matrix, is primarily composed of structural proteins and water. It is an important contributing factor to the mechanical integrity of several soft tissues [22, 24, 25, 79]. Collagen is the main structural protein of most connective tissues including arteries and plays an important role in the overall stability of the tissue [75, 80, 81]. In section 4.1, assessment of (collagen) matrix stability and hydration starting from bulk tissue to molecular level assessment is reviewed (see Table 1.2).

Bulk tissue property (gross) measurements

Bulk tissue properties such as weight, opacity [82] and physical dimensions (e.g. shrinkage during collagen denaturation [83-85]) provide gross assessment of the matrix stability and hydration. Changes in the net weight of the tissue are usually assumed to be largely due

to the bulk water loss. As water occupies the spaces between matrix fibers, dehydration has been suggested to reduce the interfibrillar spacing, which in turn may affect the stability [86]. Previous studies in artificial tissues [87] have reported tissue dehydration following freeze-thaw.

Opacity is also an useful tool for gross measurement of matrix stability [82, 88]. Pierce and Johnson review the use of changes in opacity to study changes in matrix stability during collagen denaturation [88]. In another study involving a collagen based tissue equivalent, Neidert et. al. showed that the opacity reduces significantly post freeze-thaw [82] although it is unclear whether freezing induced collagen denaturation or simply rearranged the interfibrillar spacing in [82].

Matrix stability can also be indirectly measured through changes in physical dimensions. Shrinkage has also been used to quantify collagen denaturation in several studies [83-85]. While bulk tissue properties such as weight, opacity and physical dimensions provide qualitative insights, sophisticated spectroscopic, calorimetric and computational techniques reviewed in the next section can help quantify molecular level changes.

Molecular level measurements

Arguably, the most important structural protein in the ECM is collagen. The collagen matrix is hierarchically built starting from a fundamental triple helical molecule, tropocollagen (see Fig. 1.7). Reviews on hierarchical arrangement of collagen matrix and its role in overall stability of the matrix exist [75, 80]. Briefly, three polypeptide chains wrap around each other forming the tropocollagen whose stability is established by the heat-labile hydrogen bonds between the helices. Five of these tropocollagen molecules form a micro-fibril that in turn self-assembles into fibrils and then the fibers. This structure is enforced by the chemical bonds within and among different hierarchical levels and influences the stability of the matrix. In this review, some of the commonly used measurement techniques for thermal stability of collagen are reviewed.

Spectroscopic Methods

Spectroscopy has been used extensively in the analysis of secondary structure of polypeptides and proteins [89, 90]. Among the various existing spectroscopic approaches,

Circular Dichroism (CD), Fourier transform infrared (FTIR), Nuclear Magnetic Resonance (NMR) and Raman spectroscopic techniques are the most frequently used. Among these methods, NMR spectroscopy requires very high concentration of the sample and is usually expensive [91]. Moreover, as Raman spectroscopy has not been used frequently in the assessment of thermal stability of collagen, this review is limited to studies that have used CD and FTIR in studying collagen stability (see Table 1.2).

Circular Dichroism (CD)

CD is a spectroscopic technique that uses differential absorption of polarized light in order to determine the structure of macromolecules [90-96]. CD experiments are typically very quick (~30mins), non-destructive and can be performed using both near and far ultraviolet (UV) spectra using small samples [91]. A detailed review on use of CD to study protein secondary structure has been presented by Johnson [90]. Briefly, CD spectra can be used to determine the α-helix, β-sheet, β-turn and random coil content of proteins. While α-helix, β-sheet and random coil structures have intense positive bands at 192 nm, 198 nm and 210 nm respectively, β-turn has an intense negative band at 198nm. Additionally, α-helix also has an intense negative band at about 222 nm, and another reasonably intense negative band at 208 nm. In another review, Kelly and Price review the use of CD in studying folding and unfolding of proteins [91]. During collagen denaturation, triple helical structures unfold and form random coil structures, kinetics of which can be studied from the variation in the intensity of the CD bands as reported in previous studies [92-95]. In addition to CD, FTIR spectroscopy has also been used to study the secondary structures of proteins and is reviewed in the following section.

Fourier Transform Infrared (FTIR) spectroscopy

FTIR is another well established spectroscopic measurement technique used vastly in the measurement of macromolecular structures such as proteins and lipids. Application of FTIR in studying protein structures has been reviewed in detail by Kong and Yu [89]. Secondary structure analyses of proteins are typically carried using the amide bands. Amide-I and amide-II are intense bands corresponding to the α-helical or triple helical content in the sample (see Fig. 1.4). Amide- III is a band (1320-1180 cm^{-1}) corresponding

to the β-sheet and random coil structures [97, 98]. Heat induced denaturation of collagen can be measured by either analyzing the decrease in triple-helical content from the Amide-I or Amide-II band peak area or increase in random coil structures from the Amide-III band peak area[99]. An amide-III analysis is often better for studying denaturation in tissues because the amide-I and amide-II bands are distorted when large sample thicknesses are involved [99]. Other analyses such as measurement of changes in absorption peak ratio in the amide bands [100] and decrease in CH_2 stretch peak [101] have also been used to study thermal stability of collagen. In addition to spectroscopy, calorimetric techniques such as the differential scanning calorimetry (DSC) have been used extensively in studying thermal stability of collagen [86, 102-104].

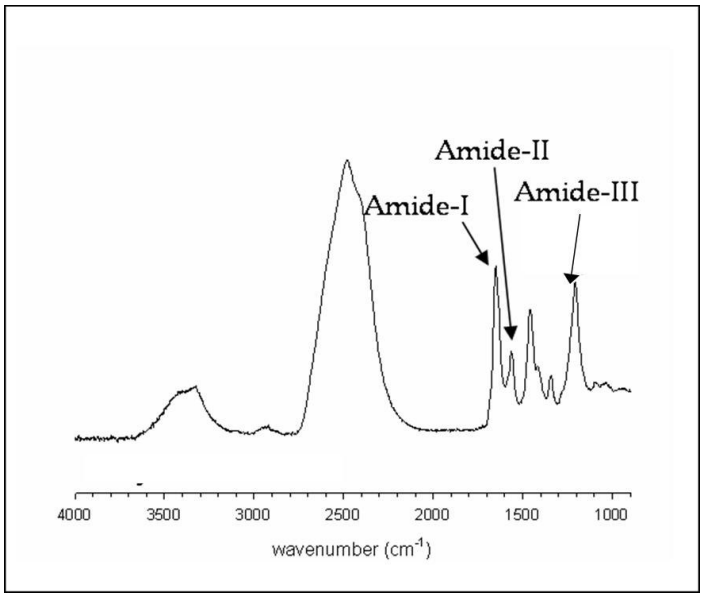

Figure 1.4 FTIR spectra with the different amide bands characteristic of protein secondary structures.

Calorimetric Method - Differential Scanning Calorimetry (DSC)

DSC is used to study endothermic and exothermic phase change processes including collagen denaturation [86, 102-104] (Fig. 1.5). Sturtvent et. al. present a detailed review on the different biomedical applications of DSC and particularly how enthalpy and onset temperature for a phase change process be obtained [102] (see Fig. 1.5). Among the

numerous DSC studies on thermal stability of proteins, those from Miles et. al. [86, 103, 104] are classic examples of the use of DSC in the assessment of thermal stability of collagen in different tissues. As DSC is a well established technique and there exists several reviews on the use of DSC for the assessment of thermal stability of proteins [105], this review shall not further elaborate on this topic. However, it should be noted that while DSC provides enthalpic information, spectroscopic techniques provide information on the structural changes occurring at the molecular level. In addition to spectroscopic methods, development of advanced computational capabilities has enabled the use of molecular dynamics to visualize the structural changes occurring in a single molecule (Figs. 1.7 and 1.8).

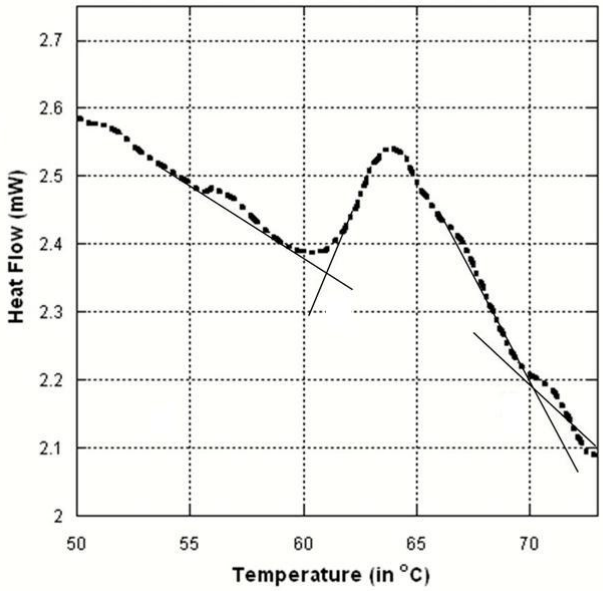

Figure 1.5 Measurement of thermal stability of collagen using DSC: denaturation endotherm of a) rat tail tendon and b) arterial collagen

Computational Method - Molecular Dynamics

MD is probably the most realistic simulation technique that allows examination of nanoscale behavior of proteins (Fig. 1.6). Collagen, at the nanoscale, consists of triple helical tropocollagen molecules that have a length of 300 nm and diameter of 1.5 nm. Through MD simulations, it is now possible to understand the events happening in a single tropocollagen molecule at nanoscale which is the first step towards a multiscale understanding of thermal stability from a molecule to tissues.

MD has been previously used to describe kinetic pathways of several important reactions and thereby provide molecular level insights [106, 107]. Unfolding kinetics of helical proteins such as tropocollagen can be analyzed by studying the variation of root mean squared displacement (RMSD) of the α-carbon in the amino acid residue with time or temperature as shown in Fig. 1.7. Additionally, variation in the helical content of the protein molecule with time or temperature can also be used to study the unfolding kinetics. The helical content is calculated based on the fraction of residues satisfying the dihedral angle (φ, ψ) criterion obtained from the ramachandran plot for different secondary structures (left helix, α-helix, β-sheet, etc.) [108].

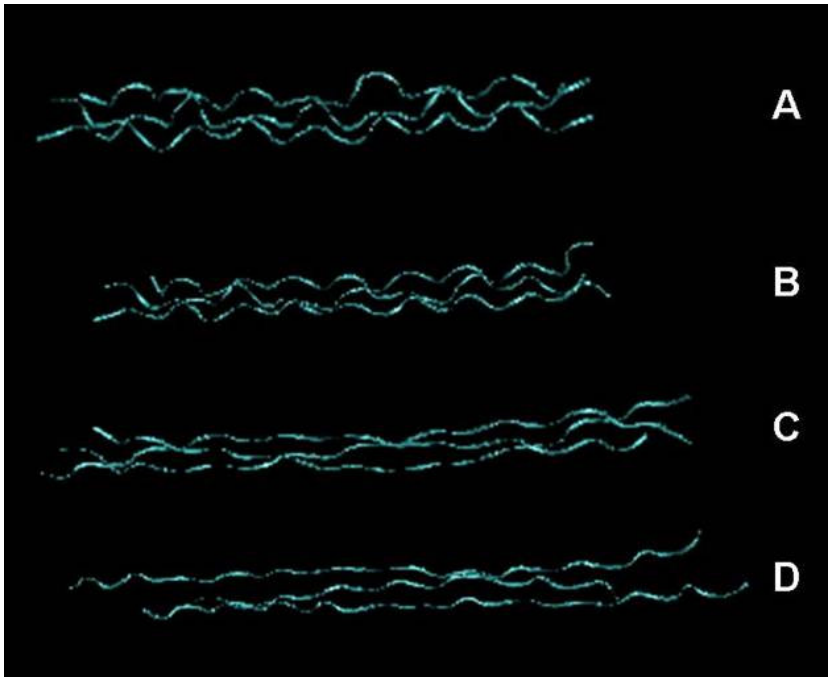

Figure 1.6 Visualization of thermal unfolding of tropocollagen using molecular dynamics (A-D)

Despite MD's ability to provide molecular insights on the transition state structures (dihedral angles of the protein backbone, hydrogen bonds, etc.), the use of extremely high temperature for unfolding under computationally accessible timescale (nanoseconds) has invoked criticism on its validity in the supra-physiological (<95^{o}C) temperature regime. However, the agreement between the simulations and experiment for different proteins [109-111], suggests that the unfolding pathways are independent of the

temperature and the process is merely accelerated by increasing the temperature in MD [106]. Additionally, the development of nano second laser pulses for ablation of biological tissues provides a scope for experimentally verifying MD simulations [112]. Conclusively, MD simulations, if used with caution, can be very useful in precisely understanding the changes (e.g. thermal stability) at the level of a single molecule. Development of effective multi-scale models that connect these molecular mechanisms to biomechanical changes in arteries at tissue level will be very useful controlling the mechanical property changes due to thermal treatments.

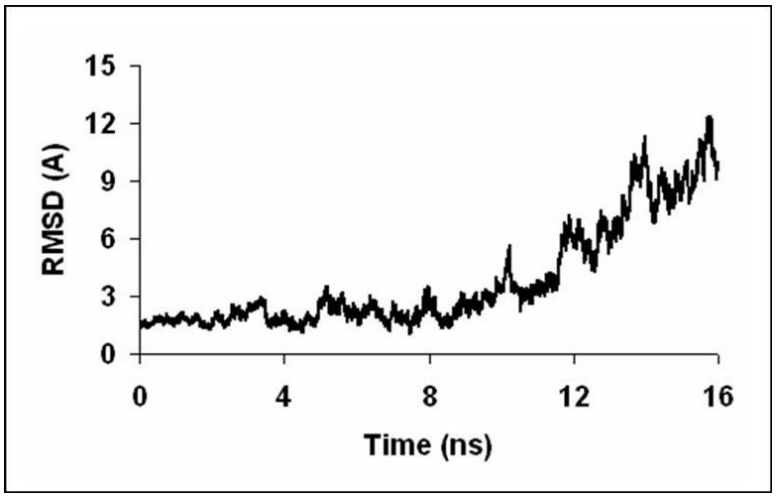

Figure 1.7 Thermal stability of single tropocollagen molecule assessed from MD simulations: change in RMSD vs. time.

1.4.2 Measurement of cell viability or function

In addition to the collagen matrix, cells also play an important role in determining the biomechanical response of tissues. It is therefore important that in addition matrix stability changes, thermally induced cellular level changes be measured as well. Commonly used established approaches include assessment of viability through histological evaluation, biochemical assays and measurement of cellular functioning in tissues by studying their response to certain chemicals [113] (e.g. SMC response to norepinephrine and acetylcholine [114]). Recent advancements in the force measurement techniques have made it possible to mechanically probe the cell and then correlate them

to its function. Zhu et. al. 2000 [115] and Suresh 2007 [116] provide a detailed review on cell mechanics.

1.4.3 Thermally induced ECM and cellular changes in arteries

In the previous section, different techniques used in the measurement of cellular and molecular level changes were reviewed. While some techniques presented in section 4.2 have already been employed to perform molecular level measurements in tissues including arteries, the remaining offer the scope to further our understanding in these areas. In the following section, ECM and cellular changes induced due to both freeze-thaw as well as heating are reviewed (see Table 1.2).

Changes due to freeze-thaw

SMCs and collagen matrix form the most important components of an arterial wall [76]. As the overall arterial biomechanical response is governed by these components, changes to them during treatments such as freeze-thaw need to be quantified. Freeze-thaw studies in artificial [87] tissues have reported tissue dehydration post treatment thereby affecting the ECM structure [82] and stability . In an artificial tissue scaffold study [87], it was reported that the freeze-thaw induced dehydration ultimately resulting in closer packing of the collagen fibers in the matrix. Neidert et al. also observed water movement due to freezing by observing the loss of opacity in frozen artificial tissue samples [82]. They additionally reported that the weight loss correlates with the size and extent of ice crystallization. In a separate study in rat tail tendon, an increase in thermal stability of the collagen matrix due to dehydration was observed by Miles et. al. [86]. These studies suggest that freeze-thaw induced dehydration could potentially change the thermal stability of the collagen matrix and needs to be understood better.

In addition to the ECM, SMCs also are important components of arteries. Previous studies involving freeze-thaw have reported significant reduction in SMC viability [117, 118] that varies depending on different treatment parameters (cooling rate, end temperature, etc.). While these studies offer good preliminary insights, they have been carried out in different *in-vitro* model systems (monolayer, fibrin gel [117, 118] or tissue equivalents [118]), which may differ from the native vessel behavior.

Changes due to heating

Similar to freeze-thaw, heating also results in changes in both ECM and cells that ultimately cause the overall biomechanical changes. Collagen, an important component of ECM, denatures when heated to temperatures higher than 55°C for sufficient time [80]. Several treatments involving heating (thermal keratoplasty, skin re-surfacing, tissue welding, etc.[119]) are based on collagen denaturation because of which it has been extensively studied for decades. Wright and Humphrey review the collagen denaturation process in detail [80]. At the molecular level, denaturation involves unfolding of tropocollagen molecule and involves breaking of both the intermolecular hydrogen bonds (within the tropocollagen triple helix structure causing it to unfold) and the heat-labile intramolecular cross-links [83]. Denaturation can also be measured calorimetrically by the endothermic heat release in DSC (Fig 1.5), spectroscopically by the changes in the secondary structure in CD or FTIR (Fig. 1.4), optically by loss of birefringence [120] and mechanically by shrinkage measurements [83-85]. Denaturation of collagen has been shown to be a function of both temperature and the time of heating [80, 83, 84, 103]. The denaturation ratio (or accumulated thermal damage) can be represented as an Arrhenius damage integral ($\Omega(\tau)$, representing the temperature history of the material $0<t<\tau$), where t is the time, E is the activation energy, A is the frequency factor, R is the universal gas constant, T is the temperature. $C(0)$ represents the initial concentration of collagen at the "native" state and $C(\tau)$ represents the concentration of collagen at the "native" state at $t=\tau$ [83].

$$\Omega(\tau) = \ln\left[\frac{C(0)}{C(\tau)}\right] \qquad \Omega(\tau) = \int_0^{\tau} A e^{-\frac{E}{RT}} dt \tag{1.5}$$

In addition to the ECM changes, heating also results in cell death when heated to suitably high temperatures. Orihara et. al. 2002 reported that exposing the SMCs to 43°C for 2hours causes complete destruction [121]. Exposure of cells to higher temperatures causes death at an earlier time point.

1.5 SUMMARY

Atherosclerosis is an arterial disease that results in the formation of plaque or hard fatty deposits on the inner wall thereby causing narrowing of the artery. In the last few years, the clinical importance of thermal treatments for atherosclerosis involving both freezing (cryoplasty, cryopreservation of vascular grafts) and heating (in-stent inductive heating) has increased significantly. As artery biomechanics directly impacts hemodynamics and cellular functioning, it is important to understand the biomechanical changes due to the thermal treatments and their underlying mechanisms. As reviewed in this chapter, freeze-thaw and heating both can induce changes to the ECM and cells that lead to overall biomechanical changes in arteries. Optimization of thermal treatments, for e.g. freeze-thaw as in the case of cryoplasty, requires understanding of the biomechanical changes induced due to these treatments and their underlying mechanisms that motivates this dissertation research.

1.6 RESEARCH GOALS AND SPECIFIC AIMS

The goal of this research was to investigate the biomechanical changes in arteries induced by freeze-thaw and the mechanisms underlying these changes (see Fig. A). In this dissertation, two specific aims (SAs) were pursued. SA1 involved quantification of freeze-thaw induced mechanical property changes in arteries using both uniaxial tensile tests and indentation. While uniaxial tensile tests were chosen for relatively easy sample preparation and testing, indentation was performed in order to study a more localized biomechanical response to characterize diseased artery response. SA2 involved investigation of the mechanisms underlying the biomechanical changes. This primarily involved understanding the changes to the collagen matrix and SMCs following thermal treatments (SA2a). Changes to collagen matrix stability were assessed by quantifying the changes to the amide-III band using FTIR spectroscopy. Changes in SMC function were studied from the response of arteries to norepinephrine (NE) and acetylcholine (AC). Finally, MD simulations were performed as a tool to further investigate dehydration

induced increase in thermal stability of the collagen matrix due to freeze-thaw at the molecular level (SA2b). The specific aims of the dissertation are summarized as follows:

SA1. Quantification of freeze-thaw induced biomechanical changes in arteries

a. Changes in uniaxial tensile response

b. Changes in indentation response

SA2. Investigation of mechanisms underlying freeze-thaw induced biomechanical changes

a. Role of collagen matrix and SMCs

b. Dehydration induced changes in stability of single tropocollagen molecule

1.7 OVERVIEW OF DISSERTATION

This dissertation is organized into four chapters. Each chapter consists of a specific research project to study the specific aims outlined in the previous section. An overview of each chapter is given below.

Chapter 2: Freeze-thaw Induced Biomechanical Changes in Arteries -I: Uniaxial Tensile Response

Chapter 2 describes the experiments conducted to study the effect of freeze-thaw on biomechanical properties of arteries as more work is needed to understand the post-cryosurgical or post-cryopreservation changes in mechanical properties of the arteries. Porcine femoral arteries were frozen using two methods: a) in a controlled rate freezer to -80^{o}C at 1^{o}C/min in the presence of cryoprotective agent (CPA) simulating cryopreservation and b) using an aluminum probe to -20C for 2-5mins in the absence of CPA simulating cryoplasty. Following freeze-thaw, artery samples were subjected to uniaxial tensile testing and the changes in weight measured. The results from this study suggest that arterial stiffness increases with freeze-thaw, which was relatively less in the presence of CPA. Additionally, significant reduction in weight of the tissue was observed indicating the importance of bulk water redistribution as one underlying mechanism.

Finally, the extent of stiffening and weight reduction was greatly attenuated in samples frozen in the presence of CPA suggesting the ability of CPA to help hold water within the tissue.

The results from this chapter were published in the following citation:

Venkatasubramanian, R.T., Grassl, E.D., Barocas, V. H., Lafontaine, D. and Bischof, J.C. (2006) "Effect of freezing and cryopreservation on the mechanical properties of arteries." *Annals of Biomedical Engineering* **34**(5): p823-832.

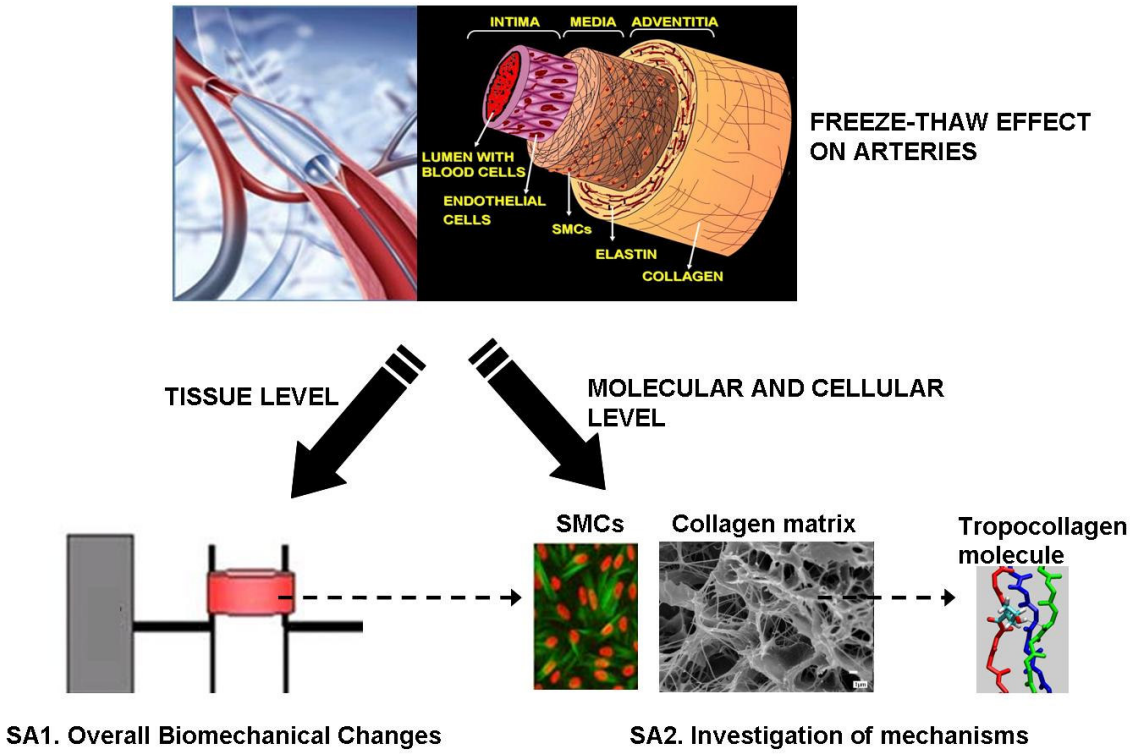

Figure 1.8 Mechanistic understanding of thermobiomechanics of arteries: an overview

Chapter 3: Freeze-thaw Induced Biomechanical Changes in Arteries -II: Indentation Response

Chapter 3 describes the indentation experiments conducted to study the effect of freeze-thaw on localized biomechanical properties of arteries. Biomechanics of normal and diseased arteries, as well as changes in them following freeze-thaw, were measured using an indentation technique that provides localized information at the same time requiring only small tissue samples. Normal human arteries, obtained from an autopsy, were tested and their biomechanics compared with that of diseased human arteries, obtained from donors who underwent bypass surgeries. Due to reduced availability of normal human tissues, normal porcine arteries were also used to understand the freeze-thaw effect on normal arteries. It was observed that the diseased human artery response was approximately 6.2 times stiffer than that of normal human artery but normal porcine arteries were stiffer than both normal (~14 times) and diseased human arteries i.e. E_∞ (normal porcine) > E_∞ (diseased human) > E_∞ (normal human) where E_∞ is the equilibrium modulus. Following freeze-thaw, the diseased human arteries showed no significant change whereas the moduli of normal porcine arteries were found to increase significantly (~1.5-2.3 times). No significant changes were observed in the viscoelastic parameters (g, τ_1 and τ_2) of both normal porcine and diseased human arteries following freeze-thaw. As arterial stiffness increases following cryoplasty in normal arteries, alterations in hemodynamics are expected. Such alterations in hemodynamics have been reported in vascular grafts with a mechanical property mismatch and hypothesized as potential mechanism for downstream pathology. Finally, the results from the current study can provide bracketing behavior (i.e. elastic modulus of normal and diseased arteries as well as changes in them following cryoplasty) for emerging computational models that account for solid-fluid coupling at the artery wall to further investigate hemodynamics in a cryoplasty treated artery. Additionally, measurements from this study can form a baseline to which mechanical properties measured *in vivo* using elastography techniques, i.e., intravascular ultrasound (IVUS) elastography and optical coherence tomography (OCT) can be compared. This may ultimately help form the basis of a diagnosis with IVUS or OCT of disease or pathology within the artery.

The results from this chapter have been submitted as the following citation that is presently in review at the time of dissertation submission:

Venkatasubramanian, R.T., Simha, N.H., Tatsutani, K. and Bischof, J.C. (2008) "Effect of cryoplasty on mechanical properties of human and porcine arteries using indentation." *Cryobiology* (In review at the time of dissertation submission).

Chapter 4: Mechanisms Underlying Freeze-thaw Induced Changes: Role of Collagen Matrix and SMCs

Chapter 4 describes the experiments that investigate the freeze-thaw effect on the arterial components (collagen, smooth muscle cells or SMCs), as well as the components' contribution to the overall artery biomechanics to ultimately understand the mechanisms underlying the biomechanical changes induced by freeze-thaw. It was observed that freeze-thaw of normal arteries caused significant tissue dehydration (15% weight reduction), a consequent increase in thermal stability of the collagen matrix (~6.4^{o}C increase in denaturation onset temperature), and SMC destruction (no contraction and relaxation response to norepinephrine (NE) or acetylcholine (AC) respectively). In addition to freeze-thaw, the arteries were also subjected to hyperthermia and osmotic treatments (0.05M, 0.1M and 0.2M mannitol) that preferentially altered either the smooth muscle cells (SMCs) or collagen matrix (hydration/stability) respectively. While hyperthermia treatment also caused complete SMC destruction, no tissue dehydration was observed. On the other hand, mannitol (0.2M) treatment significantly increased the thermal stability (~4.9^{o}C increase in denaturation onset) but did not change the SMC function. However, freeze-thaw, hyperthermia and 0.2M mannitol treatments all resulted in significant reduction in toe region. The toe region of the freeze-thaw, hyperthermia and 0.2M mannitol treated arteries normalized to their respective controls were 0.61 ± 0.14, 0.81 ± 0.05 and 0.73 ± 0.14 respectively with minimum toe region observed after freeze-thaw. These studies suggest that both increased thermal stability due to tissue dehydration, as well as SMC destruction occurring during freeze-thaw, are important mechanisms of the freeze-thaw induced biomechanical changes.

The results from this chapter have been submitted as the following citation that is presently in review at the time of dissertation submission:

Venkatasubramanian, R.T., Wolkers, W., Barocas, V.H., Lafontaine, D., Soule, C., Iaizzo, P., and Bischof, J.C. (2008) "Freeze-thaw induced biomechanical changes in arteries: Role of collagen matrix and smooth muscle cells." *Annals of Biomedical Engineering* (In review at the time of dissertation submission).

Chapter 5: Thermal Stability of Single Tropocollagen Molecule and Dehydration Induced Changes

This chapter describes the MD simulations that were performed as a tool to further investigate dehydration induced increase in thermal stability of the collagen matrix due to freeze-thaw at the molecular level. The simulations investigated short time (ns) and high temperature (> 500 K) denaturation events within hydrated (in a 60 Å x 100 Å x 32 Å waterbox), partially dehydrated (surrounded by a water skin of thickness 5.5 Å) and fully dehydrated (*in vacuo*) tropocollagen under constant pressure and constant volume conditions. Changes in root mean squared displacement (RMSD) of C_α (central carbon atom of an amino acid to which the sidechain and amino group are attached to), helical content and hydrogen bonding during unfolding events were assessed. It was concluded that following dehydration, despite reduction in protein-water hydrogen bonds due to absence of water molecules, new intra-protein hydrogen bonds that are backbone-sidechain in nature were formed that ultimately led to an increase in thermal stability of tropocollagen. It has been speculated that formation of new intra-protein hydrogen bonds within tropocollagen atleast in part govern the mechanism underlying the increased thermal stability of arterial collagen matrix following mannitol and freeze-thaw treatments observed in previous experimental studies.

The results from this chapter are being prepared for the following citation: Venkatasubramanian, R.T., Perlmutter, J., Sachs, J. and Bischof, J.C. (2008) "Nanoscale unfolding of a single tropocollagen molecule." *Cellular and Molecular Bioengineering* (In preparation at the time of dissertation submission).

Chapter 6: Summary and Conclusion

Chapter 6 presents the overall conclusions of the studies presented in this dissertation

Appendix A: Thermal modeling of Cryoplasty

In appendix A, the thermal history in arteries during cryoplasty was predicted for different balloon temperatures using a thermal model. Based on the predicted temperature distribution, conservative estimates of injury regimes in the artery during cryoplasty were predicted. A thermal model of cryoplasty is useful in predicting the temperature distribution during cryoplasty; which in turn would be ultimately beneficial for further optimization of the technique.

The results from this chapter were published in the following citation:
Balasubramanian, S.K., Venkatasubramanian, R.T., Menon, A. and Bischof, J.C. (2008) "Thermal injury prediction during cryoplasty through *in vitro* characterization of smooth muscle cell biophysics and viability" *Annals of Biomedical Engineering* **36**(1): p86-101.

---

2 FREEZE-THAW INDUCED BIOMECHANICAL CHANGES IN ARTERIES –I: UNIAXIAL TENSILE RESPONSE

This chapter describes the uniaxial tensile tests performed to quantify the biomechanical changes in arteries due to freeze-thaw. The present author performed all the biomechanical experiments and data analysis. The histological analysis was carried out in collaboration with Dr. James Coad of the Department of Pathology at West Virginia University. The present author also created and edited the manuscript for publication. The results from this chapter were published in the following citation:

i. Venkatasubramanian, R.T., Grassl, E.D., Barocas, V. H., Lafontaine, D. and Bischof, J.C. (2006) "Effect of freezing and cryopreservation on the mechanical properties of arteries." *Annals of Biomedical Engineering* **34**(5): p823-832.

Abstract

This chapter describes the experiments conducted to study the effect of freeze-thaw on biomechanical properties of arteries as more work is needed to understand the post-cryosurgical or post-cryopreservation changes in mechanical properties of the arteries. Porcine femoral arteries were frozen using two methods: a) in a controlled rate freezer to -80^{o}C at 1^{o}C/min in the presence of cryoprotective agent (CPA) simulating cryopreservation and b) using an aluminum probe to -20C for 2-5mins in the absence of CPA simulating cryoplasty. Following freeze-thaw, artery samples were subjected to uniaxial tensile testing and the changes in weight measured. The results from this study suggest that arterial stiffness increases with freeze-thaw, which was relatively less in the presence of CPA. Additionally, significant reduction in weight of the tissue was observed indicating the importance of bulk water redistribution as one underlying mechanism. Finally, the extent of stiffening and weight reduction was greatly attenuated in samples frozen in the presence of CPA suggesting the ability of CPA to help hold water within the tissue.

2.1 INTRODUCTION

Atherosclerosis is an important disease with an increasing mortality rate worldwide. In the United States, 400,000 angioplasties are performed every year for the treatment of atherosclerosis [4, 5]. However, 40% of these result in restenosis [4, 5], indicating the need of improvement in the procedure. Cryoplasty, a freezing therapy, involves opening of narrowed arteries using liquid nitrous oxide to simultaneously inflate and cool the dilatation balloon, wherein the diseased arteries are frozen to about -10° to -20°C. While the efficacy of this treatment is being examined in terms of clinical symptoms and histological changes [12, 17], little is known about how the mechanical properties of the tissues are affected by the treatment. One motivation to study the changes in mechanical properties is the possibility of altered hemodynamics, thereby influencing the progression of secondary vascular disease [122, 123]. Cryopreservation, on the other hand, is a process where cells or whole tissues are preserved by cooling to low sub-zero temperatures, such as (typically) -80°C or -196°C. As cryopreserved arteries are extensively used as vascular grafts [124, 125], it is necessary to understand the changes in mechanical properties post-cryopreservation.

Most studies on the effects of freezing on blood vessels have focused on cryopreservation of native and engineered vessels for use as grafts in vascular surgery. Little has been done to examine the mechanical effect of freezing post cryoplasty, which is performed in the absence of cryoprotective agents (CPA). The studies with CPA and the few without CPA have given widely varying results, which appear to depend on the particular vessel studied and the type of mechanical test performed on them. From the varying results in the presence of CPA and lack of results in the absence of CPA it is clear that there is no definitive answer as to what the effects of freezing are on the mechanical properties of arteries, and that more work is needed to determine what mechanical effects, if any, cryoplasty and cryopreservation will have on the arteries.

The purpose of this study was to begin to examine potential mechanical effects of cryoplasty and cryopreservation on blood vessels. To do this, pig femoral arteries were frozen in a controlled rate freezer and using a probe in the absence of CPA. Following a passive thaw at room temperature, the samples were subjected to uniaxial tensile tests to

assess differences in mechanical properties. The results suggest that there are mechanical property changes following freeze/thaw, particularly in the physiological or low stress (up to 50 kPa) region. Weights of the tissues before and after freezing were also measured. The results indicated that there is a bulk reduction in weight of samples frozen in the absence of CPA or serum, thereby suggesting bulk water movement as one underlying mechanism. To examine these changes further, and to study the changes following cryopreservation, we also froze arteries in the presence of CPA.

2.2. METHODS

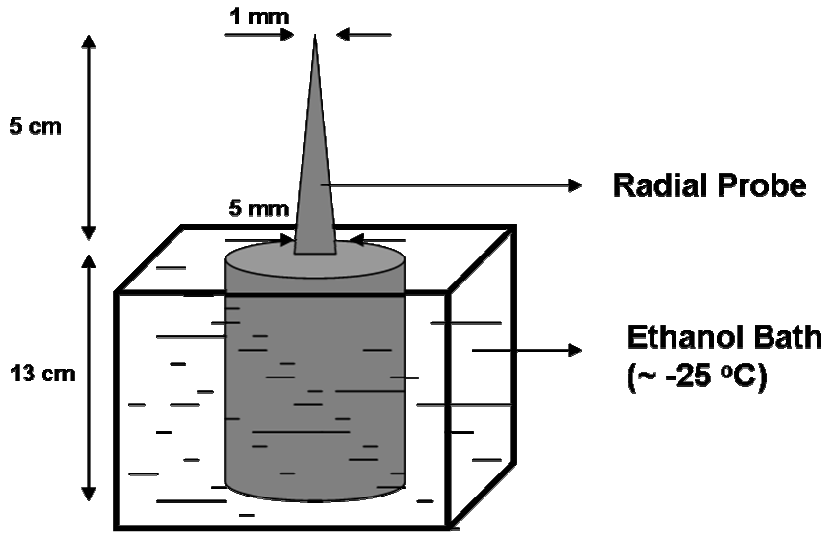

Figure 2.1 The tapered aluminum probe used for radial freeze to simulate cryoplasty

2.2.1 Harvesting and preparation of vessels

Femoral arteries were obtained from domestic pigs used for physiology studies. The average age of the pigs used was 3-4 months while the mean weight of the pigs was about 40 kg. All the pigs used for the study were IACUC approved. Although some of the pigs were used for cardiovascular physiology studies, the femoral arteries were not directly involved at any point and to our knowledge there were no significant systemic effects from the previous studies. Vessels were removed within 1 hour of death and transported to the lab in phosphate buffered saline (PBS) on ice. The vessels were rinsed with fresh PBS, cleaned of any remaining fatty tissue, and cut into 3 mm rings. Rings were kept in

PBS prior to freezing or mechanical testing for not more than one hour at room temperature.

2.2.2 Freezing procedures

Freezing was performed using two protocols, which were chosen based on standard cryoplasty conditions. In one of them, arterial rings were frozen in a controlled-rate freezer (Planer) by maintaining the samples at -20^{o}C for 5 mins. In the other, radial freezing was performed using an aluminum probe as shown in Fig. 2.1. The cylindrical portion of the probe was placed in an ethanol bath and the tapered portion was set to -20^{o}C by maintaining the bath at an appropriate temperature. A tapered probe was used for freezing as the arterial rings had varying diameters. Some of the samples were frozen in radial direction with load. Load was applied during freezing by pulling the arteries down the tapered probe leading to a strain of approximately 60%. The hold time for radial freeze was 2mins. In both cases, samples were passively thawed at room temperature and placed in PBS after which they were uniaxially tested. The weights of the samples were measured before and after freeze/thaw to assess any bulk water movement during freezing.

2.2.3 Cryopreservation procedures

For studies of the effect of cryopreservation on mechanical properties, segments of the arteries were agitated in a rotator with increasing concentrations of a solution of dimethyl sulfoxide (DMSO) in DMEM with 2.5 % chondroitin sulfate, based on the procedure in Pegg et al. [27]. The arteries were agitated in a rotator for 10 minutes at each CPA concentration and 20 minutes at the final concentration of 15% DMSO. The segments were then cut into 3 mm rings and placed in a 24 well plate with 1 ml of the 15% DMSO solution. The samples were then frozen in a controlled-rate freezer (Planer), at -1 ºC/min to -80 ºC. After a 4 minute hold, the vials were thawed in a 37 ºC water bath. The freezing and thawing parameters were chosen because Pegg et al. [27] saw no fractures in rabbit common carotid arteries frozen under similar conditions. The CPA was removed from the thawed samples, by again agitating them in decreasing concentrations of DMSO in DMEM with 2.5 % chondroitin sulfate and 3% mannitol for 5 minutes at each step [126].

Samples were then placed in PBS and immediately taken for uniaxial tensile testing. To further compare the effect of CPA on the biomechanics of arteries post freeze/thaw, some samples were frozen under similar conditions, i.e. at -1^{o}C/min to -80^{o}C in PBS and in culture media (RKO media containing serum) respectively, in the controlled rate freezer. In addition, to understand the mechanism of water movement and the role played by serum, if any, in preventing the outside water movement through possible hydrogen bonding [104], some samples were frozen in media (containing no serum) and weights of the tissue samples were measured before and after freezing after wiping off the excess water from the tissue explants.

2.2.4 Histology

Histology of all the samples was reported after assessment by Dr. James Coad, a surgical pathologist at West Virginia University. Cell/ECM injury was assessed in each sample using light microscopy and blind analysis. Fresh and frozen samples for histological examination were maintained in Dulbecco's modified Eagle's medium (DMEM) supplemented with 1% penicillin-streptomycin and 10% fetal bovine serum at room temperature for 72 hours. This culture method allows for the irreversibly injured cells to manifest damage histologically, while uninjured cells maintain histologic viability [127]. After culture, the samples were fixed in neutral buffered formalin and paraffin-embedded. Tissue blocks were sectioned at 5 μm, mounted on a slide and stained with hematoxylin and eosin prior to microscope histological exam.

2.2.5 Mechanical testing procedures

Vessel dimensions were measured prior to mechanical testing, just after thawing. Wall thickness was measured by photographing rings under 4x magnification, measuring the in pixels, and then converting to mm. Following measurements, samples were kept in PBS until testing. The rings were subjected to uniaxial tensile testing on an MTS MicroBionix biomaterials testing machine (MTS Systems, Eden Prairie, MN). As described previously for tissue-equivalent rings [128], the arterial rings were mounted on parallel T-bars (Fig. 1.2a) such that one side of each "T" projected through the lumen. One T-bar was connected to the actuator, with the other connected to a 5 N load cell, allowing

continuous measurement of the stress response to a constant extension rate of 2 mm/min (~ strain rate of 0.8% per sec) in the circumferential direction. Samples were preconditioned by repetitively opening and closing the T-bars approximately to a strain of 20% until the stress-strain curve did not significantly change, with 6 repeats typically sufficient. Samples were then stretched at an extension rate of 2 mm/min until reaching the limit of the load cell. True stress (σ) and true strain (γ) were calculated as shown below.

$$\sigma = \frac{F(t)}{A_0 \frac{L_0}{L(t)}} \tag{2.1}$$

$$\gamma = \ln\left(\frac{L(t)}{L_0}\right) \tag{2.2}$$

where $F(t)$ is the measured force at time t, A_0 is the initial cross-sectional area of the ring, L_0 is the initial displacement (Fig. 1.2), and $L(t)$ is the displacement at time t. Due to the variability in the small strain region of the stress-strain curves, the reported moduli are defined as the slope of the large strain linear region of true stress vs. true strain, which is more appropriate than engineering strain, i.e. $(L(t)/L_0)$- 1, at the large strains investigated. A toe region was defined by extending the linear region to the x-axis and recording the intercept (Fig. 1.2b). Initial Length (L_0) (referred to as Length in result plots) and the linear elastic modulus were the other parameters measured (Fig. 1.2b). The ultimate tensile strength (UTS) was not measured because the associated force was greater than the limit of the load cell.

2.2.6 Statistics

Data are given as the mean +/- standard deviation with n = 6-13 for all of the tests except for the tests performed on samples frozen in radial direction without load where n = 4. Samples from contralateral segments were considered independent and for the purpose of statistical analysis; the values for each sample were normalized to control (fresh samples from the same segment), to account for variability. Student's t-test was used to test

significance between specific cases, with an adjusted maximum p-value of 0.01 to account for multiple comparisons.

2.3 RESULTS

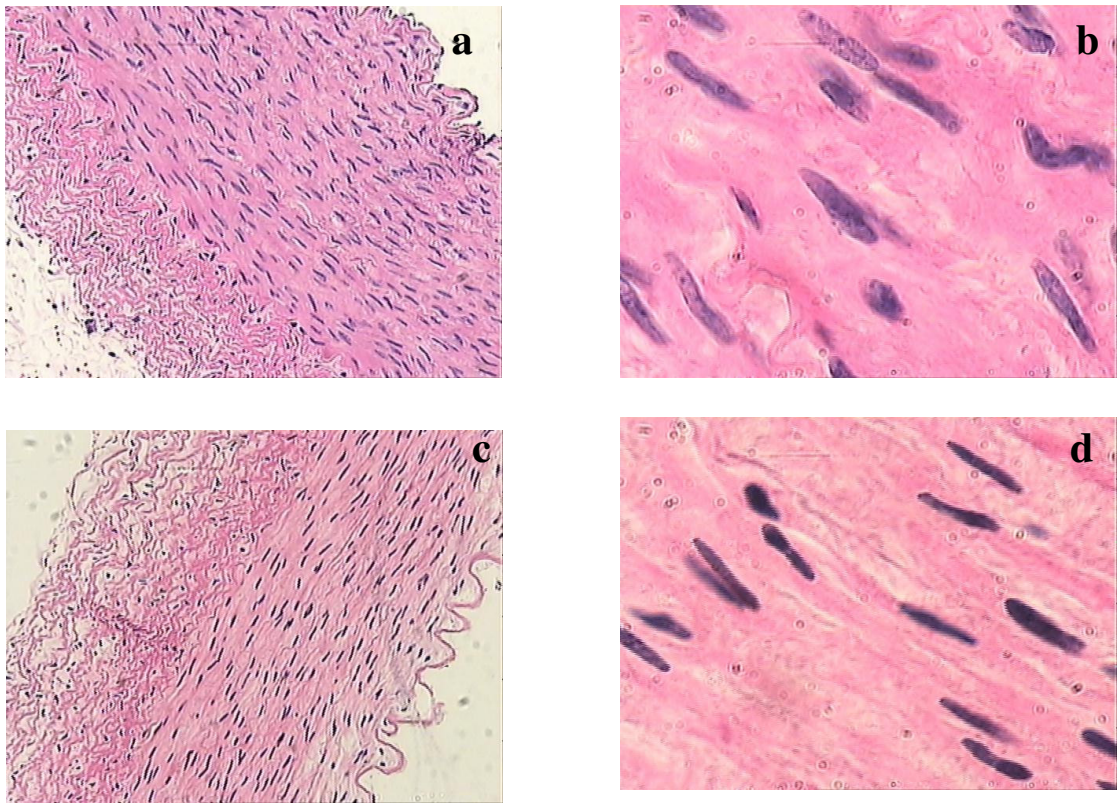

Figure 2.2 Hematoxylin and eosin stained section of fresh (a, b) and frozen (c, d) arteries, original magnification 10x (a, c) and 60x (b, d). Note the condensed nuclei in the frozen samples (c and especially d) indicating smooth muscle cell injury.

2.3.1 Macroscopic and histological changes with freezing

Following freezing in the controlled-rate freezer or the ethanol bath, the rings appeared to increase in $_{\text{length (Lo)}}$. This is reflected in the values reported for initial starting length for the mechanical testing, reported in Fig. 2.5. There was a significant difference in the starting length of frozen samples when compared to the fresh samples.

Histological evaluation revealed cell injury in the samples frozen in the absence of CPA. Signs of cell stress including cytoplasmic contraction, mild hypereosinophilic staining, and nuclear condensation can be observed in the frozen sample in Fig. 2.2b,

compared to the unfrozen in Fig. 2.2a. In addition, approximately 10% of the smooth muscle cells showed necrosis with nuclear breakdown and moderate hypereosinophilia. These necrotic cells varied in density around the circumference. Despite the evidence of cell injury, no significant damage to the ECM structure was observed.

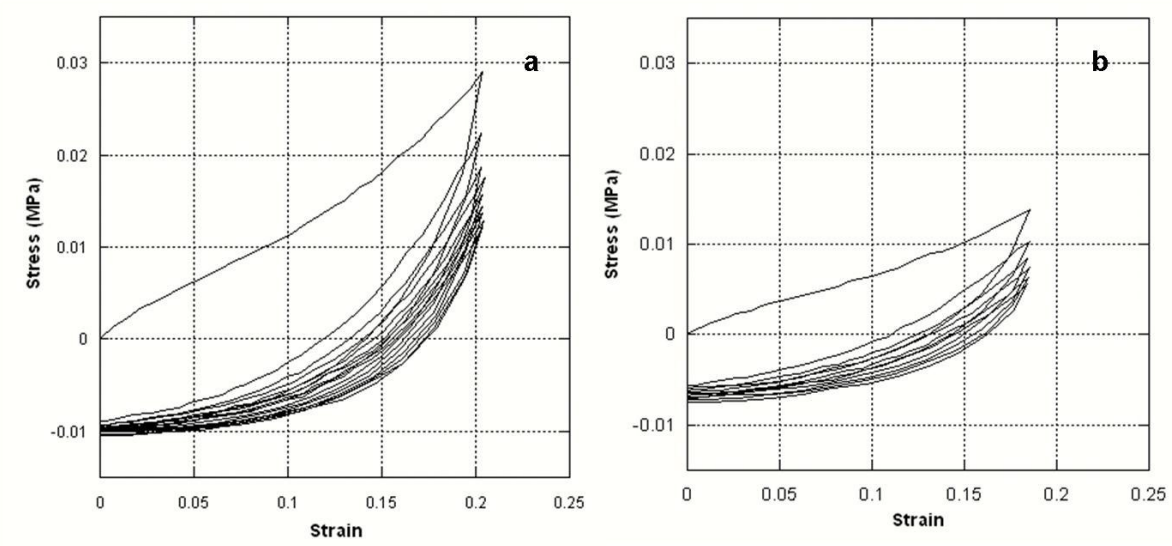

Figure 2.3 Preconditioning curves for (a) fresh and (b) frozen-thawed samples.

2.3.2 Stress-strain characteristics of frozen arteries

Each sample was preconditioned to a strain of 20% before testing. Fresh samples exhibited greater hysteresis in the first preconditioning loop and took more cycles to reach repeatable stress-strain curves than frozen samples (Fig. 2.3). Following preconditioning, the samples were stretched at 2 mm/min to the upper limit of the load cell. Figure 2.4a shows representative stress-strain curves for fresh and frozen samples, while Fig. 2.4b focuses on the lower stress region (up to 50kPa) to demonstrate the large differences in this region. The physiological region is calculated based on the Laplace relation between transmural pressure and circumferential stress [46, 47]

$$\sigma_c = \left(\frac{Pa}{h} \right) \tag{2.3}$$

$$a = \frac{2L(t) + 2\pi R}{2\pi} \tag{2.4}$$

where a is the internal diameter, P is the transmural pressure and R, the radius of the pins of the t-bars. The arteries are assumed to be circular and cylindrical thin tubes [67].

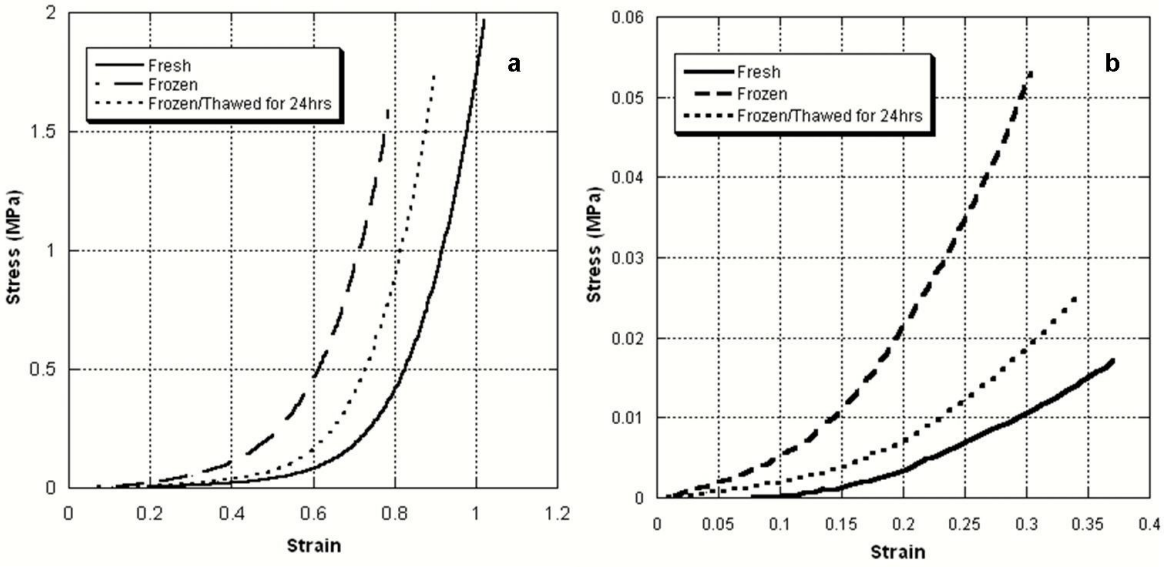

Figure 2.4 (a) Stress-strain curve for fresh samples, samples frozen in Controlled rate freezer (CRF) and samples frozen in CRF and thawed for 24 hrs. (b) Stress – strain response in the physiological regime.

The linear regime in the stress-strain curve for fresh samples started at higher strains while it was considerably lower for frozen samples. After thawing the frozen samples and culturing at 37^{o}C for 24 hours, a shift towards the fresh behavior was observed, though not completely (Fig. 2.4). All the parameters measured were normalized to control (fresh) for comparison (Fig. 2.5). While the toe region decreased in frozen samples, the length Lo increased. The linear modulus also decreased in frozen samples, however it can be clearly seen (Fig. 2.4) that the average modulus of elasticity was higher in frozen samples in the physiological regime, i.e. lower stress regime.

The stress-strain curve for samples frozen without CPA in radial direction also showed similar trends (Fig. 2.6). When compared to samples frozen in the controlled-rate freezer (CRF), the samples frozen in radial direction with and without load showed further drift away from the fresh behavior, with the ones loaded showing maximum drift. Figure 2.7 shows the parameters comparing the fresh and different frozen samples, all normalized to control.

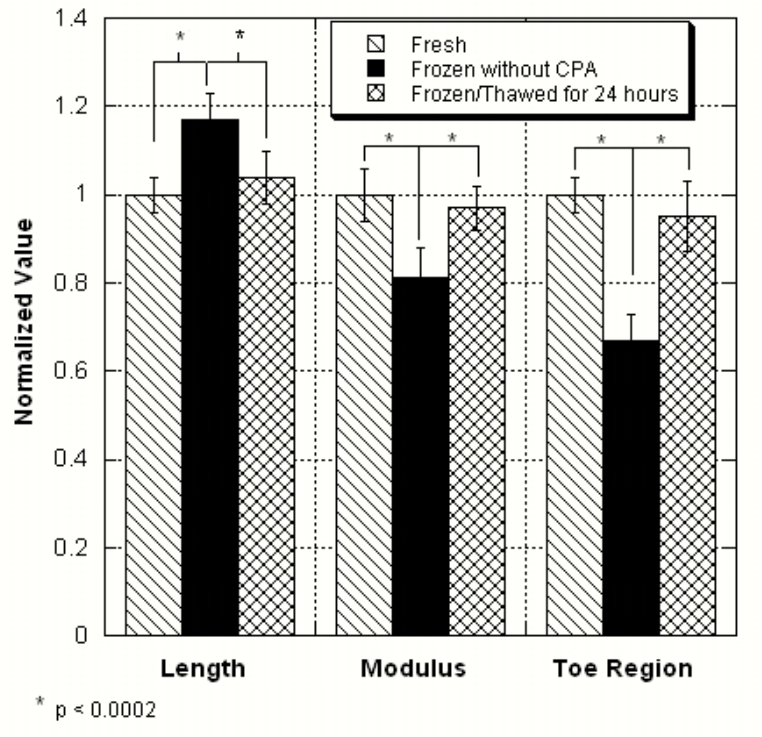

Figure 2.5 Comparison of normalized values of properties for fresh (n=13), samples frozen in CRF (n=6), and samples frozen in CRF and thawed in media for 24 hours (n=6).

2.3.3 Changes in mechanical characteristics following cryopreservation

There were no significant changes in the L_0 for samples frozen with CPA. Pre-conditioning curves were not different and the number of cycles to achieve repeatability was similar to fresh samples. However, a smaller shift could be seen in the stress-strain curves (Fig. 2.8). Changes in the modulus and toe region were also observed (Fig. 2.9); both were less than that of the fresh samples.

Comparison of freezing in PBS and culture media containing serum under similar conditions as that of cryopreservation showed shifts from fresh behavior. The degree of shift from the fresh behavior was the maximum in samples frozen in PBS, while the next were the samples frozen in media (Fig. 2.8). Samples frozen with CPA showed the closest behavior to that of fresh samples. The different parameters measured also indicated that samples frozen with CPA show the closest resemblance to fresh behavior (Fig. 2.9) compared to others, although there were significant deviations in these samples.

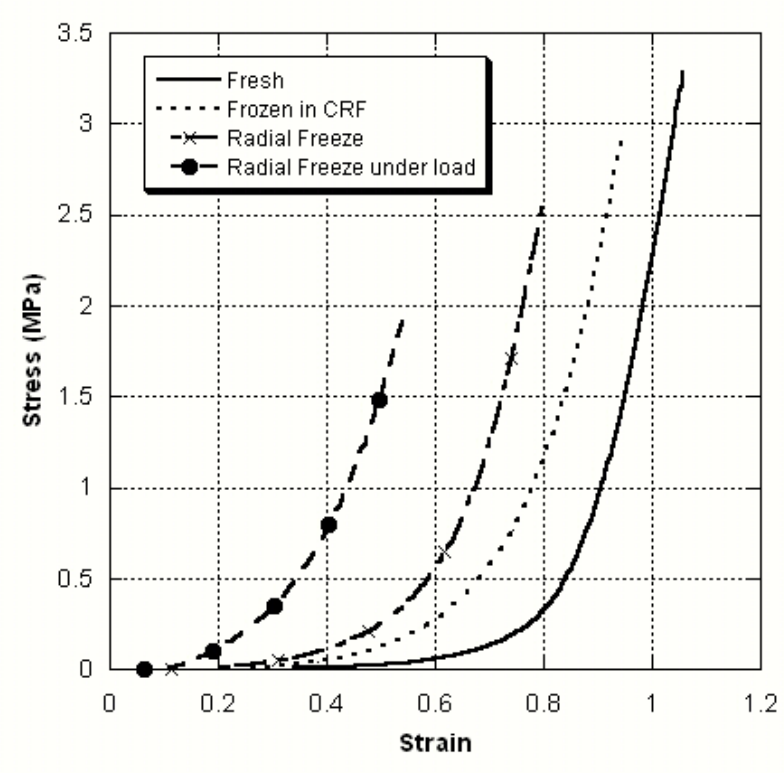

Figure 2.6 Stress-strain curves for fresh samples and samples frozen in radial direction with and without load.

2.4 DISCUSSION

2.4.1 Extension rate and preconditioning

The extension rate used for the current study was 2 mm/min (~ strain rate of 0.8% per sec). This rate is low compared to rates that have been previously used in the literature [42, 68, 69, 129] to study the mechanical response of native fresh and frozen tissues. This rate is also comparable with some of the rates that have been previously used [130, 131] in tissue equivalents. It has been previously shown [43] in soft tissues that there exists a range of rates where the extension rate doesn't not affect the mechanical response. It was therefore assumed that the chosen extension rate was sufficiently low to be in the range where the stress-strain curves of both the fresh and frozen tissues were independent of the extension rate. Preconditioning was performed to approximately a strain of 20% in both fresh and frozen tissues at the same extension rate that was used to stretch the samples. Preconditioning is a common practice [82, 130, 131] used to reduce variability in biomechanical measurements and is described elsewhere [60, 132]. It was again assumed that

the preconditioning sensitivity held true for frozen samples as in case of fresh tissue samples. However, it might be interesting to study the variation, if any, of the strain rate and preconditioning sensitivity in frozen samples.

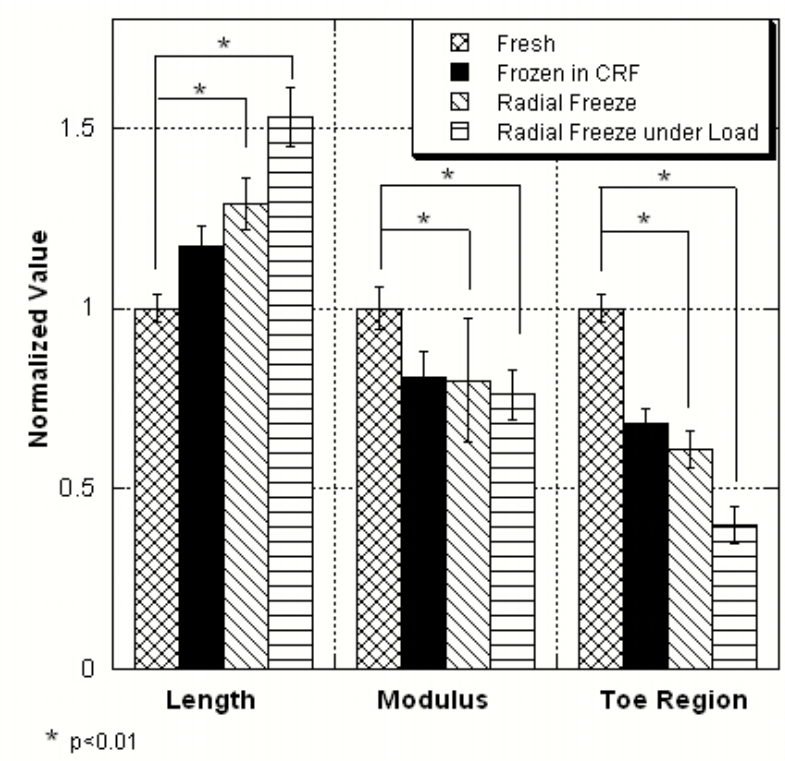

Figure 2.7 Comparison of normalized values of properties for fresh (n=13), samples frozen in CRF (n=10), samples frozen in radial direction with (n = 4) and without load (n=6).

2.4.2 Macroscopic and histological changes

The mechanism for the change in vessel length (L_o) after freezing is not clear from these studies. The formation of ice may cause changes in the structure, including changing the alignment of the fibers. In addition, the movement of water in and out of the tissue may have caused changes in the vessel microstructure and hence the dimensions. Damage to the ECM was not apparent from the histological sections. A clear understanding of these changes may require more in-depth examination, such as using birefringence techniques [133-135] or electron microscopy [136].

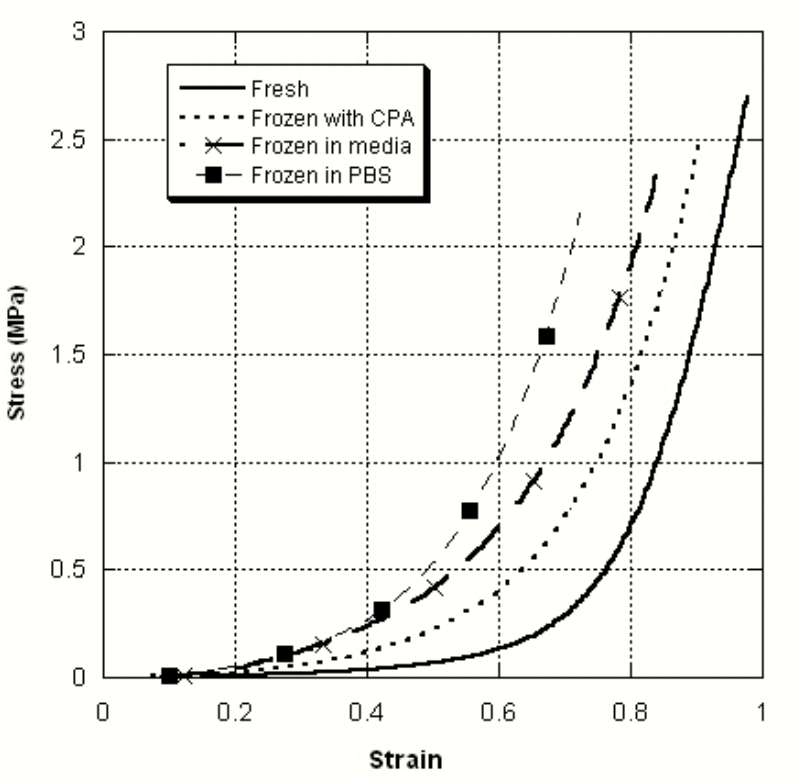

Figure 2.8 Stress-strain curves for fresh samples, samples frozen in PBS, samples frozen in media and samples frozen with CPA.

2.4.3 Differences in stress-strain curves for frozen arteries

Given the non-linearity of tissue mechanics and complexity of the arterial pressure waveform, caution must be taken in drawing general conclusions from this single strain rate study. The differences in the preconditioning loops (Fig. 2.3) as well as the stress-strain curves (Fig. 2.4) suggest that freezing may result in some changes in structure that are similar to the changes induced by preconditioning. This may be due to irreversible damage, such as breaking of crosslinks, or a change in alignment, increasing in the circumferential direction. The frozen samples start at a longer length and increase in stress more rapidly than the fresh tissue. This could mean that the fibers are already aligned and are engaged all at once, whereas in the fresh tissue the fibers are gradually pulled into alignment, resulting in a gradual increase in force as more fibers become aligned and engaged. The shift in the stress-strain curve could also be due to the change in L_0, which is a result of change in the tissue properties.

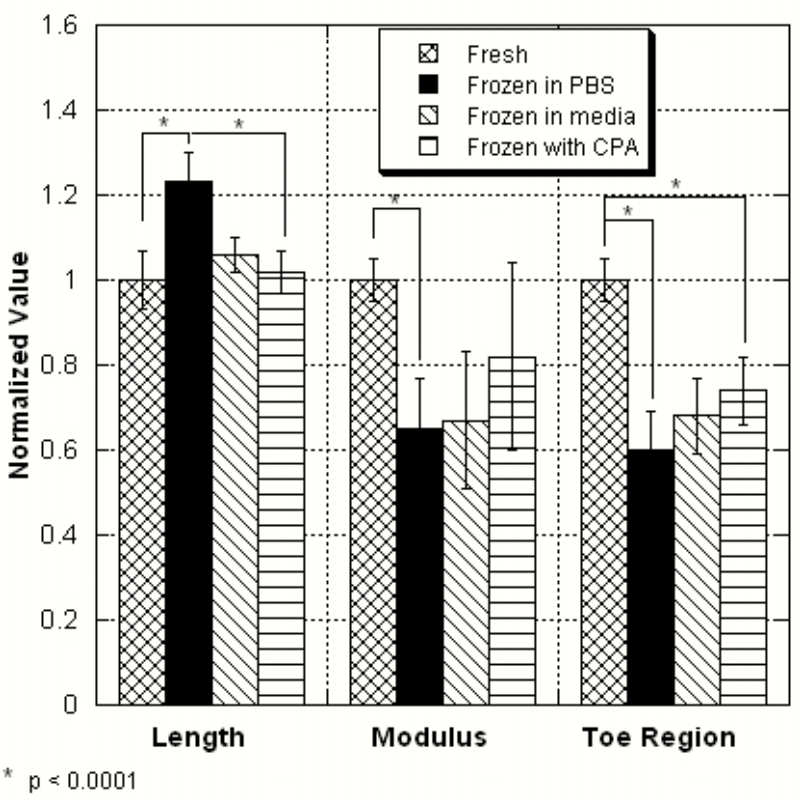

Figure 2.9 Comparison of normalized values of properties for fresh samples (n=13), samples frozen in PBS (n=8), samples frozen in media (n=6) and samples frozen with CPA (n=6).

Considerable reduction in weight in tissues following freeze/thaw indicates that there is a bulk water movement phenomena occurring during the freezing [82]. Moreover, we could assume that there is some amount of water movement into the tissues following 24 hours of incubation of the samples in media. The shift of the stress-strain curve towards fresh behavior after 24 hours of incubation in media post-freezing (Fig. 2.4) further emphasizes the water redistribution phenomena and its effect on the mechanical behavior of the arteries.

The structural and mechanical effects could also be the result of a lack of contribution from the smooth muscle. However, we found it difficult to separate the contribution of the ECM from the contribution of the smooth muscle from these experiments. The changes in length (L_o) and mechanical properties could be due to a loss in smooth muscle viability, damage to the ECM, or a combination of both. Future experiments should address the effect of freezing on matrix components independent of smooth muscle.

2.4.4 Freeze-thaw vs. cryopreservation

The differences seen between frozen-thawed and cryopreserved arteries may be a result of differences in the movement of water and ice formation. The frozen arteries most likely lost some water during the freeze-thaw process, whereas the cryopreserved arteries were more likely to retain water because of the CPA. This may explain why the frozen arteries exhibited an increase in length (L_o) and a change in the preconditioning behavior, while the cryopreserved arteries did not. Drastic reduction of weight in tissue samples frozen without CPA (or in media not containing serum) over samples frozen in the presence of CPA (or in a media containing serum) indicates the prevention of bulk water movement by CPA or serum. CPA or serum could be imagined to be media that prevents water movement out of the tissue, probably through hydrogen bonding [104]. A closer examination of the vessel structure following the freeze-thaw cycle is necessary to explain how the differences in water movement and ice formation may have changed the structure, and therefore the mechanical response.

2.4.5 Hemodynamic variations due to mechanical property changes

Following the changes in mechanical properties post freeze/thaw, it is important to understand the changes in hemodynamics caused by the changes in mechanical properties. The wave equation for the blood in arteries is obtained through

$$c = \sqrt{\frac{Eh}{2\rho a}} \tag{5}$$

assuming the flow to be pulsatile and arteries to be thin cylindrical tubes with elastic walls [38]. This yields the Moens-Korteweg equation

where

c is the wave speed of the blood flow

E is the Elastic modulus of the arterial wall

h is the arterial wall thickness

ρ is the density of blood

a is the internal radius of the artery

It was found that the wave speed increases in frozen samples (7.93m/s) when compared to fresh samples (5.43m/s). This is due to increase in the elastic modulus in the physiological region. The localized blood flow changes due to altered biomechanics of arteries from freezing can be compared to one during an insertion of vessel graft with different biomechanical properties than that of the native vessel [40]. Future work should be aimed at studying, in detail, the effects of changes in mechanical properties during freezing on the blood flow of arteries as localized differences in hemodynamic conditions, including change in velocity profiles and recirculation zones, make the region more prone to plaque formation [31, 137, 138]. Another interesting study would be to understand the effect on blood flow under damped conditions, which would be a more realistic model.

The biomechanical changes in the section of the artery where cryoplasty is performed, further cause variations in characteristic impedances, thereby resulting in reflection and alteration in the transmission of pulsatile flow [38]. These effects could also be seen during the use of vascular grafts, as their mechanical properties might be different from the recipient vessel properties. Changes in impedances results in energy being partially transmitted and reflected at the junction of treated and untreated arterial sections. Further, geometric variations viz. increase in length (L_o) of the treated arterial section could also bring about changes in the pulsatile blood flow. Future studies should be aimed at understanding these alterations thoroughly as they could result in chronic blood flow disorders.

2.4.6 Comparison to other work

As mentioned previously, most of the work looking at the effect of freezing on arterial tissue has been in the presence of CPA. The results have been mixed depending on the particular artery and test used. For example, in a pulsed flow loop experiment, Rosset et al. saw a change in the response of cryopreserved human common carotid artery (CCA) after freezing, but did not see a change in cryopreserved superficial femoral artery (SFA) [70]. Also, Pukacki et al. [69] measured the compliance and elastic modulus of DMSO cryopreserved iliofemoral arteries and compared them with fresh samples. They saw no changes in cryopreserved arteries. However, Blondel et al. did see a difference in

cryopreserved SFA subjected to inflation tests [67]. The main differences observed were in the measured strains and stresses, but not in the calculated elastic moduli or compliance values. These results are difficult to compare directly to our results since the type of test was different. However, Adham et al. [42] performed uniaxial tests similar to ours on cryopreserved thoracic aortas and they observed a decrease in the high stress modulus, as we did, but it was not statistically significant. They did not comment or report on differences in the shape of the stress-strain curve or on sample dimensions, so it is not possible to fully compare our results.

It is difficult to make any direct comparisons between our work with the frozen samples and work in the literature because the few studies of arteries frozen in the absence of CPA have not measured or reported the same properties as we have here. Schaar et al. [139] saw no changes in frozen samples stored at -80°C through intravascular elastography. Litwin et al. [68] studied the tensile behavior of canine aortic tissue after sterilization and preservation procedures, including deep freezing. They observed a difference in tensile strength with freezing (only in the thoracic region), but they did not comment on or report modulus or toe region data.

Studies of the effect of freezing on the mechanical behavior of other tissues have given mixed results as well. In a study of the effect of storage conditions on ligament mechanical behavior, Viidik and Lewin [62] did not see a variation in the gross shape of the load-elongation curve, failure load, or elongation at rupture after deep freezing, but did see a difference in the failure energy. Woo et al. [65] saw no significant difference in the failure energy of ligaments frozen at -20 ºC for 3 months, but did see a decrease in the area of hysteresis during cyclic testing in the frozen samples, similar to what we saw with the frozen arteries. Krag and Andreassen [140] saw changes in the mechanical behavior of lens capsule rings after freezing to -80 ºC. There was no significant difference in the reported ultimate stiffness (analogous to our reported linear modulus), but there was a difference in the elastic modulus calculated at low strains. This is similar to what we saw in the arteries, in that the differences were primarily in the low strain region. The mixed results given by these different tissues and studies may be the result of various factors including tissue composition and structure, freezing protocol, and the specific mechanical testing protocol used.

In a study of freezing artificial tissues, Devireddy et al. suggested the possibility of fiber alignment as the reason for decreased opacity during freezing [82, 141]. They also saw water movement in samples frozen in the absence of CPA. Our study extends this possibility further to native tissues. Our weight measurements before and after freezing suggest that water movement could be an important phenomenon that causes the changes in mechanical behavior. Water could be seen as a medium responsible for randomness in the orientation of the fibers and once the water moves out; the fibers realign themselves, thereby causing the observed changes in mechanical behavior.

2.5 SUMMARY

As biomechanical properties of arteries play an important role in hemodynamics, an attempt was made to quantify the biomechanical property changes in arteries following freeze-thaw treatments. Porcine arteries were subjected to two types of freeze-thaw treatments both in the presence and absence of CPA based of the two applications, cryoplasty and cryopreservation, respectively. The results from this study are summarized below:

i. Freeze-thaw in the absence of CPA does affect the mechanical properties of the porcine femoral arteries as measured from the uniaxial tensile response. Specifically, freezing caused a significant increase in length (L_o) and decrease in the toe region, with only a small change in linear modulus. However, freezing caused a significant increase in the average elastic modulus in the physiological regime.

ii. Cryopreservation, on the other hand, does not result in an increase in L_o, but does affect the toe region and linear modulus.

The exact mechanisms for these changes are not known; although some data suggests that changes in water content could be important underlying phenomena. Changes in the ECM and loss of smooth muscle viability could also play an important role. In chapter 2, the biomechanical changes induced by freeze-thaw as measured using an indentation technique that can capture localized mechanical properties compared to uniaxial tensile

testing is discussed. In chapters 3 and 4, the mechanisms underlying the freeze-thaw induced changes were investigated in detail.

Acknowledgements

The authors would like to thank Dr. James Coad of the Department of Pathology at West Virginia University for histological analysis. The authors would also like to thank Dr. Paul Iaizzo and Lynn Hartman from the Experimental surgical services (ESS) at the University of Minnesota for access to fresh pig tissue. The authors would also like to thank David Swanlund for technical assistance. Funding from Boston Scientific is gratefully acknowledged.

3 FREEZE-THAW INDUCED BIOMECHANICAL CHANGES IN ARTERIES –II: INDENTATION RESPONSE

This chapter describes the indentation tests performed to quantify the biomechanical changes in arteries due to freeze-thaw. The present author performed all the biomechanical experiments, data analysis, created and edited the manuscript for publication. The results from this chapter have been submitted as the following citation that is presently in review at the time of dissertation submission:

i. Venkatasubramanian, R.T., Simha, N.H., Tatsutani, K. and Bischof, J.C. (2008) "Effect of cryoplasty on mechanical properties of human and porcine arteries using indentation." *Cryobiology* (In review at the time of dissertation submission).

Abstract

This chapter describes the indentation experiments conducted to study the effect of freeze-thaw on localized biomechanical properties of arteries. Biomechanics of normal and diseased arteries, as well as changes in them following freeze-thaw, were measured using an indentation technique that provides localized information at the same time requiring only small tissue samples. Normal human arteries, obtained from an autopsy, were tested and their biomechanics compared with that of diseased human arteries, obtained from donors who underwent bypass surgeries. Due to reduced availability of normal human tissues, normal porcine arteries were also used to understand the freeze-thaw effect on normal arteries. It was observed that the diseased human artery response was approximately 6.2 times stiffer than that of normal human artery but normal porcine arteries were stiffer than both normal (~14 times) and diseased human arteries i.e. E_∞ (normal porcine) > E_∞ (diseased human) > E_∞ (normal human) where E_∞ is the equilibrium modulus. Following freeze-thaw, the diseased human arteries showed no significant change whereas the moduli of normal porcine arteries were found to increase significantly (~1.5-2.3 times). No significant changes were observed in the viscoelastic parameters (g, τ_1 and τ_2) of both normal porcine and diseased human arteries following freeze-thaw. As arterial stiffness increases following cryoplasty in normal arteries, alterations in hemodynamics are expected. Such alterations in hemodynamics have been reported in vascular grafts with a mechanical property mismatch and hypothesized as potential mechanism for downstream pathology. Finally, the results from the current study can provide bracketing behavior (i.e. elastic modulus of normal and diseased arteries as well as changes in them following cryoplasty) for emerging computational models that account for solid-fluid coupling at the artery wall to further investigate hemodynamics in a cryoplasty treated artery. Additionally, measurements from this study can form a baseline to which mechanical properties measured *in vivo* using elastography techniques, i.e., intravascular ultrasound (IVUS) elastography and optical coherence tomography (OCT) can be compared. This may ultimately help form the basis of a diagnosis with IVUS or OCT of disease or pathology within the artery.

3.1 INTRODUCTION

Atherosclerosis is a major health care problem in the United States. While there are more than 400,000 coronary angioplasties performed in the US about 30-40% of them result in restenosis or neointimal hyperplasia[5]. Cryoplasty is a recently developed minimally invasive approach used in the treatment of atherosclerosis; currently in peripheral arteries [18]. This approach involves opening of the narrowed arteries by simultaneously inflating and freezing a catheter guided balloon filled with liquid nitrous oxide. An important advantage of cryoplasty over conventional balloon angioplasty is its potential ability to restrict restenosis by inducing apoptosis [142, 143]. Previous clinical studies aimed at evaluating the midterm results of cryoplasty have shown that the treatment demonstrated a high degree of early angiographic success over a period of 9 months [18] and efforts are now being directed towards understanding the long term implications of the treatment.

Long term efficacy of cryoplasty is likely dependant on biomechanical changes induced during the treatment as biomechanical properties play an important role in the hemodynamics [38]. For example the most important consideration while developing a vascular graft to replace a diseased artery is to match the compliance (representative of the mechanical property) of the graft with that of the native vessel[144]. Compliance and other viscoelastic property mismatch in the arteries (due to addition of grafts) could alter the hemodynamic wall shear stress and ultimately result in pathological conditions including occlusion and/or intimal hyperplasia [144, 145]. Additionally, the stress distribution in the artery is responsible for proper functioning of the smooth muscle cells (SMCs) [40]. It is therefore important to quantify normal and diseased artery biomechanics both before and after cryoplasty. These biomechanical properties would could provide a bracketing behavior for emerging computational models[146, 147] that account for solid-fluid coupling at the artery wall and can be potentially used to further investigate hemodynamics in a cryoplasty treated artery.

Measurement of localized arterial mechanical response is important. Artery consists of three different layers namely intima (inner layer), media (middle layer) and adventitia (outer layer). Atherosclerosis is characterized by formation of plaque or fatty deposits on the intima. It also involves activation and proliferation of SMCs in the media

and their migration to the intima [1]. An atherosclerotic artery location primarily consists of diseased and remnant non-diseased sections along the axial and circumferential directions possibly resulting in variation in the local mechanical properties, i.e. E (r_{artery}, θ, z). Understanding the biomechanical response of a diseased artery completely therefore requires studying the localized mechanical response; which is not possible using conventional uniaxial or multiaxial tests. Localized *ex-vivo* measurements of normal and diseased artery biomechanics also form a baseline to which mechanical properties measured from *in-vivo* measurements such as intravascular ultrasound (IVUS) elastography or optical coherence tomography (OCT) can be compared to for detection of diseased state[54, 55].Finally, uniaxial and multiaxial tests require large tissue samples which are often difficult to obtain in human arteries suggesting the need for alternative techniques.

The current study involves measurement of normal (porcine, human) and diseased (human) artery biomechanics (modulus and viscoelastic relaxation parameters) both before and after freeze-thaw using a novel indentation technique that provides localized information at the same time requiring only small tissue samples. Mechanical property changes between normal and diseased arteries are reported along with their changes following freeze-thaw separately. Our results suggest that diseased human arteries are stiffer in their indentation response compared to the normal human arteries. Following cryoplasty, a stiffer indentation response is observed in normal porcine arteries while no significant differences are observed in diseased human arteries. The results from this study suggest that the mechanical behavior of cryoplasty treated artery section is similar to an inserted vascular graft with significantly high stiffness.

3.2 MATERIALS AND METHODS

3.2.1 Tissue Harvesting and Freezing Protocol

Normal porcine iliofemoral arteries (N = 4), sections of length 3-5 cms each, were obtained from domestic pigs used for other IACUC approved studies, in which the iliofemoral arteries were not directly involved. Normal or undiseased human iliac (from lower abdomen region) artery sections (N = 2) of length 3-4cms each were obtained

during an autopsy (of a 50 year old male) associated with other IRB approved studies at the University of Minnesota and it was visually confirmed that no atherosclerotic plaque was present in these samples. Finally, diseased human femoral artery sections (N = 4) of length 2-3 cms each, were obtained from undisclosed donors undergoing bypass surgery from the Veterans Affairs Medical Center, Minneapolis, MN. It should be noted that anatomically the femoral artery is only an extension of the iliac artery outside the abdomen region and the two arteries are often referred to as iliofemoral arteries due to their similarities[148]. The diseased arteries were completely occluded, as a result of which plaques were removed by the surgeon with minimal damage to the arterial wall following which artery sections were brought to the laboratory in physiological saline solution. All arteries were rinsed in 1X phosphate buffered saline (PBS) solution and were cleaned of any adipose tissue. For freeze-thaw treatment, the arteries were cut into ~1 cm long rings and were then frozen in a radial fashion inside out similar to cryoplasty. Freezing was performed by exposing the entire arterial ring to -20 ^{o}C for 120 s using an ethanol chilled tapered aluminum probe. Following freezing, the samples were passively thawed at room temperature and prepared for indentation. Artery wall thickness was measured by photographing the rings under 4X magnification, measuring them in pixels, and then converting them to mm ($\pm$0.01mm). Indentation of diseased arteries was performed in different artery samples with multiple locations within each sample.

3.2.2 Mechanical Testing

Indentation on normal porcine and diseased human arteries was performed using ElectroForce (ELF) 3100 (Bose Corporation, Eden Prairie, Minnesota, USA) as shown in Fig. 3.1a. Following freeze-thaw, artery rings were cut open and glued to the surface of a Petri dish with the lumen side on top. The Petri dish was then filled with phosphate buffered saline (PBS) and indentation was performed using a cylindrical indenter with a tip diameter of 2 mm on the luminal side as the arteries were frozen inside out and the biomechanical changes, if any, would be more prominent on the luminal side. The intimal and medial layers of the arteries would majorly govern the mechanical response in such a case. On the other hand, if the indentation were to be performed from the outside, the contributions from the adventitial layer may dominate. All arteries were subjected to a

two-step indentation protocol with each step consisting of a ramp at 2 mm/s to a depth of approximately 1/4th or 1/5th the arterial wall thickness (depth ~ 0.1-0.25 mm) followed by a hold of 300-500 s for stress relaxation.

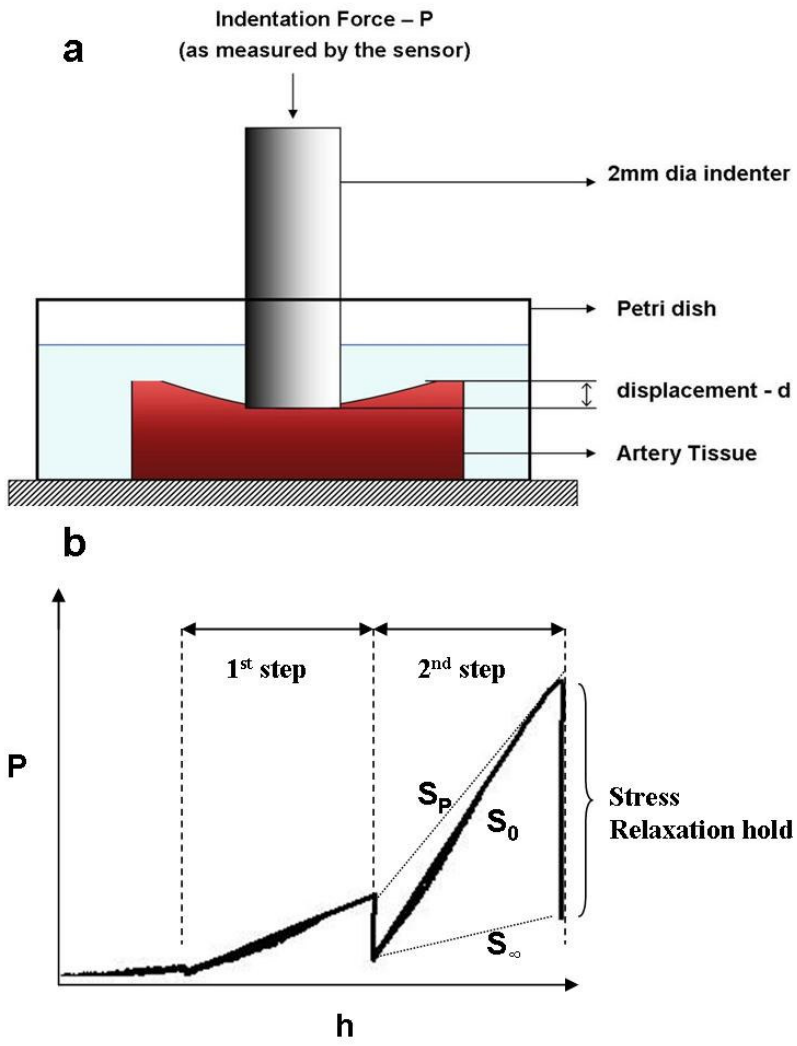

Figure 3.1 Mechanical testing in arteries using indentation: a) experimental set up (not to scale) b) Typical force-displacement curve. Peak (S_P), equilibrium (S_∞) and Initial (S_0) stiffness are the slopes of the lines shown.

Indentation was also performed on normal human arteries using Nanoindenter XP instrument (MTS Inc., Eden Prairie, Minnesota, USA) with a 1mm diameter cylindrical tip. Normal porcine arteries, also tested using the ELF system described above, were additionally tested using this method as a control between the two testing systems (ELF/Nanoindenter). The normal (measured using Nanoindenter) and diseased (measured using ELF) human artery response, normalized to normal porcine response from the respective systems, were then compared and reported (see results). The indentation protocol in the Nanoindenter also consisted of two steps; with each step consisting of a ramp at 10 mN/s to a depth of approximately 0.1mm followed by a hold of 400s. The artery thickness was directly determined by additionally indenting on the flat surface of the stage without the artery and comparing the displacements. The arteries were kept moist by keeping them immersed in 1X PBS solution during indentation.

3.2.3 Data Analysis

For indentation of an isotropic, homogenous, linear elastic layer bonded to a rigid surface by a cylindrical indenter, the indentation force P and stiffness S are related to the indentation depth h as [149] :

$$P = \frac{Ehb\kappa}{(1-\nu^2)} \tag{3.1}$$

$$S = \frac{dP}{dh} = \frac{Eb\kappa}{(1-\nu^2)} \tag{3.2}$$

where E is the Young's modulus, b the indenter tip diameter, ν the Poisson's ratio and $\kappa = \kappa\ (b/t,\ \nu)$ accounts for the finite layer thickness t. Equation 1 can be modified to obtain the relationship (Eqn. 3.2) between the stiffness $(S=dP/dh)$ and modulus (E). The peak (E_P), equilibrium (E_∞) and initial (E_0) moduli were used to characterize the mechanical response. The peak (S_P), equilibrium (S_∞) and initial stiffness (S_0) were initially calculated using the slopes of the indentation force-depth response (as shown in Fig. 3.1b) and the corresponding moduli were then calculated from Eqn. 3.2 with the artery

wall assumed to be incompressible at all times (i.e. ν = 0.5)[150]. While S_P and S_∞ were calculated from the difference in force levels obtained at the start and end of the stress relaxation holds respectively, S_0 was obtained from the ramp data of the second step. The ramp data for the relaxation hold in each sample was fit linearly such that $R^2 > 0.92$ and S_0 was thus obtained from its slope. For the indentation using the Nanoindenter system, only the S_∞ and the corresponding E_∞ were calculated as the maximum loading rate that could be achieved in this system was significantly lower than that compared to the rates in ELF and the peak or initial stiffness was not actually representative of the initial mechanical response of the arteries.

In addition to extracting the elastic modulus, viscoelastic relaxation response was quantified for tests performed on the ELF system using a three parameter relaxation model (Eqn. 3.3) as follows:

$$P(t) = P_0\left[1 - g\sum_{i=1}^{2}(1 - e^{t/\tau_i})\right] \tag{3.3}$$

where $P(t)$ and P_0 are the current and initial indentation force respectively; g the material parameter; τ_1 and τ_2 the time constants. The relaxation data was fit to the relaxation model using a nonlinear least-squares curve fitting technique using commercially available software (Kaleidagraph 3.5, Synergy Software, Reading, PA) and the viscoelastic parameters g, τ_1 and τ_2 extracted. The optimal fit for the viscoelastic relaxation was obtained by selecting the parameters such that the goodness of fit parameter (R^2) was always maximized. Due to some displacement that was observed during the hold steps in the Nanoindenter system (note the increase in indentation depth in Fig. 3.2a), the viscoelastic relaxation constant were not extracted for the tests performed in this system. Nevertheless, the equilibrium stiffness (S_∞) and modulus (E_∞) obtained from this system could still be extracted from these tests which were used to compare the normal vs. diseased human artery response.

3.2.4 Statistics

Data are given as the mean +/- standard deviation of mechanical behavior recorded for 'n' number of tests performed under each experimental group i.e. normal porcine: n = 4/6

(fresh/frozen-thawed), normal human: n = 5, diseased human: n = 8/9 (fresh/frozen-thawed). The total number of artery sections "N" obtained under each experimental group are: normal porcine (N = 4), normal human (N = 2) and diseased human (N = 4). Effects of freeze-thaw on normal porcine and diseased human arteries were normalized to their respective fresh response. The ratio of diseased human (measured using ELF) to normal human (measured using Nanoindenter) artery response, both normalized to normal porcine, were then to study the normal vs. diseased response. Two sample unequal variance (heteroscedastic) student t-tests were used for comparison between groups. Differences between groups were reported as statistically significant if $p \leq 0.05$.

3.3 RESULTS

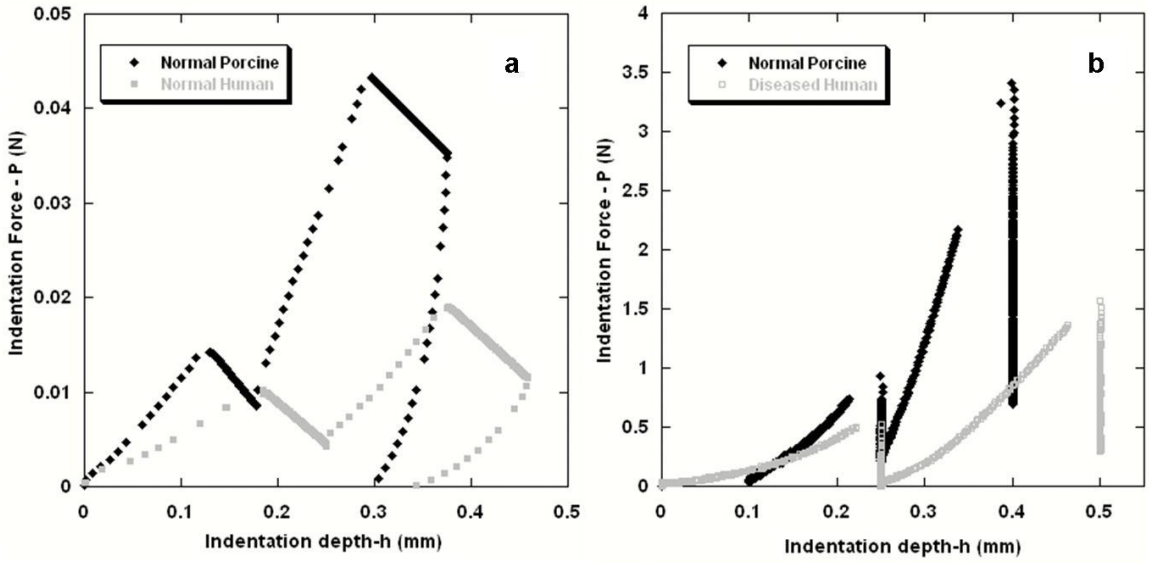

Figure 3.2 Representative indentation response of a) normal porcine vs. normal human and b) normal porcine vs. diseased human artery

3.3.1 Sample thickness

Sample thickness between normal human (1.55 ± 0.1 mm) and diseased human (1.02 ± 0.09 mm) arteries were compared and found to be statistically different ($p < 0.001$). Both normal and diseased human arteries were significantly thicker than normal porcine arteries (0.84 ± 0.09 mm). No statistically significant changes in thicknesses were

observed post freeze thaw in both normal porcine ($p = 0.46$) and human diseased arteries ($p = 0.29$).

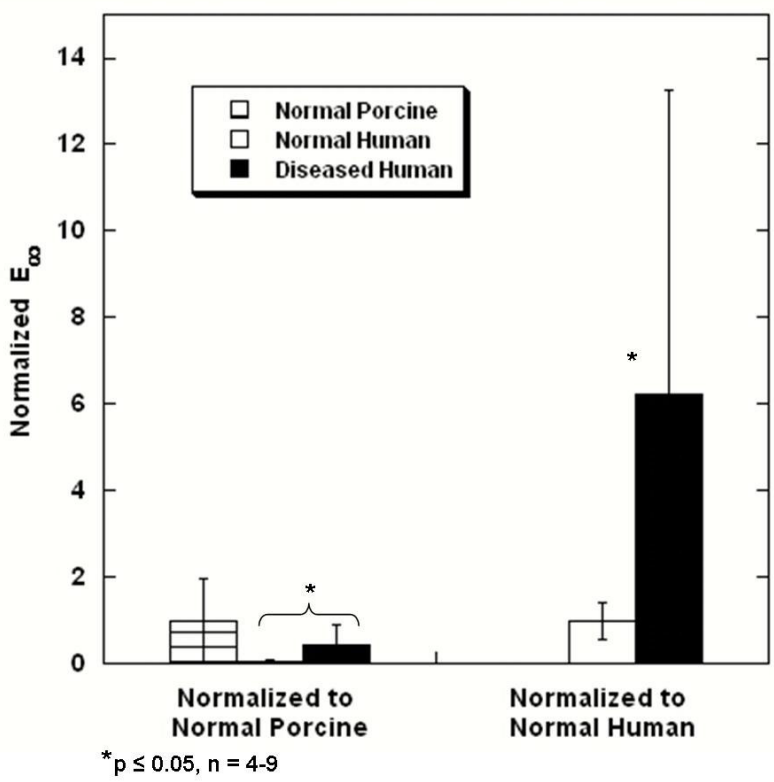

Figure 3.3 Indentation response of normal porcine, normal human and diseased human arteries: changes in equilibrium modulus (E_∞) normalized to normal porcine and normal human.

3.3.2 Normal vs. diseased response of human arteries

Diseased human arteries were found to be stiffer than the human arteries (Figs. 3.2a and 3.3). Figure 3.2 shows the representative force-displacement response for normal and diseased human arteries along with the normal porcine response in both ELF and Nanoindenter systems. Figure 3.3 shows the equilibrium moduli of normal and diseased human arteries normalized to that of normal porcine. It can be seen that both normal and diseased human arteries had a statistically lower equilibrium moduli (E_∞) compared to normal porcine arteries (Fig. 3.3). However, equilibrium modulus (E_∞) for the diseased human arteries was significantly higher than that of normal human as seen from Fig. 3.3.

The equilibrium modulus for the normal porcine, normal human and diseased human arteries were 132 ± 125 kPa, 8.9 ± 3.8 kPa and 55.1 ± 62.7 kPa respectively.

3.3.3 Fresh vs. frozen-thawed response

The overall indentation response following freeze-thaw was different for the normal, porcine and diseased human arteries. The indentation response of the normal porcine arteries following freeze-thaw was stiffer as seen in Fig. 3.4a. It can be clearly seen that freezing causes increase in different stiffness (S_P, S_∞ and S_0) as seen from the different slopes in the force-displacement response. Extending the incompressibility assumption[150] to frozen-thawed samples, i.e. $\nu = 0.5$, Eqn. 3.2 suggests that the modulus ratios of the fresh to frozen-thawed samples are the same as their stiffness ratios (i.e. $E_{frozen}/E_{fresh} = S_{frozen}/S_{fresh}$) as $\kappa\ (b/t,\ \nu)$ did not vary significantly[149]. Figure 3.5a summarizes the changes in peak, equilibrium and initial moduli (normalized to fresh) of normal porcine arteries following freeze-thaw. While peak (E_P) and equilibrium (E_∞) moduli of the frozen-thawed porcine samples were 2.3 ± 1.6 and 1.8 ± 0.6 times that of the fresh respectively, the initial modulus (E_0) was 1.6 ± 0.8 times that of fresh.

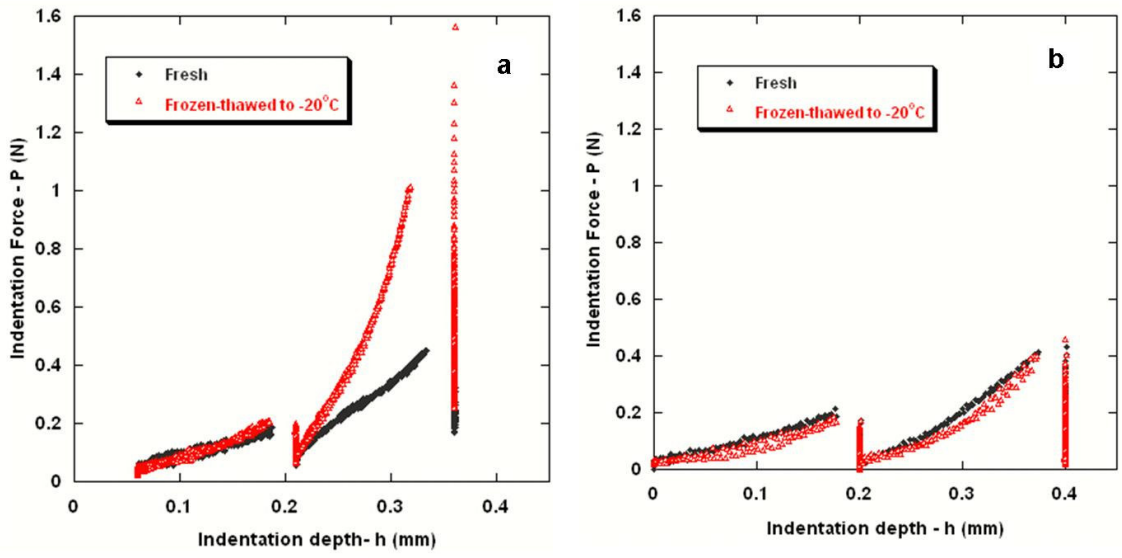

Figure 3.4 Representative indentation response of a) normal porcine and b) diseased human arteries before and after freeze-thaw.

In contrast to normal porcine arteries, no statistically significant changes were observed in the indentation response of the diseased human arteries following freeze-thaw (Figs. 3.4b and 3.5b). Additionally, the peak, equilibrium and initial moduli of both fresh and frozen-thawed arteries showed large standard deviations. While peak (E_P) and equilibrium (E_∞) moduli of the frozen-thawed human samples were 1.3 ± 1.1 and 1.1 ± 1.1 times that of the fresh respectively, the initial modulus (E_0) was 0.74 ± 0.31 times that of fresh.

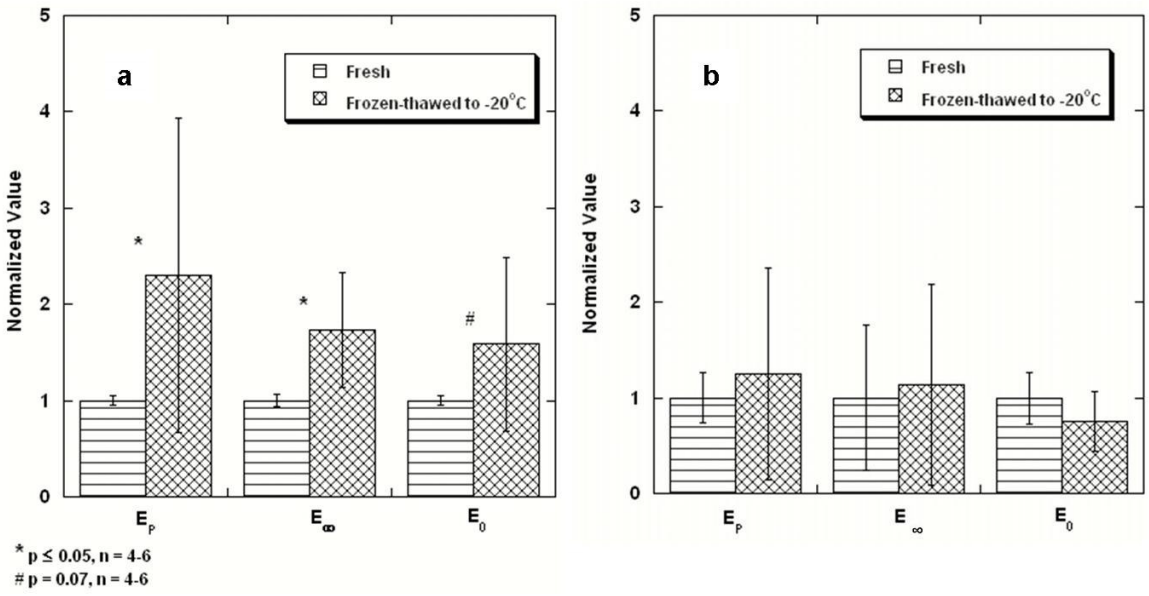

Figure 3.5 Changes in normalized peak (E_P), equilibrium (E_∞) and initial (E_0) moduli following freeze-thaw in a) normal porcine and b) diseased human arteries.

3.3.4 Changes to viscoelastic relaxation parameters

The relaxation data was fit to the three-parameter relaxation model and R^2 was used as a measure to indicate the goodness of fit (i.e. higher the R^2 better the fit). All curve fitting results presented have an R^2 value greater than or equal to 0.90, indicating good agreement between the experimental data points and the fit calculated using the estimated parameters. Table 3.1 gives the material parameter (g) and time constants (τ_1 and τ_2) for normal and diseased arteries before and after freeze-thaw. Figure 3.6 indicates the

viscoelastic relaxation profiles of the different cases as described by their respective average values of g, τ_1 and τ_2.

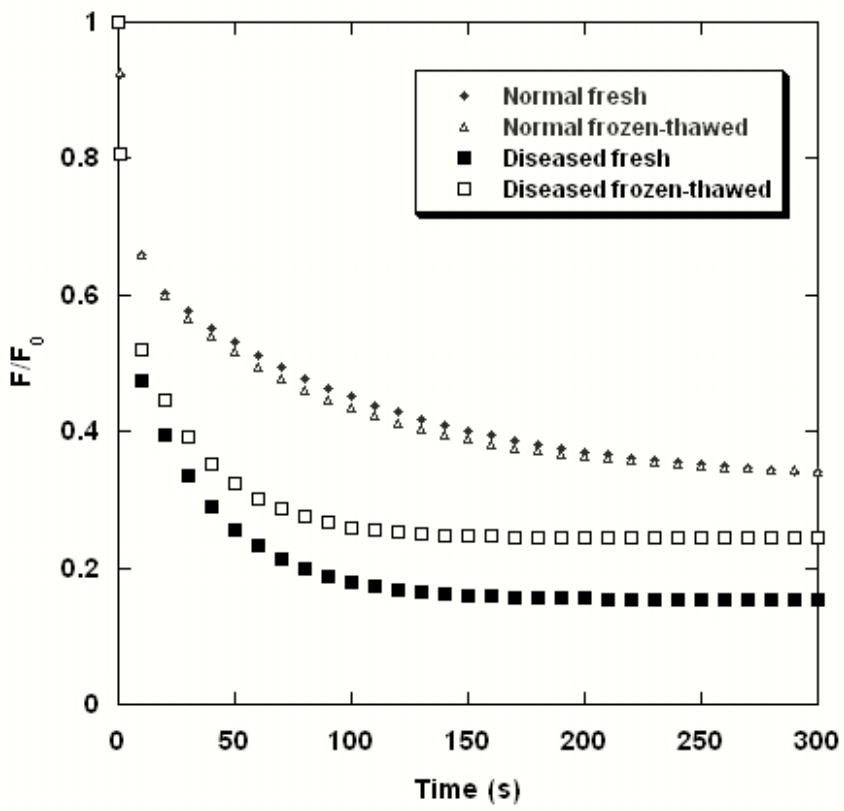

Figure 3.6 Viscoelastic relaxation of normal (porcine) and diseased (human) femoral arteries before and after freeze-thaw as described by the average values of g, τ_1 and τ_2.

There were no significant changes due to freeze-thaw on the viscoelastic relaxation profile of both normal porcine and diseased human arteries. It could be seen from Fig. 3.6 that the profiles of normal porcine arteries before and after freeze-thaw were similar. Statistical analysis of the fresh and frozen-thawed groups of the human diseased arteries indicated no significant differences between them although the profile described in Fig. 3.6 suggested some differences. This was probably due to the large standard deviations observed (see Table 3.1) in their g, τ_1 and τ_2 values.

3.4 DISCUSSION

3.4.1 Artery biomechanics and hemodynamics

Artery biomechanics plays an important role in hemodynamics [38] and therefore plays an important role in determining the long term efficacy of arterial treatments. In a study that involved determining the patency of cryopreserved saphenous veins as conduits for coronary artery bypass surgeries, Iaffaldano et. al. observed that nearly 94% of the grafts resulted in pathological conditions over a period of eight years [145]. Similar development of pathological conditions have also been observed in vascular grafts with biomechanical mismatch [144] due to the effect of artery biomechanics on hemodynamics. The Moens-Korteweg relation describes the how wave velocity during a pulsatile flow is affected by the elastic modulus of the artery ($c = \sqrt{\frac{Eh}{2\rho a}}$) where c is the wave velocity and E, the elastic modulus of the artery wall [38]. a, h and ρ are internal artery radius, artery wall thickness and density of the blood respectively. A close understanding of the hemodynamics in arteries therefore requires a model that accounts for the artery wall elasticity. However, due to the complexity of computationally studying solid-fluid coupling, most previous hemodynamics models did not account for artery wall elasticity [31, 151]. Recent advancements in the computational capabilities have allowed emerging models to begin to account for the arterial wall elasticity [146, 147]. The results from the current study can provide bracketing behavior (i.e. elastic modulus of normal and diseased arteries as well as changes in them following cryoplasty) for such emerging computational models[146, 147] that account for solid-fluid coupling at the artery wall to further investigate hemodynamics in a cryoplasty treated artery. It should however be noted that the artery is exposed to a tensile mechanical loading *in-vivo* that is different from the indentation response. A simpler approach to overcome this issue would be to come up with a correlation between the tensile and indentation properties of soft tissues, an approach that is often used in material composites [152, 153]. For instance, the physiological elastic modulus ($E_{uniaxial}$) of porcine arteries (fresh: 185±92 kPa and frozen-thawed: 506±159 kPa) measured using uniaxial tensile tests reported elsewhere [154] can be correlated to the equilibrium modulus ($E_{indentation}$) (fresh: 132±125 kPa and frozen-thawed: 322±309 kPa) reported in this indentation study.

3.4.1 Importance of local mechanical properties

Understanding the local mechanical response of the arteries both *in vivo* and *ex vivo* is important. *In vivo* techniques such as optical coherence tomography (OCT) and intravascular ultrasound (IVUS) elastography measure the local properties of arteries [54, 55]. These techniques typically measure the deformation of artery using ultrasound or OCT with the intraluminal pressure as the excitation force for calculating mechanical properties ($E= \Delta P/\Delta\varepsilon$ where P is the intraluminal pressure and ε the strain at the respective location measured using IVUS or OCT) at different arterial location[54]. The current study involving localized *ex-vivo* measurements of normal and diseased artery biomechanics can form a baseline to which mechanical properties measured *in vivo* using the elastography techniques[54, 55] can be compared to for detection of diseased state. Additionally, the local mechanical properties measured using these techniques could be applied in computational models[146, 147] to account for spatial variations in artery wall modulus particularly in diseased and treated arteries as discussed in the previous section. This provides a realistic approximation than using a single elastic modulus for the artery wall when the elastic modulus can vary spatially, i.e. $E (r_{artery}, z, \theta)$.

Artery type	g		τ_1 (s)		τ_2 (s)	
	Fresh	Frozen-Thawed	Fresh	Frozen-Thawed	Fresh	Frozen-Thawed
Normal (Porcine)	0.34 ± 0.06	0.33 ± 0.07	4.1 ± 2.4	4.2 ± 2.2	104 ± 60	84 ± 33
Diseased (Human)	0.42 ± 0.05	0.37 ± 0.09	1.8 ± 2.3	1.5 ± 1.0	36 ± 31	32 ± 21

Table 3.1 Viscoelastic relaxation parameters (g, τ_1 and τ_2) for porcine (n=4-6) and human femoral arteries (n=8) before and after freeze-thaw.

3.4.3 Normal vs. diseased artery response and freeze-thaw effect

Diseased human arteries are stiffer than normal arteries. In a study on coronary arteries, Van Popele et. al. reported that the arterial stiffness (without plaque removal) increased with the progression of atherosclerosis using a distensibility measurement system *in vivo*[155]. Our indentation study, that involved subjecting the artery to compression as

compared to tension in a distensibility measurement[155], also suggests that diseased human arteries (55.1 ± 62.7 kPa) have an equilibrium modulus approximately 6.2 times that of normal arteries (8.9 ± 3.8 kPa) (also see Fig. 3.3). Due to the difficulty in the procurement of normal human arteries, the normal artery behavior was characterized from a single donor in the current study. It should however be noted that there could be potential variation between donors especially when from different age groups. In the case of diseased arteries, the plaques were removed prior to performing cryoplasty in the current study. This was because the diseased arteries were completely occluded by plaque thereby preventing any cryoplasty to be performed in them. This was also the reason why the donors of the diseased arteries underwent bypass surgery as performing cryoplasty or angioplasty would be difficult in such cases. Nevertheless, investigating the response of the diseased artery without plaque is still useful to understand how tissue beneath the plaque, where presumably intimal hyperplasia[1] changes the biomechanical properties, responds to cryoplasty.

Normal and diseased arteries show varied response to cryoplasty. While normal arteries stiffen following cryoplasty, diseased arteries do not show any statistically significant change. It was observed that that all the three moduli (E_P, E_∞ and E_0) increase following cryoplasty in normal porcine arteries (Fig. 3.4a and 3.5a). Previously, Venkatasubramanian et. al. measured the non-linear uniaxial response of normal porcine arteries following radial freeze-thaw simulating cryoplasty and reported that freezing resulted in a stiffer mechanical response than control through a reduction in toe region[156] and an increase in physiological elastic modulus[154]. This trend agrees with our indentation results in normal porcine arteries. Care should however be taken before directly comparing the two results as these are different tests (compression vs. tensile) performed at different loading conditions. As the uniaxial tensile tests are representative of the equilibrium response due to the preconditioning and very low extension rate (2 mm/min) involved, only the equilibrium modulus (E_∞) obtained from the indentation study can be compared with the uniaxial response. Additionally, cutting open the rings during indentation removes the residual stresses and may indirectly affect the mechanical response. However, performing indentation on a tissue and extracting a modulus requires the tissue to be bonded to a rigid surface (not possible using a ring). The results in this

study involving diseased human arteries showed no statistically significant differences between the fresh and frozen-thawed samples (Fig. 3.4b and 3.5b). This could in part be due to the large standard deviations within each group. Such deviations could be due to the pathological conditions of the arteries involved. It should however be noted that these results only suggest that there are no significant biomechanical changes due to cryoplasty in diseased arteries. The primary objective of cryoplasty is destruction of smooth muscle cells which has been discussed in other studies[117, 143]. However, differential biomechanical response of normal vs. diseased arteries to cryoplasty may lead to treated arterial sections, consisting of mostly diseased (stiffer than normal) and some remnant non-diseased (stiffens following freeze-thaw) sections, with high stiffness compared to surrounding untreated normal sections. This condition is similar to insertion of a vascular graft with high stiffness and may result in chronic pathological conditions as observed following grafting [144, 145].

3.4.4 Mechanisms underlying freeze-thaw induced biomechanical changes

Controlling the mechanical property changes following freezing requires understanding the mechanism underlying these changes. The arrangement of extra-cellular matrix or ECM fibers is usually associated with the modulus of soft tissue[157]. Results from the current study suggest that freezing causes an increase in stiffness or modulus (Fig. 3.5a) in normal porcine arteries suggesting that freezing potentially causes matrix rearrangement. However, no significant in the viscoelastic properties (Table 3.1) were observed following freezing. Fluid (primarily water) flow within a soft tissue such as artery during loading is expected to play an important role in viscoelasticity[158]. Our indentation results suggest that freezing does not significantly alter the fluid flow within the matrix. However, Venkatasubramanian et al. reported that freezing resulted in almost 15% reduction in weight of the artery sample suggesting bulk water loss[156]. The possible explanation to this could be that water contributes very little to the overall viscoelasticity of the artery. Moreover, some studies in other collagenous tissues such has cartilage have shown that the collagen ECM has intrinsic viscoelasticity [159]. The results in this study suggest that such intrinsic viscoelastic effects contribute more towards the overall tissue viscoelasticity and that the water effects might not be significant. Nevertheless, water loss

following freeze-thaw could possibly re-arrange the ECM and thereby affect modulus of the arteries seen in both uniaxial and indentation results (Fig. 3.2a). Finally, as freezing of the arteries to -20^{o}C also causes SMC death, SMC contribution to the biomechanical response could also be a potential cause for the biomechanical changes. Future work should therefore be directed towards understanding the mechanisms (i.e. changes to ECM and SMCs) underlying the freeze-thaw induced biomechanical changes.

3.5 SUMMARY

This study measured the biomechanical changes in the localized response of normal (porcine, human) and diseased (human) iliofemoral arteries. The results from this study are summarized below:

i. Following freeze-thaw, the diseased human arteries showed no significant change whereas the moduli of normal porcine arteries increased significantly. No statistically significant changes in the viscoelastic relaxation parameters were observed post freeze-thaw in both normal porcine and diseased human arteries.

ii. It was observed that diseased human arteries had a significantly higher modulus compared to normal human arteries.

iii. The results from this study can provide bracketing behavior (i.e. elastic modulus of normal and diseased arteries as well as changes in them following cryoplasty) for emerging computational models that account for solid-fluid coupling at the artery wall to further investigate hemodynamics in a cryoplasty treated artery.

iv. Measurements from this study can form a baseline to which mechanical properties measured *in vivo* using the elastography techniques such as intravascular ultrasound (IVUS) elastography or optical coherence tomography (OCT) for detection of diseased state can be compared to.

The exact mechanisms for the impact of freeze-thaw on normal and diseased arteries are unknown and an improvement in the efficacy of treatments such as cryoplasty requires an investigation of the underlying mechanisms. In chapter 4, the role of collagen matrix and

SMCs, arguably the most important components of arteries, in the freeze-thaw induced biomechanical changes are investigated.

Acknowledgements

The authors are grateful to Dr. Steven Santilli from the VA medical center, Minneapolis, MN and Dr. Robert Sweet from the University of Minnesota for the help in obtaining human arteries. The authors would also like to thank Dr. Ravi Namani from Orthopaedic Surgery for his guidance during the indentation experiments. Grant from Boston Scientific and loan from Bose Corporation for ElectroForce 3100 indenter usage is acknowledged. Doctoral dissertation fellowship from the graduate school at the University of Minnesota is also acknowledged for funding.

4 MECHANISMS UNDERLYING FREEZE-THAW INDUCED BIOMECHANICAL CHANGES: ROLE OF COLLAGEN MATRIX AND SMOOTH MUSCLE CELLS

This chapter describes the studies performed to investigate the freeze-thaw effect on the arterial components (collagen, smooth muscle cells or SMCs) and subsequently the components' contribution to the overall artery biomechanics. The present author performed all the experiments and the data analysis. The histological analysis was carried out in collaboration with Dr. Schmechel of the Department of Lab Medicine and Pathology at University of Minnesota. Experiments on functional assessment of Smooth muscle cells were performed in collaboration with Dr. Paul Iaizzo of the Department of Surgery at the University of Minnesota. The results from this chapter have been submitted as the following citation that is presently in review at the time of dissertation submission:

i. Venkatasubramanian, R.T., Wolkers, W., Barocas, V.H., Lafontaine, D., Soule, C., Iaizzo, P., and Bischof, J.C. (2008) "Freeze-thaw induced biomechanical changes in arteries: Role of collagen matrix and smooth muscle cells." *Annals of Biomedical Engineering* (In review at the time of dissertation submission).

Abstract

This chapter describes the experiments that investigate the freeze-thaw effect on the arterial components (collagen, smooth muscle cells or SMCs), as well as the components' contribution to the overall artery biomechanics to ultimately understand the mechanisms underlying the biomechanical changes induced by freeze-thaw. It was observed that freeze-thaw of normal arteries caused significant tissue dehydration (15% weight reduction), a consequent increase in thermal stability of the collagen matrix (~6.4^{o}C increase in denaturation onset temperature), and SMC destruction (no contraction and relaxation response to norepinephrine (NE) or acetylcholine (AC) respectively). In addition to freeze-thaw, the arteries were also subjected to hyperthermia and osmotic treatments (0.05M, 0.1M and 0.2M mannitol) that preferentially altered either the smooth muscle cells (SMCs) or collagen matrix (hydration/stability) respectively. While hyperthermia treatment also caused complete SMC destruction, no tissue dehydration was observed. On the other hand, mannitol (0.2M) treatment significantly increased the thermal stability (~4.9^{o}C increase in denaturation onset) but did not change the SMC function. However, freeze-thaw, hyperthermia and 0.2M mannitol treatments all resulted in significant reduction in toe region. The toe region of the freeze-thaw, hyperthermia and 0.2M mannitol treated arteries normalized to their respective controls were 0.61 ± 0.14, 0.81 ± 0.05 and 0.73 ± 0.14 respectively with minimum toe region observed after freeze-thaw. These studies suggest that both increased thermal stability due to tissue dehydration, as well as SMC destruction occurring during freeze-thaw, are important mechanisms of the freeze-thaw induced biomechanical changes.

4.1 INTRODUCTION

Atherosclerosis is a major health care problem in the United States. For example, more than 400,000 coronary angioplasties are performed in the US every year, of which about 30-40% result in restenosis or neointimal hyperplasia [5]. In the last few years, the clinical use of freeze-thaw applications for treatment of atherosclerosis and the prevention of restenosis has increased significantly [18, 160-162]. Cryoplasty is a recently developed, minimally invasive technique used in the treatment of atherosclerosis that is currently being used clinically in peripheral arteries such as iliofemoral or popliteal arteries [18, 162]. This technique involves opening of the narrowed arteries by simultaneously inflating and freezing a catheter-guided balloon filled with liquid nitrous oxide. An alternative to *in vivo* therapies includes surgical replacement of the diseased artery with native [26, 160] or engineered arterial vessels [29, 82], which also requires efficient cryopreservation techniques to store and preserve the vascular grafts. In general, cryopreservation is defined as a technique where cells and/or small tissues are frozen in the presence of a chemical agent or cryoprotectant (CPA) so that subsequently following thawing, viable tissues can be recovered and used later for various purposes [26]. However, previous studies have shown that treatments such as cryoplasty and cryopreservation cause arterial stiffening [156]. Therefore, in order to further optimize these freeze-thaw techniques, the mechanism underlying the arterial stiffening that occurs post freeze-thaw must be carefully delineated, since artery biomechanics plays a significant role in hemodynamics [38].

The overall biomechanical response of an artery is governed by its structural components. Structurally, the artery wall is composed of the extracellular matrix (ECM) and several types of cells that are distributed into three layers: intima, media and adventitia. Collagen is the most important structural protein of the ECM, which also contains elastin, glucosaminoglycans, and other molecules [76]. Among the incorporated cells within an artery, smooth muscle cells (SMCs) are the predominant type which are located in the media or middle layer [76, 77]. In highly muscular arteries such as iliofemoral arteries, the collagen matrix and smooth muscle cells (SMCs) are the most important structural components [76, 77]. Hence, during treatments such as freeze-thaw, changes to these arterial components ultimately lead to the observed arterial stiffening [156]. In order to understand the mechanisms underlying these biomechanical changes, it is important to: a)

understand the changes to these components during freeze-thaw and b) understand the relative contribution of collagen matrix and SMCs to the overall artery biomechanics.

Most of the previous studies that have investigated the effects of freeze-thaw on arterial components, have primarily studied changes in cellular viability [117, 118]. These studies have often been carried out in model systems, whose behavior may differ from that of native vessels'. Additionally, very few published studies exist that look into the post-freeze-thaw changes in collagen matrix stability and/or structure [87]. Therefore, it is generally considered that more work is needed to understand both the component effects due to freeze-thaw, as well as the relative individual component contribution to the overall artery biomechanics.

The purpose of the current study was to investigate the component effects due to freeze-thaw as well as their effect on artery biomechanics and ultimately understand the mechanisms underlying freeze-thaw induced biomechanical changes. In addition to freeze-thaw, two additional treatments to preferentially alter collagen matrix (hydration/stability) or SMCs were employed. In the first treatment, designed to preferentially alter collagen matrix hydration/stability, the arteries were treated with various concentrations of a hyperosmotic agent, mannitol, which caused significant tissue dehydration or bulk water loss but minimally affected SMC function. The other treatment, designed to reduce SMC function without affecting the collagen matrix, involved subjecting the arteries to a hyperthermia; which reduced the SMC function but caused no tissue dehydration. Tissue dehydration (measured from net weight changes) was employed as an indicator of matrix stability, since dehydration affects the structural organization of the collagen fibers in the matrix, specifically, less interfibrillar water implies closer packing of the fibers. Changes in collagen matrix thermal stability were also directly measured, by assessing secondary protein structure using a novel Fourier Transform Infrared (FTIR) spectroscopy technique. Additionally, SMC function was assessed by measuring contraction and relaxation responses to norepinephrine (NE) and acetylcholine (AC), respectively. Finally, uniaxial tensile tests were performed to measure the change in overall artery biomechanics. Our results suggest that both collagen matrix and SMCs are important components whose alterations underlie the changes in overall artery biomechanics during freeze-thaw. Both tissue dehydration, and subsequent

increased thermal stability, of the collagen matrix, as well as SMC destruction observed during freeze-thaw, are important mechanisms of arterial stiffening.

4.2 MATERIALS AND METHODS

4.2.1 Tissue harvesting and sample preparation

Iliofemoral arteries were obtained from domestic pigs that had been sacrificed as part of other IACUC approved studies that did not involve modifications to either the iliac or femoral arteries. The methods for euthanasia were considered to have minimal effects of these isolated samples as we were able to record viable functional activities from prepared vascular rings (see below). The animals were approximately 3-9 months old, and weighed 40 to 85 kilograms. Artery sections were removed shortly after animal euthanasia (< ½ hour) and transported to the laboratory in 1X phosphate-buffered saline (PBS) solution. The dimensions of the artery sections were approximately; inner diameter: 3mm, thickness: 1mm and length: 5-8 cms. After rinsing in 1X PBS solution, the arteries were cleaned of any adipose tissue and cut into approximately 3 mm long rings. Artery rings were directly used for weight measurement tests and uniaxial tensile tests. For the FTIR studies, the rings were cut open and thin sections (~500 μm) were prepared by gently scrapping off tissue layers from the intimal (lumen) surface.

4.2.2 Thermal treatments

Freeze-thaw: Cryoplasty was simulated by freezing to -20^{o}C for 2 mins in the radial direction using an ethanol chilled tapered aluminum probe as previously described [156]. The arteries were then passively thawed at room temperature before being subjected to SMC contractility or FTIR testing.

Hyperthermia: Hyperthermic treatment consisted of heating the artery samples in PBS-filled microcentrifuge tubes immersed in a 43^{o}C water bath for 2 hours. This protocol was selected to produce complete SMC death [121]. After these thermal treatments, SMC contractility/relaxation and weight measurements were carried out so to study SMC functional changes and tissue dehydration.

	Name	Treatment		
		Media	Time	Temperature
Controls	Fresh	PBS	1-3 hours	20°C
	20°C	SMC	18 hours	20°C
	37°C	SMC	18 hours	37°C
	Muscle bath	Modified Krebs-Henseleit	18 hours (in the muscle bath)	37°C
	Cell death	PBS	18 hours	-196°C
Experimental Groups	Hyperthermia (Heat)	PBS	2 hours	43°C
	Mannitol (0.05M, 0.1M and 0.2M)	SMC	18 hours	20°C
	Freeze-thaw (F/T)	-	2 mins	-20°C

Table 4.1. List of controls, experimental groups and their respective treatments.

4.2.3 Osmotic (Mannitol) treatment

Osmotic treatments involved exposing the arterial rings to differing mannitol concentrations (0M mannitol control, 0.05M, 0.1M and 0.2M) in SMC media (described elsewhere [117]); the rings were incubated at 20°C (room temperature) for 18 hours with continuous shaking such that it caused significant dehydration in the arteries. Use of 20°C instead of 37°C allows for the irreversibly injured cells to manifest damage histologically, while uninjured cells appear histologically viable [127, 156, 163]. The concentrations were chosen such that osmotic stress on the cells did not induce SMC death. Following mannitol treatment, SMC contractility/relaxation, FTIR and uniaxial tests were performed to quantify changes in SMC function, collagen matrix stability and overall biomechanics respectively.

4.2.4 Weight measurement

The weights of the artery rings (n = 5 to 6) before and after the different treatments were measured (±0.1 mg), and bulk weight loss was assumed to be due to tissue dehydration. The artery rings were patted dry and any excessive water droplets remaining on the surface were wiped off before the weights were recorded. Changes in hydration ratio, i.e., the ratio of weights of the sample after to before treatment, normalized to respective controls (fresh and 20^{o}C, refer Table 4.1), were measured and reported.

4.2.5 FTIR procedure

Infrared absorption measurements were carried out with a Nicolet Magna 6700 Fourier transform infrared spectrometer (Thermo-Nicolet, Madison, WI, USA). The following acquisition parameters were used: 4 cm^{-1} resolution, 32 co-added interferograms, and 4000-900 cm^{-1} wavenumber range. Omnic software (Thermo-Nicolet, Madison, WI, USA) was used for spectral data analyses and display. All studies were performed on thin arterial samples in a temperature controlled transmission cell. The samples were sandwiched between two CaF_2 windows and hydration maintained with 1X PBS solution. The windows were separated by a mylar spacer (Thermo Electron North America Inc., Madison, WI, USA). Silicon grease was applied at the edges of the CaF_2 windows to prevent dehydration of the sample during heating. The temperature was regulated by a temperature controller (Minco Products Inc., Minneapolis, MN, USA). The temperature dependence of the FTIR spectra was studied by heating the sample from 20˚C to 90˚C at a rate of approximately 2˚C min^{-1}.

Protein secondary structure analysis and heat-induced protein denaturation studies were performed by analyzing the amide-III (1320-1180 cm^{-1}) absorption band of the protein backbones [97, 98]. The amide-I and -II bands, typically used for protein analyses, were too distorted to analyze, due to the thickness of the sample. The less intense amide-III band, however, could be used and showed shape changes upon denaturation. Specifically, the increase in random coil and β-turn structures between 20^{o}C to 90^{o}C were quantified by studying the increase in area of the difference spectra in the 1285 to 1235 cm^{-1} region [97, 98]. The difference spectrum at a given temperature is calculated by subtracting the absorption spectrum at 20^{o}C from the spectrum at that temperature. Lines were then fitted to the difference spectra area vs. temperature between 40-75^{o}C, and the

denaturation onset temperature was calculated from the intersection of these lines as shown in Fig. 4.2b.

4.2.6 Measurement of SMC contractilities and relaxations (functional assessment)

The artery segments were mounted between two horizontal steel wires within a water jacket muscle organ bath (40 ml volume), which has previously been used to study vascular rings or skeletal muscle force responses; the absolute tensions were continuously recorded by force transducers [113, 164]. The chambers were filled with a modified Krebs-Henseleit bathing medium [113] gassed with 95% O_2 and 5% CO_2. While SMC contractility was measured by studying the response to 10^{-6}M norepinephrine (NE), endothelial-cell-dependent SMC relaxation was induced by exposure to 10^{-6}M acetylcholine (AC), respectively [114]. This protocol was a slight modification of that used by Bateson and Pegg [114] : here it consisted of two initial 15 minute equilibration periods followed by a 2 to 3 hour final equilibration, all in K-H solution. The pre-load forces were all set to 2g at the beginning of each equilibration period. Following equilibration, the artery rings were exposed to NE until the force had plateaued (~10mins) and the peak determined, after which they were exposed to AC for 20mins.

Three additional control SMC studies were performed: in addition to assessing responses of fresh and 20^{o}C controls (Table 4.1). These included the following: (1) treatment with SMC media at 37^{o}C (37^{o}C control), so to account for any temperature effects between 37^{o}C and 20^{o}C; (2) treatment with liquid nitrogen for 18 hours (cell death control), to study the relative responses after complete SMC death; and (3) maintaining the arterial rings in the muscle bath (muscle bath control), so to account for differences that may have been induced on the artery rings due to removal of the rings from muscle bath (e.g., for thermal or osmotic treatments) and their remounting.

SMC contractility and relaxation were measured by recording the relative vessel ring forces at the end of the final equilibration period (F_i), the peak force upon NE addition (F_e) and the resultant force after AC treatment (F_{AC}). Typically, in previous studies SMC contractility has been only assessed by quantifying the relative increases in force ($F_e - F_i$) upon NE additions[114]. Here we also assessed the changes in τ, a time

constant that indicates the time taken for the contraction force to plateau upon NE addition; i.e., τ was determined from equation 4.1 as follows:

$$F(t) = F_i + (F_e - F_i)(1 - e^{-\frac{t}{\tau}}) \quad (4.1)$$

where *F (t)* is the force measured at any time *t* during NE treatment, such that t = 0 when NE is added. Similarly, vessel relaxation was quantified by measuring the decrease in force following the addition of AC; i.e., $F_e - F_{AC}$. The relative changes in force and time constant i.e., $(F_e - F_{i)}$, $(F_e - F_{AC})$ and τ, were all normalized to fresh controls.

4.2.7 Uniaxial Tensile Testing

Post-treatment uniaxial tensile testing was carried out within 2 hours to study the overall artery biomechanics. This procedure has been described in detail previously [156]. Briefly, the artery was initially stretched until a load of 0.05 N is detected, and the corresponding length L_o measured. The artery rings were then preconditioned to a strain of 25% (~1 mm) for 9 cycles at an extension rate of 2 mm/min, followed by uniaxially stretching to a load of 5 N. The biomechanical response of the artery, described by the true stress vs. true strain response, was quantified using toe region and linear modulus as previously mentioned [156]. Additionally, the physiological elastic modulus of the artery (E_{artery}) after different treatments was calculated and compared. The physiological elastic modulus of the artery (E_{artery}) was defined as the slope of the linear fit between the engineering stress *($P= F(t)/A_0$)* and Green strain *(ε)* in the physiological regime. The physiological regime was defined between an engineering stress of 40 kPa and 120 kPa [165]. The Green strain *(ε)* is related to the stretch ratio *($\lambda = L(t)/L_0$)* such that $\varepsilon = 0.5(\lambda^2 - 1)$ [166]. A_0, L_0, *F (t)* and *L (t)* are the initial cross section area, initial length, current force and current length displacement at time *t*.

4.2.8 Controls and experimental groups

The entire study protocol consisted of investigations on 5 controls and 3 experimental groups as described in Table 4.1. All controls groups (except the one employed as immediately fresh) were maintained for 18 hours in their respective media and prescribed

temperatures; the fresh control samples were maintained in PBS at 20°C for approximately 1 to 3 hours. The 20°C and 37°C controls were maintained in the SMC media at their respective temperatures and this comparison was performed to account for differences that may arise due to the use of 37°C over 20°C. The cell death control was maintained in PBS at -196°C and was used to compare the relative SMC destruction or loss of SMC function that may have occurred in the experimental groups. A muscle bath control was also employed in which samples were maintained in the modified Krebs-Henseleit solution, at 37°C, in the muscle baths with continuous gassing; the goal here was to account for differences due to removal and remounting of arterial rings from the muscle bath. While the mannitol treatment effect was quantified by normalizing the response to 20°C control, the freeze-thaw and hyperthermic effect was quantified by normalizing the responses post-treatment to fresh control.

4.2.9 Statistics and Curve-fitting

All data were presented as the mean +/- standard deviation, with sample sizes provided (ranging from n = 3 to n = 11). Samples obtained from contralateral vessel segments were utilized as independent samples in our statistical analyses. Student's t-tests with equal variance were performed for comparison between groups, and differences between groups were reported as statistically significant if $p \leq 0.05$. Additionally, the obtained SMC contractility data was subsequently fit to equation 4.1 using a nonlinear least-squares curve fitting technique using a commercially available software (Kaleidagraph 3.5), from which the contractility time constant, τ, was extracted. The optimal fit for the time constant was obtained such that the goodness of fit parameter (R^2) was always greater than 0.90. Physiological elastic modulus was obtained from the slope of the linear fit between the engineering stress and Green strain, again such that R^2 was always greater than 0.90.

4.3 RESULTS

In order to understand the mechanisms underlying freeze-thaw induced biomechanical changes, arteries were subjected to thermal (freeze-thaw and hyperthermic) and osmotic

treatments to differentially alter the arteries' components. Changes to collagen matrix (hydration ratio, length and thermal stability) and SMCs (contractility and histology), as well as overall biomechanical changes, were measured and reported.

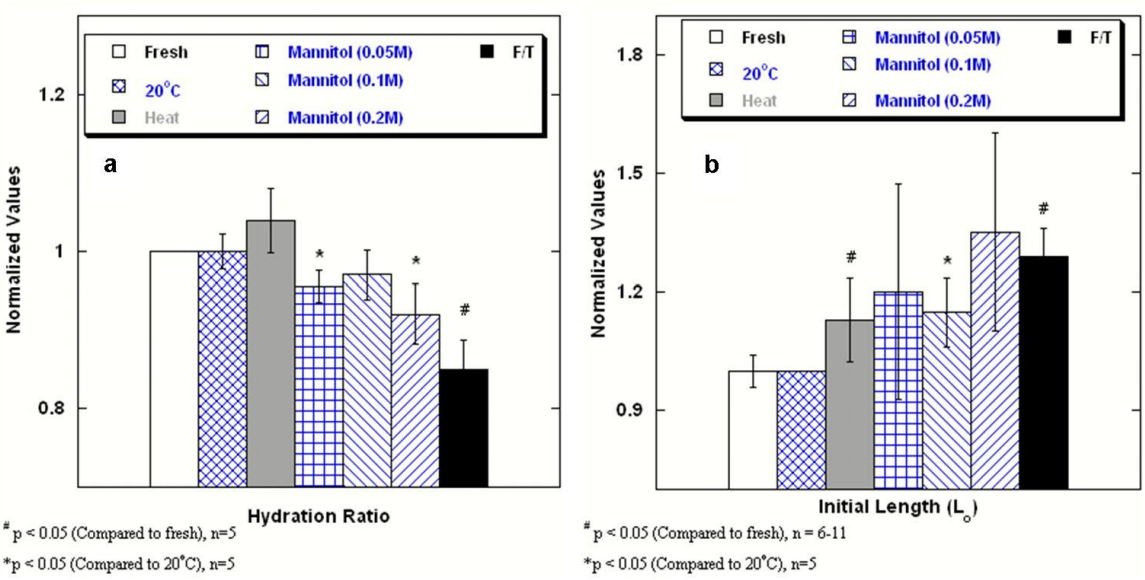

Figure 4.1 Weight and structural changes in arteries post freeze-thaw, hyperthermia and mannitol treatments (0.05M, 0.1M and 0.2M): changes in a) hydration ratio and b) initial length L_0.

4.3.1 Changes in weight and structure

Mannitol treatment, like freeze-thaw, induced significant dehydration in the artery samples (Fig. 4.1a). Statistically significant weight reductions were observed post-freeze-thaw [156] as well as post mannitol treatments. The normalized hydration ratio of the freeze-thaw and mannitol treated arteries were 0.85 ± 0.06 (freeze-thaw) [156] and 0.94 ± 0.03 (0.05M), 0.92 ± 0.10 (0.1M), 0.88 ± 0.07 (0.2M), respectively. Only the 0.05M and 0.2M mannitol groups were statistically significantly different than their respective controls (fresh and 20°C). Hyperthermic treatment, on the other hand, did not alter the weight significantly (Fig. 4.1a).

In addition to weight changes, significant structural changes, as shown by an increase in L_o following all treatments, were observed (Fig. 4.1b). The L_o (normalized to

control) following freeze-thaw, hyperthermia, 0.1M and 0.2M mannitol treatments were 1.29 ± 0.07 [156], 1.13 ± 0.11, 1.14 ± 0.09 and 1.35± 0.25, respectively.

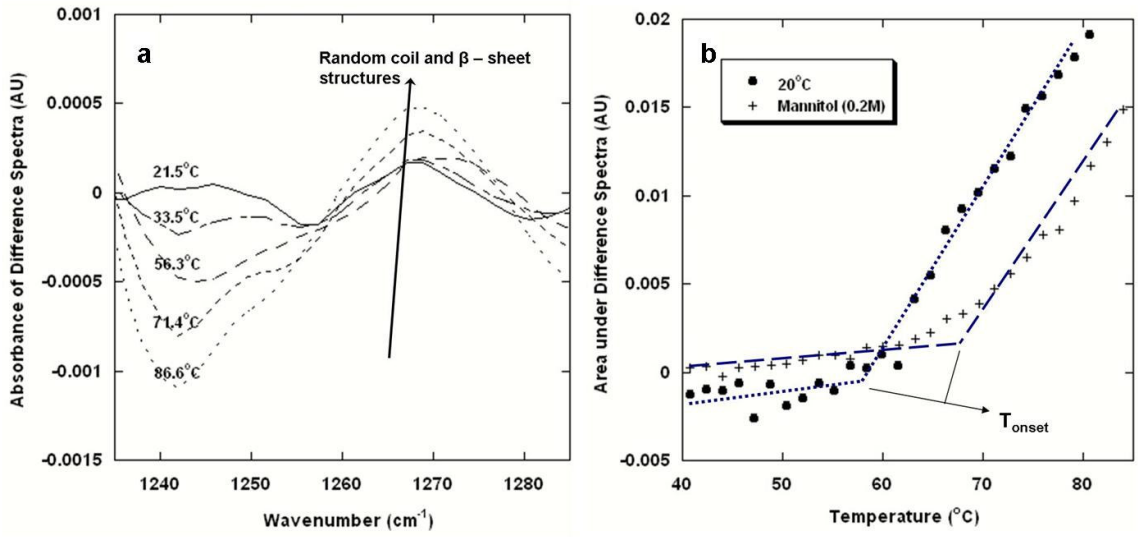

Figure 4.2 Fourier Transform Infra-red (FTIR) analysis of thermal stability of collagen matrix. a) FTIR difference spectra of artery sample (mannitol control) at different temperatures in the amide-III protein band. b) Changes in peak area under the difference spectra in 20oC control and mannitol (0.2M) treated artery samples. The sudden increase in area around 60°C-70°C represents onset of thermal denaturation of collagen.

4.3.2 Changes in thermal stability of collagen matrix

Thermal stability of the collagen matrix was assessed by studying changes in the amide-III protein band within the FTIR spectra during denaturation. Figure 4.2a shows the difference spectra, which is obtained by subtracting the initial spectrum at 20°C from the actual spectrum, for an artery sample. It can be observed from Fig. 4.2a that the area of the difference spectra between 1285-1235 cm^{-1}, which is characteristic of primarily random coil and β- turn structures [97, 98], increased with temperature. This increase in the difference spectra area indicates the increase in random coil and β- turn structures during thermal denaturation and was used to determine the onset of thermal denaturation. Figure 4.2b shows a plot of the area under the difference spectra as a function of temperature. For all artery samples, the area abruptly increased between 55 to 68°C, reflecting the onset of collagen denaturation (Fig. 4.2b), and continued to increase with temperature.

The denaturation onset was then used to assess the thermal stability of the matrix after different treatments.

The thermal stability of the collagen matrix increased after both freeze-thaw and mannitol treatments (Fig. 4.2b and Table 4.2). Statistically significant increases in the denaturation onset temperature were observed following both freeze-thaw (63.4± 4.1°C) and 0.2M mannitol (61.8 ± 3.5°C) treatments compared to their respective controls [fresh (57.0± 3.0°C) and 20°C (56.9 ± 2.4°C)]. Table 4.2 summarizes the denaturation onset temperature of arteries following control (fresh and 20°C), freeze-thaw and mannitol treatments.

	Name	Denaturation Onset Temperature (°C)
Controls	Fresh	57.0± 3.0
	20°C	56.9 ± 2.4
Experimental Groups	Mannitol (0.1M)	58.5 ± 1.6
	Mannitol (0.2M)	61.8 ± 3.5*
	F/T	63.4 ± 4.1#

# $p < 0.05$ (Compared to fresh), n = 4-5
* $p < 0.05$ (Compared to 20°C), n = 5

Table 4.2 Denaturation onset temperature as measured using FTIR in control, mannitol and freeze-thaw treated artery samples.

4.3.3 SMC contractility and relaxation

Changes in SMC function following different treatments were assessed by studying the pharmacological contraction and relaxation responses. Figure 4.3a shows a representative contractility/relaxation response for fresh and treated arteries. In the control responses (fresh and 20°C), it was observed that NE addition resulted in significant SMC contractions; AC on the other hand, caused endothelial-cell-dependent relaxation and, therefore, induced decreases in tension. It should be noted that occasionally the AC treatment caused either no response or a brief contraction (~2 min), after which the arteries then relaxed over the next 20 minute time period; such behaviors were considered

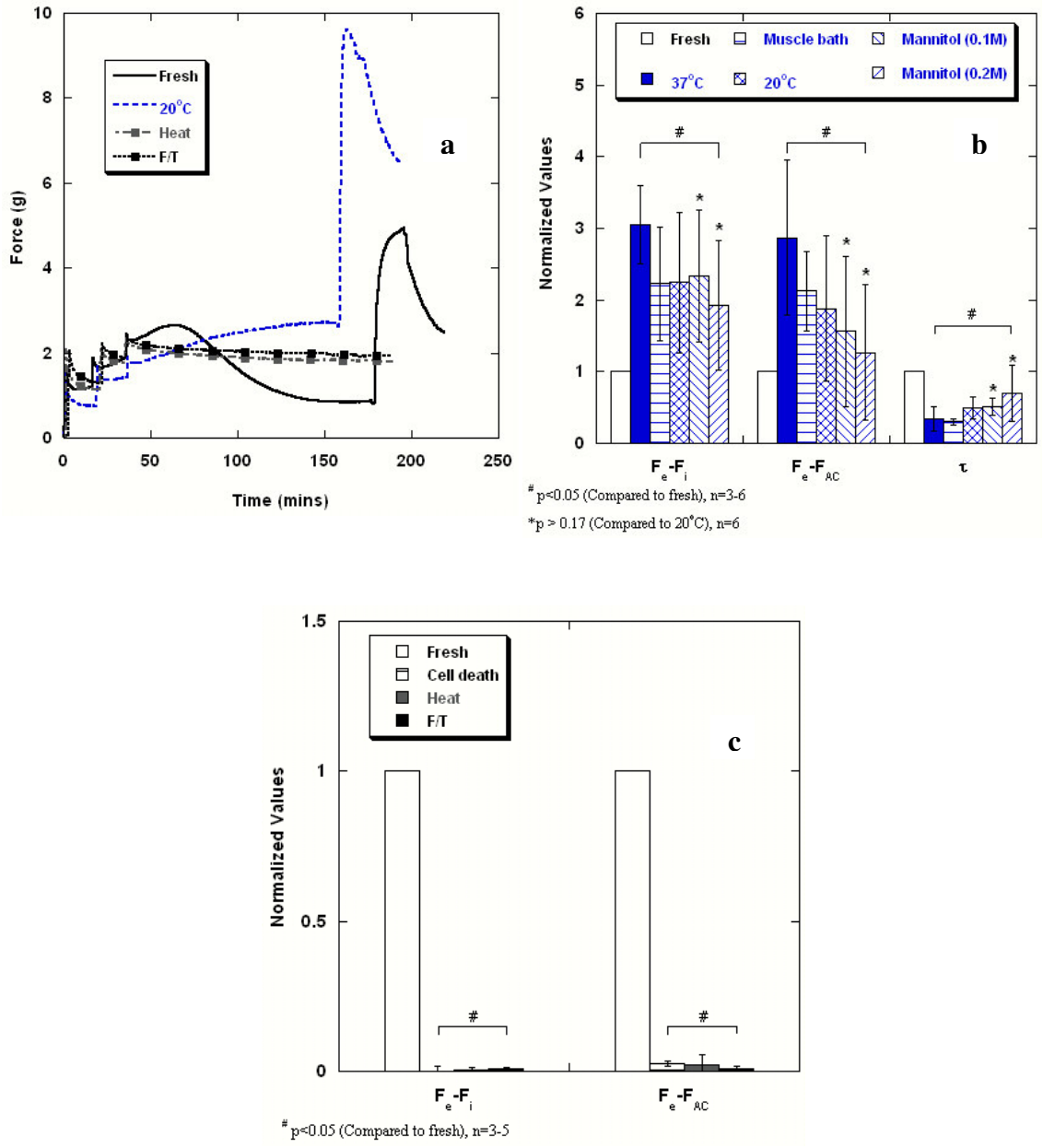

Figure 4.3 SMC contractility and relaxation response: a) representative force-time response, b) changes in normalized (F_e-F_i), (F_e-F_{AC}) and τ in control and mannitol treated arteries and c) changes in normalized (F_e-F_i) and (F_e-F_{AC}) in cell death control, hyperthermia and freeze-thaw treated arteries.

to be possibly due to endothelial cell damage. Nevertheless, no contractile or relaxation responses were observed in the vessel groups defined as cell death control, frozen-thawed, or hyperthermia treated arteries (Fig. 4.3a, b). Using Eqn. 4.1 as described above, the contraction and relaxation responses and changes in the SMC function were then

assessed by quantifying the ($F_e - F_i$), ($F_e - F_{AC}$) and τ (normalized to fresh control) for different treatments (Fig. 4.3b, c).

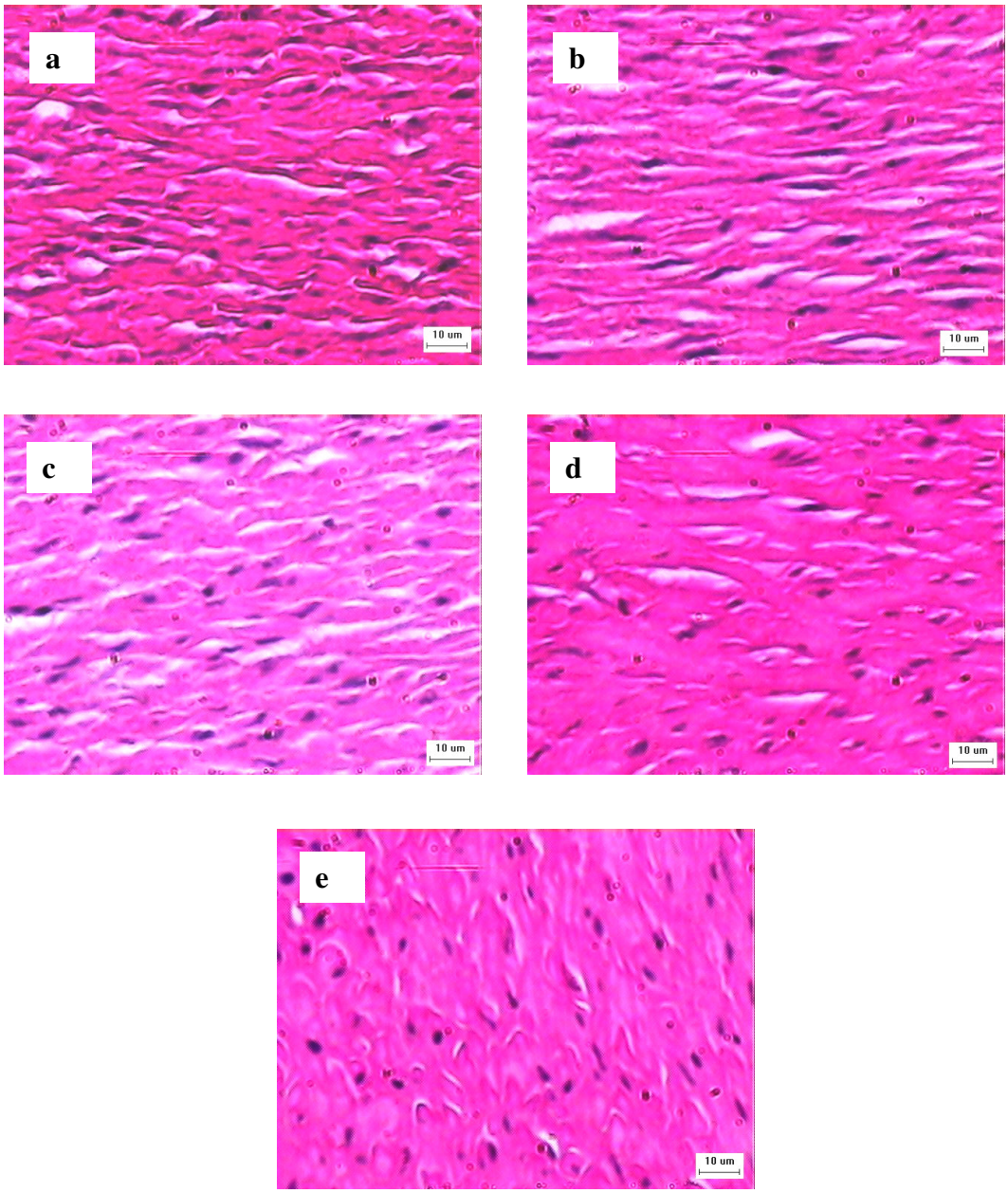

Figure 4.4 Hematoxylin and eosin stained section of fresh control (a), mannitol control (b) and mannitol treated arteries - 0.05M (c), 0.1M (d) and 0.2M (e) under 40X magnification.

Significant reduction in SMC functions were observed following freeze-thaw and hyperthermia treatments, but not after the mannitol exposure (Fig. 4.3a, b). Specifically, in the freeze-thaw and hyperthermia treated arterial rings, the typical contraction and relaxation responses were absent. As a result, normalized ($F_e - F_i$) and ($F_e - F_{AC}$) for these treatments were approximately zero, and therefore τ did not apply (Fig. 4.3a, b). In the mannitol treated arteries, the normalized ($F_e - F_i$), ($F_e - F_{AC}$) and τ did not change significantly compared to their matched controls (20^oC group). Further, there were no statistically significant differences in ($F_e - F_i$), ($F_e - F_{AC}$) and τ between the 20^oC, 37^oC and muscle bath control groups (Fig. 4.3c). However, significant increases in ($F_e - F_i$) and ($F_e - F_{AC}$) and a reduction in τ were observed after mannitol treatment, as well as in certain controls (20^oC, 37^oC, muscle bath) when compared to fresh control group (Fig. 4.3c).

4.3.4 Histology

In addition to SMC contractility and relaxation assessments, histological analyses were performed and they revealed no clear signs of any SMC injury in the control (20^oC) or mannitol treated groups (Fig. 4.4). This was considered to support the functional assessments, although a reduction in the cell size was visible with increasing mannitol concentrations (from 0.05M to 0.2M) (Fig. 4.4). Specifically, while the cell nuclei appears elongated in fresh and 20^oC control cells, the nuclei were apparently smaller in the 0.2M mannitol treated samples (Fig. 4.4a-e).

4.3.5 Artery Biomechanics

The overall biomechanical response assessments showed that the artery stiffened following freeze-thaw [156], hyperthermia and/or mannitol treatments compared to their respective controls (Fig. 4.5 and 6, refer Table 4.1 for different controls). Figure 4.5a shows the true stress vs. true strain responses in the circumferential direction for both control (fresh and 20^oC) and treated arteries. These responses were clearly nonlinear, with a distinct toe and linear regions. Freeze-thaw [156], mannitol (0.1M and 0.2M) and hyperthermia treatments all caused significant reductions in the toe regions compared to their controls (Fig. 4.5a, b). The normalized toe regions for the freeze-thaw,

hyperthermia, 0.1M and 0.2M mannitol treated arteries reduced to 0.61 ± 0.14 [156], 0.81 ± 0.05, 0.84 ± 0.07 and 0.73 ± 0.14, respectively (Fig. 4.5b). No statistically significant changes were observed in the moduli for these isolated arteries following any treatments except for freeze-thaw [156] and 0.05M mannitol treatments (Fig. 4.5b); both of which showed a reduction in the modulus.

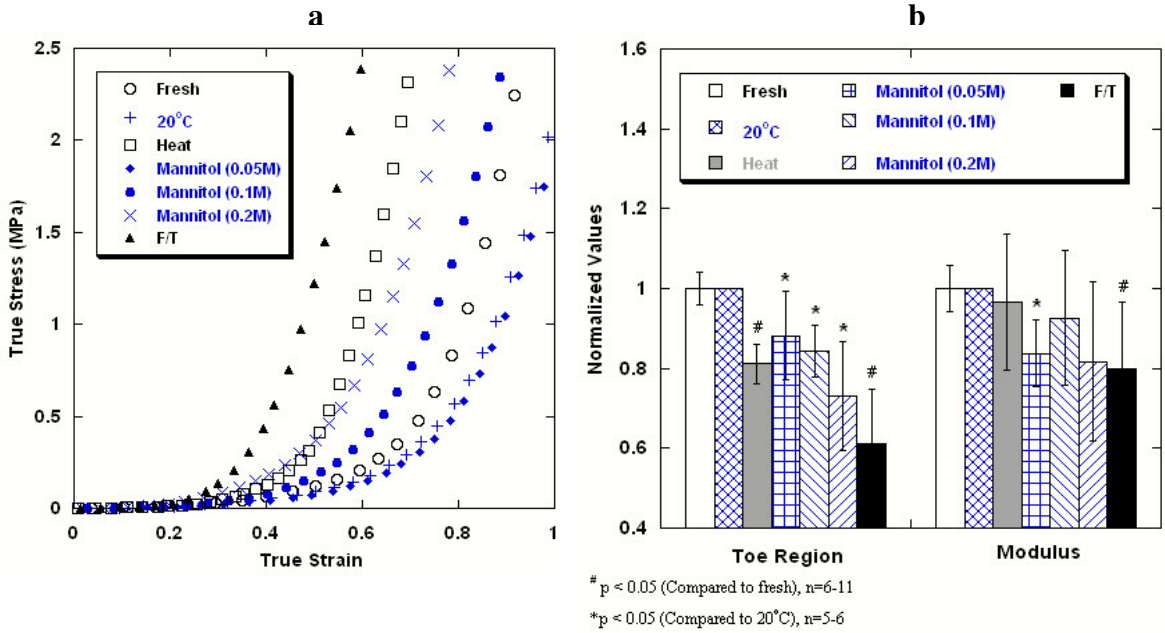

Figure 4.5 Overall artery biomechanics of fresh control, mannitol control and other treated artery samples: a) representative mechanical response (i.e. true stress vs. true strain curve) and b) normalized changes in toe region and modulus.

In the physiological regime, freeze-thaw (506±159 kPa), hyperthermia (268±132 kPa) and 0.2M mannitol (304±125 kPa) treatments all induced significant increases in the physiological elastic moduli (E_{artery}) compared to the fresh controls (185±92 kPa) (Fig. 4.6). Intragroup comparisons further showed that the freeze-thaw treatment caused a statistically higher E_{artery} than hyperthermia or mannitol treated arteries. In addition, for arterial rings subjected to a decellularization protocol (686±85 kPa) as described elsewhere [167], the resultant E_{artery} were significantly higher than even those derived for the frozen-thawed arteries (Fig. 4.6). The decellularized arteries are considered as an extreme case to better explain the mechanisms; to be described later in the paper.

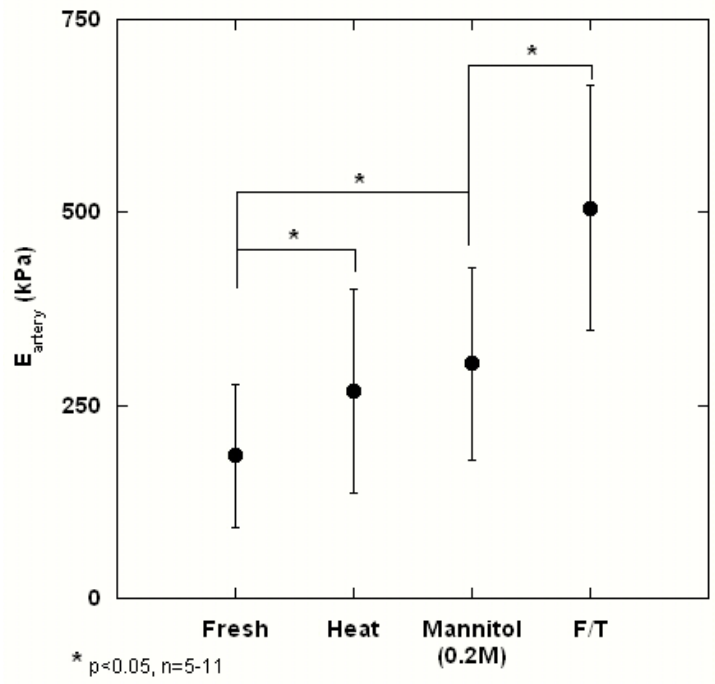

Figure 4.6 Physiological elastic modulus (Eartery) of artery post different treatments. E_{artery} is obtained from the slope of engineering stress vs. Green strain response (see text).

4.4 DISCUSSION

Understanding the mechanisms underlying freeze-thaw induced biomechanical changes requires examination of component alterations due to freeze-thaw, as well as the components' effects on artery biomechanics. In the current study, freeze-thaw induced component alterations (i.e., SMC function and collagen matrix stability) were directly studied by measuring the SMC contraction/relaxation responses (Fig. 4.3a, c), and by assessing onset of collagen denaturation by FTIR (Fig. 4.2a, b and Table 4.2). Additionally, two treatments (hyperthermia and mannitol treatment, refer to Table 4.1) designed to preferentially alter either the collagen matrix or SMCs were performed to better identify the individual component contributions to overall artery biomechanics. Treating the samples with mannitol caused significant tissue dehydration, or bulk water loss, and increased collagen matrix thermal stability (Fig. 4.1a) but maintained the SMC function (Figs. 4.3, 4.4). In contrast, hyperthermic treatment reduced the SMC function significantly (Fig. 4.3), but caused no tissue dehydration (Fig. 4.1a).

4.4.1 Freeze-thaw induced effects on artery components

SMCs and collagen matrix form the most important components of an arterial wall [76]. As the overall arterial biomechanical response is governed by these components, changes to them during treatments such as freeze-thaw need to be quantified. Previous studies involving freeze-thaw therapies have reported that cryoplasty causes significant reduction in SMC viability [117, 118] that varies depending on different treatment parameters (cooling rate, end temperature, etc.). While these studies offer good preliminary insights, they have been carried out in model systems (*in-vitro* monolayer, fibrin gel [117, 118] or tissue equivalents [118]), whose responses to freeze-thaw may differ from the native vessel behavior. In the current study, SMC function was assessed by studying the contraction and relaxation response of the SMCs within native arteries. We observed that radial freeze-thaw at -20^{o}C for 2mins, simulating cryoplasty, caused almost complete SMC destruction (Fig. 4.3a, b); a notable result similar to the effects reported for other model systems [117, 118].

In addition to SMCs, collagen matrix is another important component of the artery, therefore any collagen matrix changes due to freeze-thaw need to be understood. In a previous study, it was reported that freeze-thaw treatments such as cryoplasty resulted in tissue dehydration (bulk water loss) in arteries (Fig. 4.1a). In another study involving an artificial tissue scaffold, Miller reported that the freeze-thaw resulted in dehydration[87]. Additionally, using scanning electron microscopy (SEM), Miller reported that freeze-thaw to an end temperature of -20^{o}C resulted in structural changes in the tissue scaffold. Following freeze-thaw, the fibers were thicker, farther apart and displayed some bunching[87]. The current study also suggest that freeze-thaw induced dehydration increases the thermal stability of the collagen matrix (Fig. 4.2b, Table 4.2) which perhaps is due to structural changes in the collagen matrix leading to increased interactions that ultimately cause an increased thermal stability. The effect of dehydration on the thermal stability of the collagen matrix is discussed in detail in the following section.

4.4.2 Collagen matrix: Dehydration and its effect on thermal stability

The main structural element of connective tissues, such as tendon, ligament, cornea, skin and blood vessels, is collagen [80]. Hierarchically, the collagen matrix is built with a triple

helical tropocollagen molecule into micro-fibril, which assembles to form a fibril, which in turn form fibers [80]. The stability of a given collagen matrix determines the mechanical and thermal loads that this matrix can tolerate. Therefore, the ability to quantify matrix changes is needed for optimization of treatments involving both heating (thermal keratoplasty, skin re-surfacing, tissue welding, etc. [119]) and/or freezing (cryoplasty, cryopreservation).

The thermal stability of a collagen matrix has been typically measured by studying the kinetics of thermal denaturation that occurs during heating to 55^{o}C to 75^{o}C. During denaturation, hydrogen bonds that stabilize the triple helical structure are broken and the molecule irreversibly unfolds from an organized helical- to a random-coil or β-sheet structure. In the current study, a novel method based on the amide-III protein band of artery FTIR spectra was used to quantify the increase in random coil and β-sheet structures during collagen denaturation (Fig. 4.4). Note that arterial collagen, similar to collagen found in other tissues [83, 103], denatured between 55^{o}C to 65^{o}C (Fig. 4.2b, Table 4.2).

In general, the dehydration of an artery results in increased thermal stability of the collagen matrix; specifically, dehydration (Fig. 4.1a) due to either freeze-thaw or mannitol treatments cause an increase in the onset temperature of denaturation (Fig. 4.2b, Table 4.2). It is considered that such increases are likely due to increased inter-fibrillar interactions in the collagen matrix, which has more closely packed fibers after dehydration [86]. For example, in a rat tail tendon study by Miles et. al, the denaturation temperature following dehydration was shown to increase significantly [86]. In that study, Differential Scanning Calorimetry (DSC) was used to measure the thermal denaturation of collagen in rat tail tendon samples, which had been dried by exposure to air to vary the volume fraction of water in the tissue samples. Similarly, our freeze-thaw and mannitol treatments produced dehydration of the arteries, with a subsequent increase in the thermal denaturation onset temperature (Fig. 4.2b and Table 4.2).

An increase in the thermal stability of the collagen matrix can also be explained by changes in the activation Gibbs free energy for denaturation [168]. The increase in activation Gibbs free energy due to the addition of mannitol has been explained by Meng et. al. [169]. Specifically, the presence of mannitol molecules increases the free energy of

the protein due to an increase in net unfavorable solvophobic interactions between the sugar and protein molecules [169]. Such unfavorable interactions also reduce the effective hydration of the protein molecule [169]. The increase in the free energy of the protein is greater in the transition state, when protein begins to unfold, than in the folded or native state, due to increased solvophobic interactions in the former. The increased free energy of the protein ultimately causes an increase in the net activation Gibbs free energy (ΔG_S^*) of denaturation in the presence of sugar molecules, given by:

$$\Delta G_S^* = \Delta G_0^* + (g_T - g_N) \tag{4.2}$$

where g_T and g_N are the increases in Gibbs free energy due to the addition of sugar in the transition and native states, respectively ($g_T > g_N$).

4.4.3 Role of arterial components in freeze-thaw induced biomechanical changes

The current study investigated the relative roles of the collagen matrix and SMCs in the freeze-thaw induced biomechanical changes. To accomplish this, two treatments: a) mannitol and b) hyperthermia were employed to modify preferentially either the collagen matrix or SMCs, respectively. Changes in thermal stability of the collagen matrix and SMC function were measured along with the overall biomechanical changes to provide insights into the mechanisms.

Both increased collagen matrix stability following dehydration and SMC destruction during freeze-thaw are considered important mechanisms responsible for the observed overall biomechanical changes. Mannitol treatments caused significant tissue dehydrations (Fig. 4.1a) and increased thermal stability of the collagen matrix (Fig. 4.2b, Table 4.2), but did not result in SMC destruction or loss of their function (Fig. 4.3b). However, the overall biomechanical response of mannitol-treated arteries showed a statistically significant reduction in the toe region (Fig. 4.5a, b) compared to control (20^oC). Similar effects were also observed following freeze-thaw (Figs. 4.1, 4.5 and Table 4.2), suggesting that tissue dehydration, and the consequent increase in collagen matrix stability, is an important mechanism underlying the freeze-thaw induced biomechanical changes. SMC destruction or loss of SMC function is another important

mechanism responsible for the observed biomechanical changes. Interestingly, imposed hyperthermia caused complete SMC death (Fig. 4.3a, 3b) with no tissue dehydration (Fig. 4.1a), which nevertheless resulted in a statistically significant lower toe region compared to control (fresh), similar to freeze-thaw results (Fig. 4.5a, b). Further, although freeze-thaw and 0.2M mannitol treatments both caused comparable tissue dehydrations ($p = 0.26$) and thermal stability increases ($p=0.27$) (Fig. 4.1a, Table 4.2), freeze-thaw resulted in a significantly lower toe region ($p = 0.04$) and higher physiological elastic modulus E_{artery} ($p = 0.02$) compared to 0.2M mannitol treatment (Fig. 4.5a, b). Similarly, although freeze-thaw and hyperthermia both caused complete SMC destruction (Fig. 4.3a-c), freeze-thaw resulted in a significantly lower toe region ($p = 0.002$) and an higher physiological elastic modulus E_{artery} ($p = 0.006$) compared to hyperthermia. These results suggest that both increased collagen matrix stability due to tissue dehydration, and SMC destruction are important mechanisms in freeze-thaw induced biomechanical changes in arteries.

4.5 SUMMARY

In this chapter, the freeze-thaw induced overall biomechanical changes observed in arteries were decomposed into collagen matrix and SMC component effects to probe the underlying mechanisms. This required investigation of the freeze-thaw effect on the arterial components, as well as the components' contribution to the overall artery biomechanics. To accomplish this, arteries were subjected to thermal and osmotic treatments that preferentially altered either the collagen matrix or smooth muscle cells (SMCs), respectively. The results from this study are summarized as follows:

i. Freeze-thaw caused significant tissue dehydration and, consequently, an increased thermal stability of the collagen matrix as well as complete SMC destruction. The exact mechanism at the molecular level of dehydration induced increased thermal stability of collagen is still unclear and needs more work.

ii. While hyperthermia treatment also caused complete SMC destruction, no tissue dehydration was observed. On the other hand, mannitol (0.2M)

treatment significantly increased the thermal stability but caused no change in SMC function. Both hyperthermia and mannitol (0.2M) treatments, however, caused significant toe region reduction compared to control similar to freeze-thaw effect.

iii. Arteries stiffened, as observed by reduced toe region and increase physiological elastic modulus (E_{artery}), following freeze-thaw, hyperthermia and 0.2M mannitol treatment with maximum stiffening observed following freeze-thaw.

iv. These studies suggest that both increased thermal stability due to tissue dehydration, as well as SMC destruction occurring during freeze-thaw, are important mechanisms of the freeze-thaw induced biomechanical changes.

More work is needed to understand the molecular level changes during dehydration that ultimately lead to increased thermal stability of collagen. In order to further investigate this, thermal stability of a single tropocollagen molecule and its changes in a dehydrated condition were studied using molecular dynamics simulations as described in chapter 5. Future work should also be directed towards understanding the structural changes (at the level of fibers/fibril) in the collagen matrix using scanning/transmission electron microscopy or similar techniques.

Acknowledgement

The authors would like to thank Dr. Schmechel for the histological analysis. The authors would also like to thank the Experimental surgical services (ESS) and the Visible Heart laboratory at the University of Minnesota for access to fresh pig arteries. The authors would also like to thank Dr. Alptekin Aksan for the numerous discussions during the course of the study as well as Sue Clemmings for proofreading the manuscript. Funding from Boston Scientific and the Doctoral Dissertation Fellowship from the University of Minnesota graduate school is gratefully acknowledged.

5 THERMAL STABILITY OF SINGLE TROPOCOLLAGEN MOLECULE AND DEHYDRATION INDUCED CHANGES

This chapter describes the molecular dynamics simulations performed on a single tropocollagen molecule to study the thermal stability and the molecular level changes induced by dehydration. The present author performed all the simulations in collaboration with Dr. Jonathan Sachs and Jason Perlmutter from the Department of Biomedical Engineering at the University of Minnesota. The present author also created and edited the manuscript for publication. The results from this chapter are being prepared for the following citation:

i. Venkatasubramanian, R.T., Perlmutter, J., Sachs, J. and Bischof, J.C. (2008) "Nanoscale unfolding of a single tropocollagen molecule." *Cellular and Molecular Bioengineering* (In preparation at the time of dissertation submission).

Abstract

This chapter describes the MD simulations that were performed as a tool to further investigate dehydration induced increase in thermal stability of the collagen matrix due to freeze-thaw at the molecular level. The simulations investigated short time (ns) and high temperature (> 500 K) denaturation events within hydrated (in a 60 Å x 100 Å x 32 Å waterbox), partially dehydrated (surrounded by a water skin of thickness 5.5 Å) and fully dehydrated (*in vacuo*) tropocollagen under constant pressure and constant volume conditions. Changes in root mean squared displacement (RMSD) of C_α (central carbon atom of an amino acid to which the sidechain and amino group are attached to), helical content and hydrogen bonding during unfolding events were assessed. It was concluded that following dehydration, despite reduction in protein-water hydrogen bonds due to absence of water molecules, new intra-protein hydrogen bonds that are backbone-sidechain in nature were formed that ultimately led to an increase in thermal stability of tropocollagen. It has been speculated that formation of new intra-protein hydrogen bonds within tropocollagen atleast in part governs the mechanism underlying the increased thermal stability of arterial collagen matrix following mannitol and freeze-thaw treatments observed in previous experimental studies.

5.1 INTRODUCTION

The main structural element of extra-cellular matrix (ECM) of connective tissues like tendon, ligament, cornea, skin and arteries is collagen. Collagen, at the nanoscale, consists of tropocollagen molecules that have a length of 300 nm and diameter of 1.5 nm [170-172]. The tropocollagen molecule is formed by three left handed helices supercoiled right handed around a common axis (Fig. 5.1). These molecules are arranged in a staggered manner to form micro-fibrils that in turn self-assembles, into fibrils and then fibers that ultimately form the ECM [80, 173]. The matrix is stabilized by hydrogen bonds that are both intra-protein and protein-water in nature (see Fig. 5.1) at the molecular level and cross linking between different hierarchical levels that influence the response of the tissue to thermodynamic interventions (i.e. mechanical, thermal, or chemical stimuli). High tensile strength and thermal stability are characteristic macroscopic properties of collagen that are often linked to the extensive hydrogen bonding present in collagen matrix network [80].

Thermal stability of the collagen has been an important field of study for several decades because of its current and potential applications [105]. While collagen stability is critical in understanding burn injuries in skin [174, 175], it also directly impacts the outcome of several treatments such as thermal keratoplasty (corneal treatment for farsightedness), skin re-surfacing, tissue welding, thermal capsulorraphy (laser or radiofrequency heating of shoulder joint), etc [119]. When collagen is heated to certain temperature (55-75^{o}C), it results in thermal denaturation. In previously reported experimental studies, thermal stability of collagen has been quantified by studying the kinetics of collagen denaturation [83, 86, 103]. Wright and Humphrey provide an excellent review on different studies and applications of studying collagen denaturation [80].

Due to the importance of thermal denaturation of collagen, the thermodynamics of the denaturation process has been widely studied [84, 86, 103, 104]. Recently, a multi-scale model that incorporates the molecular level phenomena to explain the tissue level behavior was developed [176]. This model, although extremely insightful, uses the Arrhenius parameters of tropocollagen unfolding derived from tissue level experimental approaches[83]. These rather indirect determinations of kinetic parameters of nanoscale

tropocollagen unfolding are not wholly representative of the actual molecular level phenomena. Additionally, varying the thermal stability of collagen through chemical (i.e. dehydration) [86] or mechanical [83] modifications has been of significant interest to researchers. Specifically, dehydration (Fig. 4.1a) due to either freeze-thaw or mannitol treatments cause an increase in the onset temperature of denaturation (Fig. 4.2b, Table 4.2). While it is speculated that such increases are likely due to increased inter-fibrillar interactions in the collagen matrix, which has more closely packed fibers after dehydration [86], understanding of molecular level changes during dehydration is still lacking. Recent advancements in the field of molecular dynamics (MD), which is probably the most realistic simulation technique that allows examination of nanoscale behavior of proteins, allow direct investigation of these events.

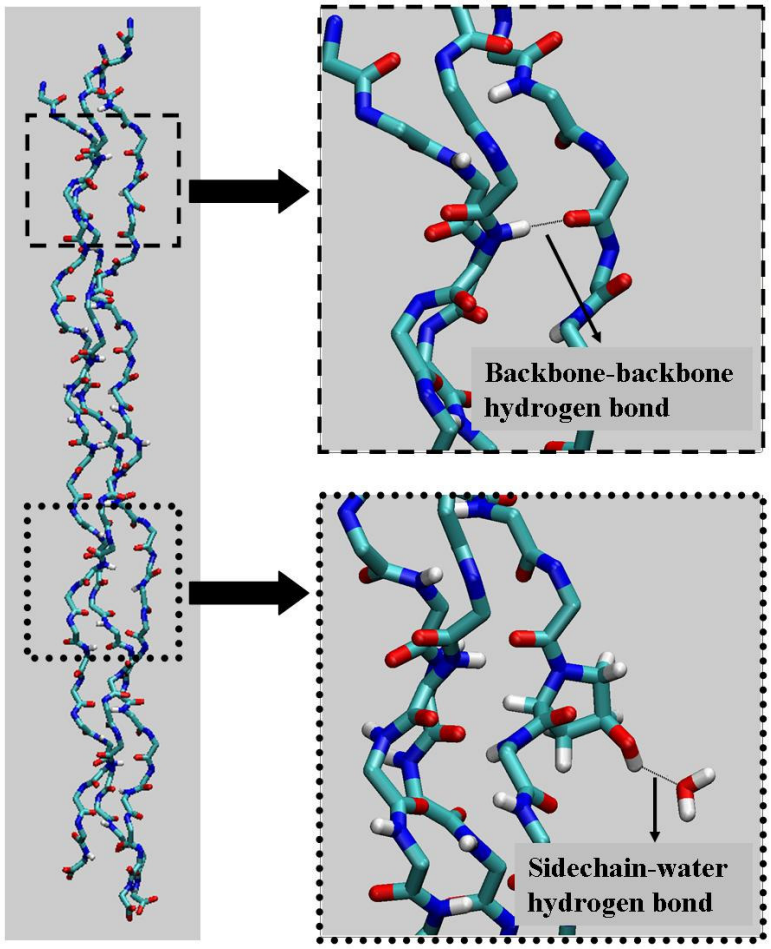

Figure 5.1 Triple helical structure of tropocollagen in the fully hydrated state. The intra-protein (backbone-backbone) and protein-water (sidechain-water) hydrogen bonds shown stabilize the native structure.

MD studies involving tropocollagen started only recently [177-179]. Moreover, most of these studies have focused on understanding only the mechanical properties [179] and fracture mechanics [177, 178] at the nano-scale. There have also been other studies that have investigated the existence of water bridges with potential stabilizing properties for different collagen-like peptides [180]. Despite the importance of thermal denaturation of collagen, unfortunately, till date no study on thermal unfolding of tropocollagen using MD has been ever reported. The MD approach has, however, been previously used to study single molecule thermal unfolding kinetics in other proteins [181, 182] including the kinetics of α-helix protein (polyalanine) denaturation [108]. Daggett presents a good review on studying protein folding and unfolding pathways using the MD approach [183].

The current study describes the MD simulations that were performed as a tool to to further investigate freeze-thaw caused dehydration induced increase in thermal stability of the collagen matrix at the molecular level. The simulations investigated short time (ns) and high temperature (> 500 K) denaturation events within hydrated, partially dehydrated (thin watershell) and fully dehydrated (*in vacuo*) tropocollagen under constant pressure and constant volume conditions. Changes in root mean squared displacement (RMSD) of C_α atom, helical content and hydrogen bonding during unfolding events were assessed. It was concluded that following dehydration, despite reduction in protein-water hydrogen bonds due to absence of water molecules, new intra-protein hydrogen bonds that are backbone-sidechain in nature were formed that ultimately led to an increase in thermal stability of tropocollagen. Similar thermal stability increase of the arterial collagen matrix following dehydration was also observed following mannitol and freeze-thaw treatments.

5.2 METHODS

5.2.1 Molecular Dynamics

All simulations were performed using the all atom force field CHARMM [184], implemented in the molecular dynamics program NAMD [185]. The CHARMM force field is widely used in the protein and biophysics community, and provides a basic description of the different (covalent, ionic, van der Waals and hydrogen bonding) interactions in proteins. The molecular structure was visualized using the visual molecular dynamics (VMD) program [186].

The initial atomic coordinates of a tropocollagen molecule were derived from the protein data bank (PDB ID 1QSU [187]). The crystal structure had a 1.75 Å resolution, a short sequence of tropocollagen molecule of length ~ 8.4 nm. The 1QSU is a triple-helical type II collagen-like molecule with sequence $(Pro\text{-}Hyp\text{-}Gly)_4$-Glu-Lys-Gly-$(Pro\text{-}Hyp\text{-}Gly)_5$. This structure (i.e. sequence) serves as a simple representation of longer tropocollagen molecules extracted from tissues and has been used in other MD studies involving tropocollagen[178, 179]. However, it should be noted that finite length effects may alter the behavior of the system in such cases. Periodic boundary conditions, as used in other MD studies on thermal unfolding of proteins[108], were also used in the current study. The size of the water box was chosen to be sufficiently large to avoid confinement effects such that the tropocollagen was solvated by atleast 10A of water molecules in each orthogonal direction which is a common practice followed in MD studies[188, 189].

5.2.2 Constant Volume Simulations

Four types of fully hydrated constant volume (CV1, CV2, CV3 and CV4) simulations were performed (Table 5.1) with an initial pressure of 1.013×10^5 Pa. The system comprised of tropocollagen molecule in a water box of size 60 by 32 by 100 Å. In all the cases, the system was initially equilibrated at 250K for 2ns followed by heating from 300K to 500K in steps of 50K with a hold time of 1ns at each temperature (Fig. 5.2a). This was followed by another heating starting from 525K or 550K until an end temperature (675K, 700K or 725K) in steps of 25K or 50K with a hold time of 1ns at each temperature (Fig. 5.2b). The final hold at the end temperature was for 8-10ns (Fig. 5.2b). The simulations (CV1, CV2, CV3 and CV4) differed in the temperature step size and end temperature as seen from Table 5.1.

MD simulations representing a partially and completely dehydrated (Table 5.1) tropocollagen molecule system were additionally performed at constant volume (60 by 32 by 100 Å). In the partially dehydrated case, a water skin of thickness 5.5 Å (determined based on the water shell distribution reported elsewhere [190]) was added surrounding the tropocollagen molecule. Complete dehydration was simulated without any water *in vacuo*. In all these cases, the system was initially equilibrated at 250K for 2ns followed by heating from 300K to 700K in steps of 50K with a hold time of 1ns at each temperature. The partially dehydrated case alone was additionally heated from 800K to 1100K in steps of 100K with 0.5ns hold at each temperature.

No.	Type	Name	Hydration box/layer	Description
1	Constant Pressure	CP1	60 x 32 x 100 Å (Initial)	a) 250K, 40ps hold b) 300K-750K, 20ps hold at every 50K step
2		CP2	60 x 32 x 100 Å (Initial)	a) 250K, 400ps hold b) 300K-700K, 200ps hold at every 50K step
3		CP3	60 x 32 x 100 Å (Initial)	a) 250K, 2ns hold b) 300K-600K, 1ns hold at every 50K step
4	Constant Volume (All constant volume simulations had an initial step of 2ns hold at 250K followed by 1ns hold at each temperature in steps of 50K until 500K)	CV1	60 x 32 x 100 Å	a) 525K-650K, 1ns hold at every 25K step b) 675K, 10ns hold
5		CV2	60 x 32 x 100 Å	a) 525K-675K, 1ns hold at every 25K step b) 700K, 8ns hold
6		CV3	60 x 32 x 100 Å	a) 550K-650K, 1ns hold at every 50K step b) 700K, 10ns hold
7		CV4	60 x 32 x 100 Å	a) 525K-700K, 1ns hold at every 25K step b) 725K, 10ns hold
8		Complete dehydration	*In vacuo*	a) 550K-650K, 1ns hold at every 50K step b) 700K, 10ns hold
10		Partial dehydration	Water skin of 5.5Å thickness	a) 550K-650K, 1ns hold at every 50K step b) 700K, 10ns hold c) 800K-1100K, 0.5ns hold at every 100K step

Table 5.1 List of MD simulations on tropocollagen under constant pressure and volume.

5.2.3 Constant Pressure Simulations

Three types (CP1, CP2 and CP3) of constant pressure (1 bar) simulations were additionally performed under fully hydrated conditions (Table 5.1). In all these cases, the system comprised of tropocollagen molecule in a water box of initial size 60 by 32 by 100 Å. CP1, CP2 and CP3 all had an initial equilibration at 250K for 40ps, 400ps and 2ns

respectively (Fig. 5.2c). This was followed by heating (by increasing the temperature) from 300K up to 700K in steps of 50K with a hold time of 20ps, 200ps and 1ns at each temperature in the respective cases (Fig. 5.2c). The different cases can be compared to application of different heating rates.

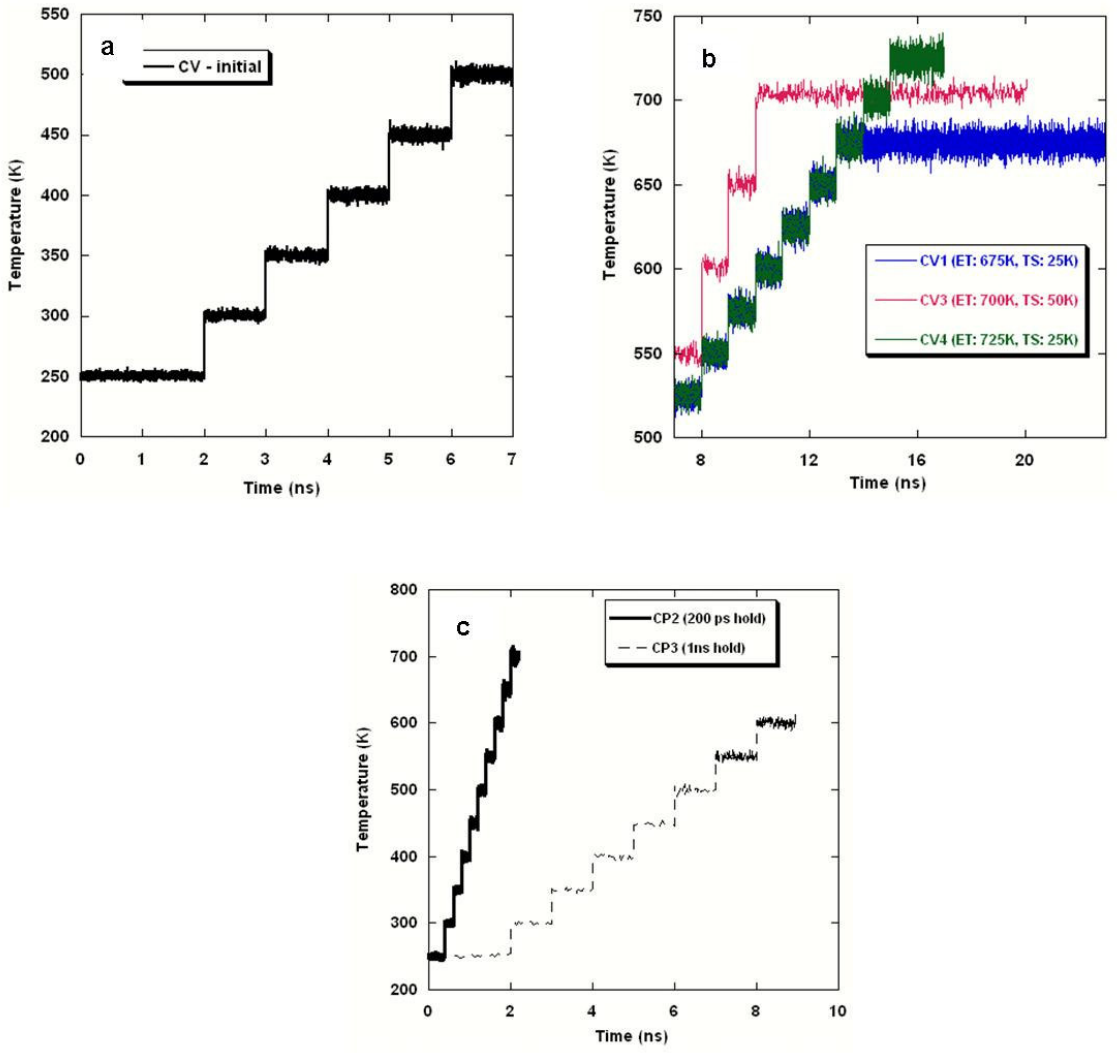

Figure 5.2 Step wise heating of a fully hydrated tropocollagen under constant volume (CV1, CV3 and CV4) and pressure (CP2 and CP3) conditions. Temperature vs. time response under constant volume ((a): 0-7ns and (b): > 7ns) and constant pressure (c) conditions. Refer to Table 5.1 for the description of different simulations.

5.2.4 Post processing and Data Analysis

Postprocessing was performed using CHARMM [191] and the simulation data analyzed in both CHARMM as well as MATLAB v7.1 (The Mathworks Inc., Natick, MA) to obtain changes in different parameters during unfolding. Hydrogen bonds were determined based on a cut-off of 2.4 Å of distance. Based on previously published studies on helix denaturation [108], root mean squared deviation (RMSD) of C_α atoms from the native structure and fraction of helical content in the molecule were used to quantify thermal unfolding. The fraction of helical content in the molecule was calculated based on the dihedral angles (φ, ψ) for each residue of the protein backbone. It was defined as the fraction of residues that satisfied the condition for triple helix, i.e. $-130^o < \varphi < -20^o$ and $90^o < \psi < 180^o$. The range of the dihedral angles (φ, ψ) for the triple helix criterion was chosen by observing the changes in the Ramachandran plot (φ vs. ψ) of the protein backbone during unfolding.

5.3 RESULTS

5.3.1 Constant Volume Simulations

Heating caused unfolding of tropocollagen in all constant volume simulations (CV1, CV2, CV3, and CV4) under fully hydrated conditions (Fig. 5.3). The backbone-backbone hydrogen bonds that stabilize the triple helix are broken upon heating resulting in uncoiling of triple helix structure as shown in Fig. 5.3a. Figure 5.3b shows reduction in both backbone-backbone hydrogen bonding as well as helical fraction in the molecule. The unfolding also resulted in significant increase in the RMSD (Fig. 5.4). Figure 5.4 shows the variation in RMSD with time for the four constant volume cases (CV1, CV2, CV3 and CV4). A clear transition marked by sudden increase in RMSD was observed (Fig. 5.4a, b) during unfolding. While there was a decrease in the helical content with time due to heating, clear transition points were not observed probably due to increased noise (not shown).

Thermal unfolding kinetics of tropocollagen under constant volume condition was dependent on the end temperature as well as the step size (25K vs 50K) during heating. Figure 5.4a shows the variation in RMSD with time during the constant volume cases CV1 and CV4. While 25K steps were used in both cases with a 1ns hold at each

temperature, the end temperature was 675K and 725K for CV1 and CV4 respectively. In both cases thermal unfolding started around 10ns (Fig. 5.4a). However, it can be observed that the rate of increase of RMSD (as indicated by the slope of the RMSD vs. time plot after 10ns) was higher in CV4 compared to CV1 (Fig. 5.4a). On the other hand, CV2 and CV3 have the same end temperature but differ in the temperature step size (comparable to the rate of heating such that CV3 < CV2). It can also be observed from Fig. 5.4b that the onset temperature for thermal unfolding was higher in CV2 (~700K) compared to CV3 (~650K). Significant difference in the rate of increase of RMSD between CV2 and CV3 can also be observed (Fig. 5.4b).

Dehydration increased the thermal stability of tropocollagen significantly. As seen in Fig. 5.5, no thermal unfolding was observed both in the partially (5.5Å watershell) and completely (*in vacuo*) dehydrated case until 20ns. Upon further increasing the temperature to 1100K, the tropocollagen molecule unfolded in the partially dehydrated case (Fig. 5.5). Similar to the fully hydrated case, unfolding was characterized by breaking of the backbone-backbone hydrogen bonds and uncoiling of the triple helix (not shown).

5.3.2 Constant Pressure Simulations

Heating under constant pressure took shorter time (≤ 8ns) and required lower temperatures (≤ 650K) compared to constant volume for the triple helix to unfold (Fig. 5.6). Similar to the constant volume cases, unfolding involved breaking of the backbone-backbone hydrogen bonds. Interestingly, the unit cell (initial size: 60 by 32 by 100 Å) that hydrated the tropocollagen molecule expanded rapidly to several times the original size (final size: 850 by 452 by 1414 Å) around the same time when the molecule unfolded. The tropocollagen molecule resembled a dehydrated state post this expansion.

Significant increase in RMSD as well as reduction in helical fraction was also observed during unfolding (Fig. 5.6). Fig 6a shows the variation in RMSD and fraction of helical content with time for the CP1 case. A clear transition marked by sudden increase in RMSD and simultaneous reduction in helical fraction can be seen around 0.18ns in the CP1 case (Fig. 5.6a). Similar transitions were observed around 1.5ns and 7.3ns in the CP2 and CP3 cases respectively (not shown).

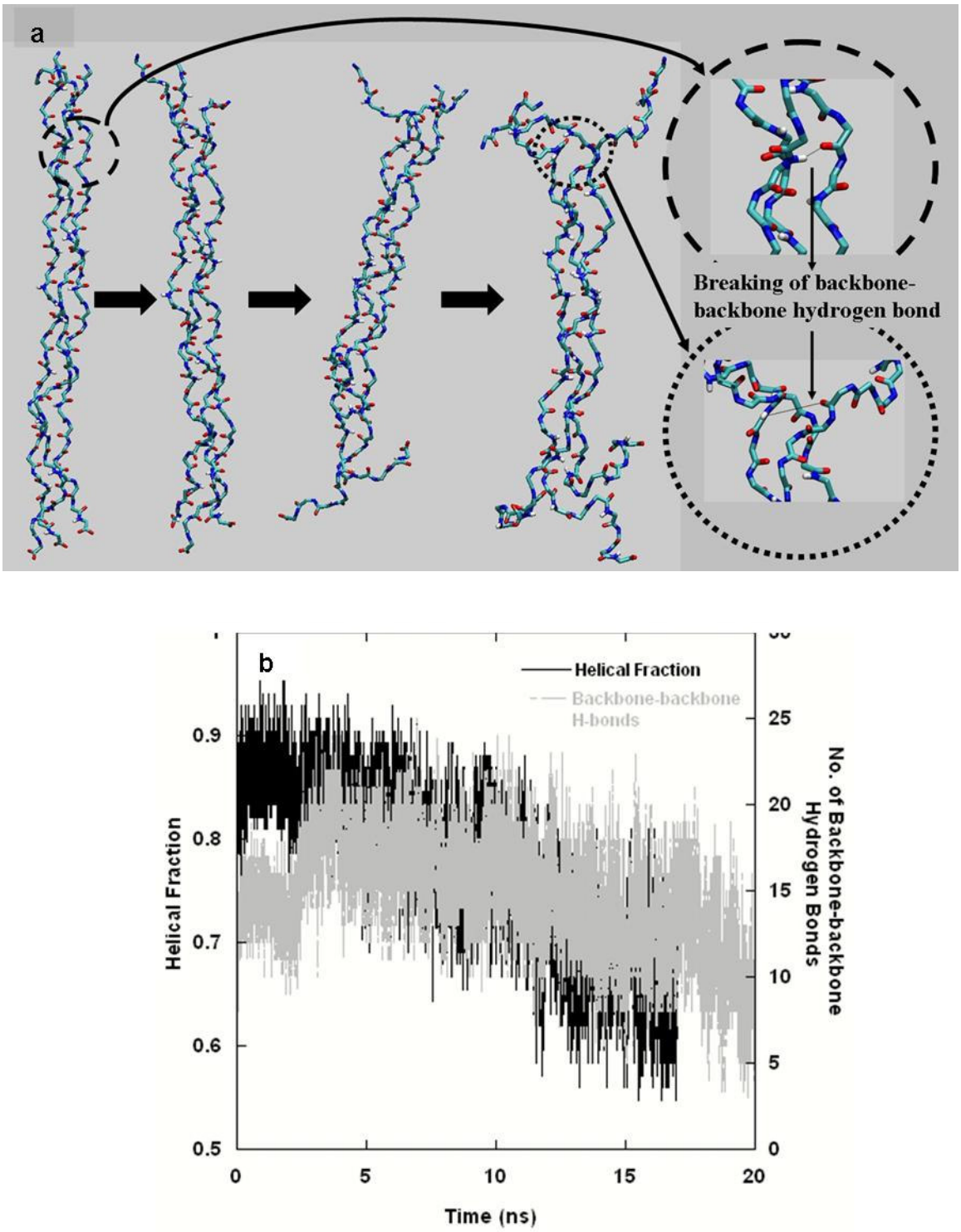

Figure 5.3 Structural changes during thermal unfolding of fully hydrated tropocollagen: a) breaking of backbone-backbone hydrogen bonds and uncoiling of the triple helix with time and b) helical fraction and backbone-backbone hydrogen bonds vs. time plot.

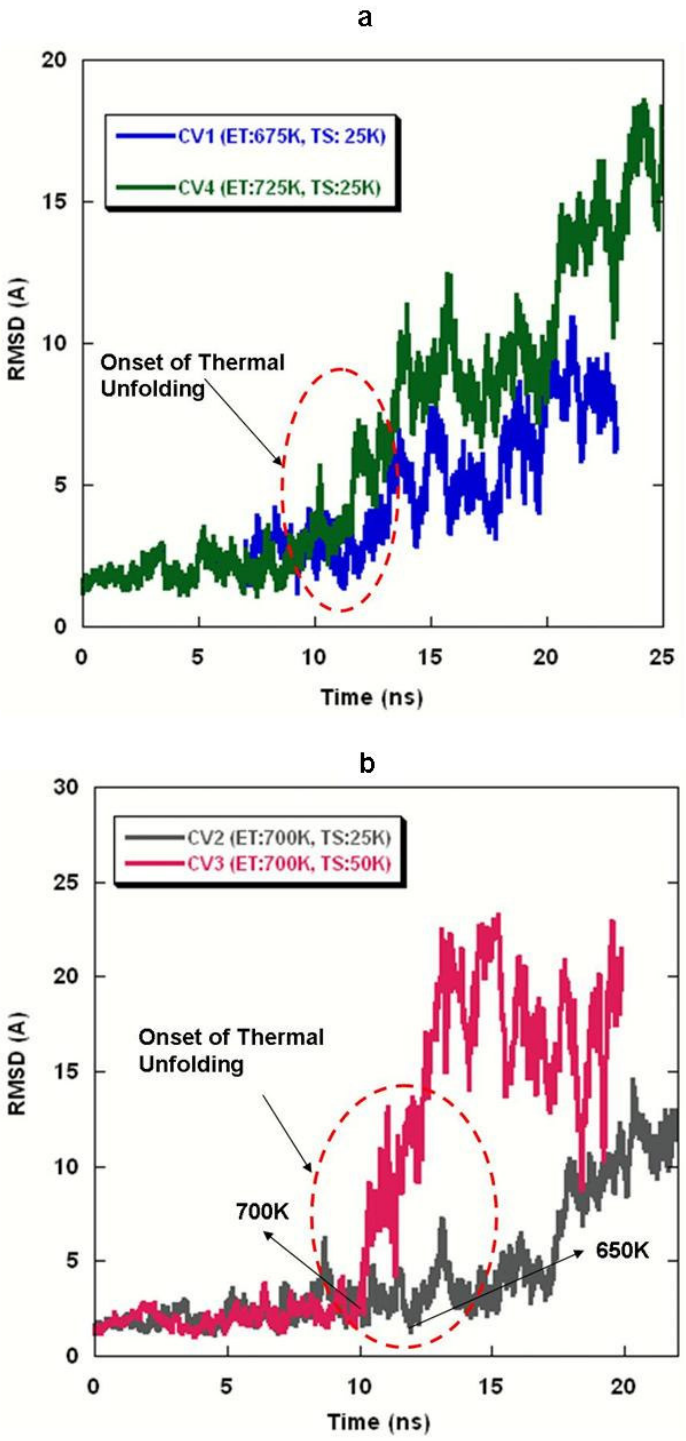

Figure 5.4 Changes in root mean squared deviation (RMSD) from the native structure during heating of a fully hydrated tropocollagen under constant volume: a) effect of end temperature; CV1 vs.CV4 and b) effect of temperature step size; CV2 vs. CV1. Refer to Table 5.1 for the description of different simulations.

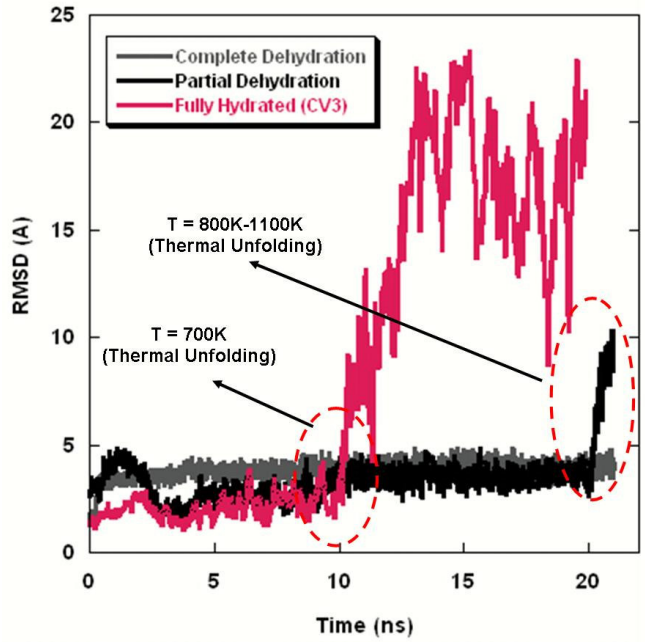

Figure 5.5 Changes in root mean squared deviation (RMSD) from the native structure during heating of completely (*in vacuo*) and partially (5Å thick water skin) dehydrated tropocollagen under constant volume. Note the increased thermal stability following dehydration as compared to the fully hydrated state.

Thermal unfolding kinetics of tropocollagen under constant pressure condition was dependent on the rate of heating (i.e. hold time and temperature). It was observed that thermal unfolding occurred at a lower temperature for the cases with larger hold times (Fig. 5.6b). It can be seen from Fig. 5.6b that while the onset temperature of thermal unfolding for the 20ps hold case (CP1) was 650K, it was 600K and 550K for the 200ps hold (CP2) and 1ns hold (CP3) cases respectively.

5.4 DISCUSSION

5.4.1 Molecular Dynamics and Nanoscale Behavior of Proteins

MD is probably the most realistic simulation technique that allows examination of nanoscale behavior of proteins. Importantly, MD can be used to describe kinetic pathways of several important reactions and thereby provide mechanistic insights. Following the first MD study on thermal protein unfolding in bovine pancreatic trypsin inhibitor [181], several studies on proteins such as chymotrypsin inhibitor 2 [106, 108, 182, 192-194],

apocytochrome [195, 196], etc. have been reported (for a review, see article by Daggett [107]). Particularly, in a study involving polyalanine, an α-helical peptide consisting of 13 residues, Daggett and Levitt studied the thermal unfolding kinetics both *in vacuo* and in the presence of a solvent [108]. In this study, changes in RMSD of the C_α–carbon atom as well as helical content with time were studied at different temperatures using the criterion for α-helicity ($-100^o < \varphi < -30^o$ and $-80^o < \psi < -5^o$) similar to that used in this study. It should however be noted that the criterion for helicity for tropocollagen (left helix) is different from polyalanine (α-helix). While MD provides tremendous insight on the transition state structures (dihedral angles of the protein backbone, hydrogen bonds, etc.) and can be very useful in studying single molecule unfolding kinetics at the nanoscale, the use of high temperature to observe the unfolding process under computationally accessible nanosecond timescale has invoked criticism on whether such an approach is valid for practical purposes. However, the agreement between the simulations and experiment for proteins such as chymotrypsin inhibitor 2 [109], the engrailed homeodomain [110] and the human yes kinase-associated protein [111] suggest that the unfolding pathways are independent of the temperature and the unfolding process is merely accelerated by increasing the temperature in MD [106].

In addition to understanding the thermal unfolding, MD can also provide insights on the nanoscale mechanical properties. The previous MD studies involving tropocollagen molecule have all mainly focused on understanding the nanoscale mechanical properties [178, 179]. These studies involved stretching of the tropocollagen molecule using a steered molecular dynamics (SMD) approach. Lorenzo et. al. subjected the single molecule to tensile strains of ~4% and reported the Young's modulus of a single tropocollagen molecule [179]. In another study, Buehler and Song showed that the collagen fibers when subjected to large deformations, at the molecular level, involved breaking of several hydrogen bonds, stretching of covalent bonds and ultimately molecular fracture [178]. Finally, despite MD studies investigating the nanoscale mechanical properties of tropocollagen as well as thermal unfolding in other proteins being reported, the current MD study is still the first to report the thermal unfolding of a single tropocollagen molecule.

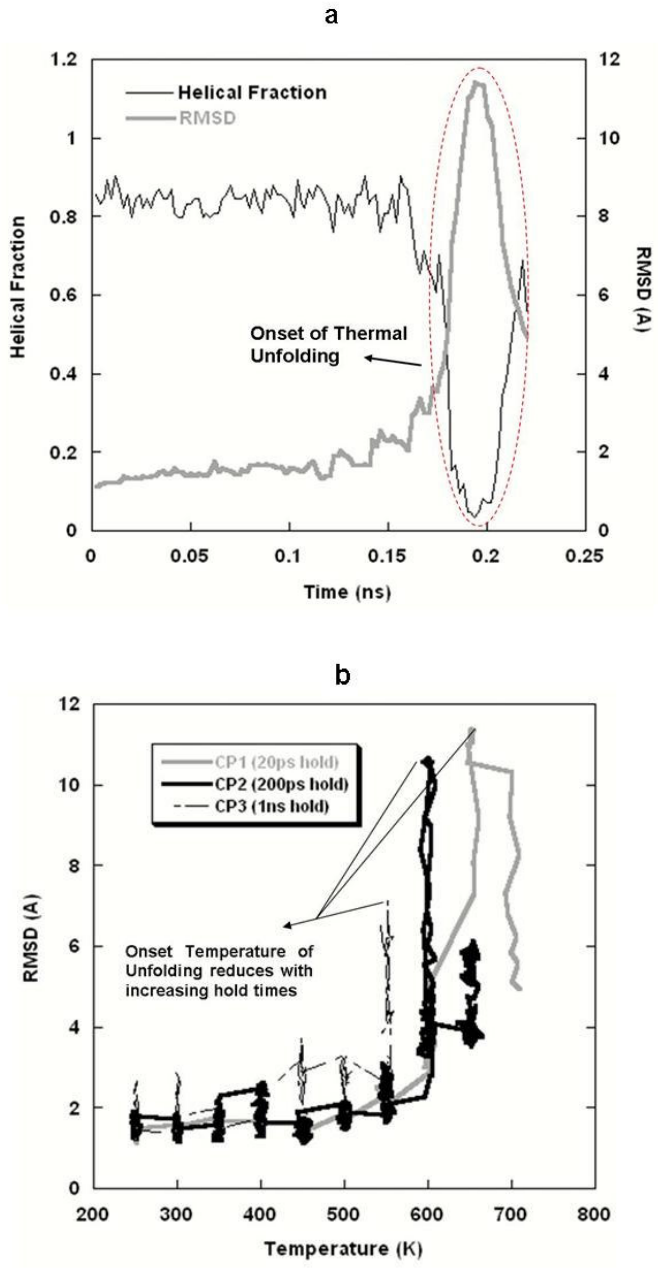

Figure 5.6 Thermal unfolding during heating of a fully hydrated tropocollagen under constant pressure. Changes in helical fraction and root mean squared deviation (RMSD) from the native structure with time: a) CP1 (20ps hold) and b) Effect of rate of heating on onset temperature of unfolding; RMSD vs. temperature changes. Refer to Table 5.1 for the description of different simulations.

5.4.2 Dehydration effect on Thermal Stability

Collagen is hierarchically arranged starting from a triple helical tropocollagen molecule into a micro-fibril, fibril and ultimately into a fiber [80, 173]. The hierarchical arrangement of

a collagen matrix differs based on the tissue type (cornea, lens capsule, aorta, tendon, etc.) thereby resulting in varying thermal stability (or mechanical strength). At the molecular level, tropocollagen is stabilized by intra-protein (mainly backbone-backbone) hydrogen bonds (Fig. 5.1). In a hydrated state, as found during physiological conditions, the tropocollagen molecule further stabilized by additional protein-water hydrogen bonds that are majorly sidechain-water in nature but also include some backbone-water bonds (Fig. 5.1). When collagen is heated, these hydrogen bonds stabilizing the tropocollagen molecule are broken and ultimately cause it to unfold (Fig. 5.3). Additionally, denaturation also involves breaking of other stabilizing bonds or crosslinks between different hierarchical levels [80].

Dehydration causes increased thermal stability of the collagen at tissue level [86]. In a rat tail tendon study by Miles et. al, the denaturation temperature following dehydration was shown to increase significantly [86]. Similarly, in another study, Venkatasubramanian et. al. showed that both freeze-thaw and mannitol treatments induced dehydration in arteries resulting in increased thermal denaturation onset temperature [154]. Increased thermal stability of tropocollagen was observed also at the nanoscale level (Figs. 5 and 9). Comparison of hydrated (Fig. 5.1) and dehydrated (Fig. 5.7) tropocollagen structure suggests that, under both conditions the tropocollagen was stabilized by backbone-backbone hydrogen bonds. While the additional protein-water hydrogen bonds stabilizing the tropocollagen in a hydrated state are reduced or absent due to partial or complete dehydration (Fig. 5.7b), dehydration results in additional intra-protein hydrogen bonds that are both backbone-sidechain and sidechain-sidechain in nature (Fig. 5.7a, c). These results therefore suggest that these intra-protein hydrogen bonds cause an increase in the thermal stability of the tropocollagen (Fig. 5.5) and ultimately collagen at the tissue level. In another MD study, Mogilner et. al. also observed that dehydration caused increased intra-protein hydrogen bonds and that the native structure of the tropocollagen was not maintained in the dehydrated state as compared to the hydrated [197]. These results suggest that while dehydration increases the thermal stability, the native structure of the tropocollagen (as in a fully hydrated case) was not preserved.

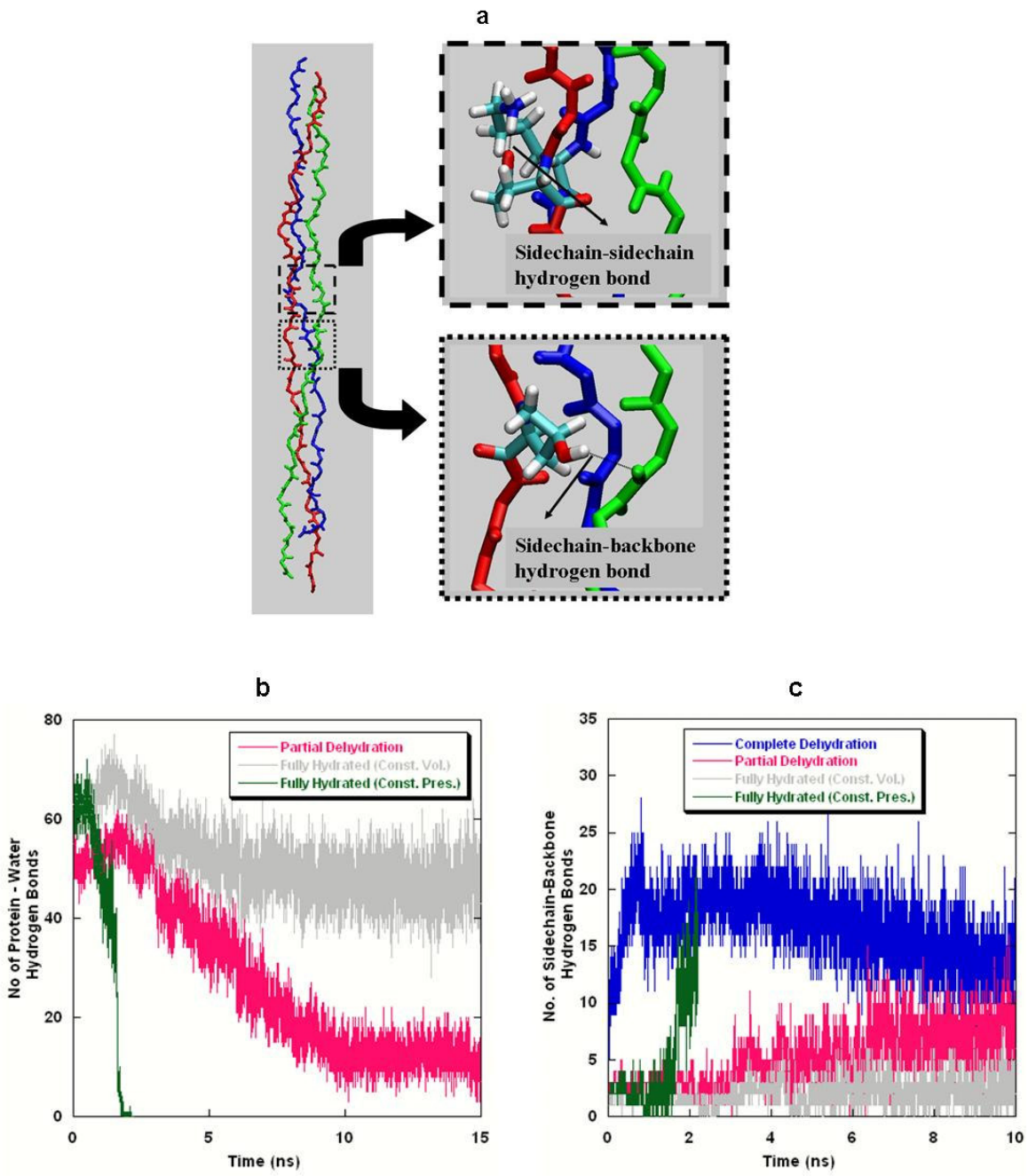

Figure 5.7 Dehydration induced variation in hydrogen bonding (stability) of tropocollagen: a) tropocollagen structure *in vacuo* (Note the newly formed intra-protein, i.e. sidechain-sidechain and sidechain-backbone hydrogen bonds), b) protein-water hydrogen bonds in fully hydrated and partially dehydrated system, and c) sidechain-backbone hydrogen bonds in completely and partially dehydrated systems.

Additionally, it can be observed from Fig. 5.7 that during heating under constant pressure conditions, the tropocollagen resembles a hydrated state initially followed by

dehydration due to expansion of the waterbox. This can be seen from through a reduction in protein-water hydrogen bonds as shown in Fig. 5.7b as well as an increase in protein-protein hydrogen bonds as shown in Fig. 5.7c.

5.5 SUMMARY

In this chapter, an attempt was made to study the nanoscale thermal unfolding of a single tropocollagen molecule using MD under hydrated and dehydrated conditions. Simulations were performed on a tropocollagen molecule in constant volume and constant pressure under fully hydrated, partially dehydrated and completely dehydrated conditions. The results from this study are summarized as follows:

i. The triple helical structure of the tropocollagen is stabilized by several hydrogen bonds that are protein-protein as well as protein-water in nature.

ii. At the molecular level, thermal unfolding involves breaking of hydrogen bonds between the protein backbones ultimately resulting in uncoiling of the triple helix. The kinetics of unfolding can also be quantified by investigating the reduction in the helical content estimated using the dihedral angle criterion and an increase in RMSD.

iii. Under dehydrated conditions, the protein-water hydrogen bonding was reduced (absent *in vacuo*) due to presence of lesser water molecules around the protein. However, increased protein-protein hydrogen bonding between the backbone and sidechains was also observed. This ultimately resulted in an increased thermal stability under dehydration conditions. These molecular mechanisms atleast in part explain the increased thermal stability of arterial collagen matrix post freeze-thaw induced dehydration reported in Chapter 4.

Acknowledgements

The authors would like to acknowledge the Minnesota Supercomputing Institute for the supercomputing resources. Doctoral Dissertation Fellowship from the University of Minnesota graduate school is acknowledged for funding.

6 RESEARCH SUMMARY

In this dissertation, studies were undertaken to investigate the freeze-thaw induced biomechanical changes in arteries and their underlying mechanisms which is ultimately required to improve the efficacy of thermal treatments. In summary, freeze-thaw induced biomechanical changes as well as arterial component changes were quantified and a component based mechanical model suggested. In addition, molecular level changes induced during dehydration, such as one during freeze-thaw, to the tropocollagen which is the building unit of a collagen matrix were also investigated using molecular dynamics approach. The important results and conclusions drawn from the studies conducted in the dissertation are summarized as follows:

Freeze-thaw induced biomechanical changes in arteries (Chapters 2 and 3)

Freeze-thaw causes significant stiffening of the arteries that can be measured using both uniaxial tensile (Chapter 2) as well as indentation (Chapter 3) responses of normal porcine arteries.

a. In the uniaxial tensile response, it was observed that the toe region in the stress-strain arterial response reduced by $39 \pm 14\%$ following radial freeze-thaw. The physiological elastic moduli (Eartery) for the fresh and frozen-thawed arteries were 185±92 kPa and 506±159 kPa respectively. It was also observed that the preconditioning loops of the frozen-thawed arteries showed lesser hysteresis and took lesser number of cycles to reach repeatable stress-strain response.
b. In the indentation response, the peak (E_P), initial (E_0) and equilibrium (E_∞) moduli of the radially frozen-thawed arteries were 2.3 ± 1.6, 1.8 ± 0.6 and 1.6 ± 0.8 times that of fresh arteries. The indentation equilibrium modulus for the fresh and frozen-thawed were 132 ± 125 kPa and 322 ± 309 kPa respectively.

Freeze-thaw induced changes to arterial components (Chapter 4)

Freeze-thaw significantly alters both collagen matrix and smooth muscle cells (SMCs) that are the most important components of an artery.

a. Radial freeze-thaw induced significant dehydration in the arteries. The hydration ratio of the arteries reduced by 15± 0.06% following freeze-thaw. Significant structural changes in the arteries were also observed. The initial length (L_o) which is representative of the inner diameter of the artery increased by 29 ± 0.07%.
b. Increased thermal stability of the collagen matrix following freeze-thaw induced dehydration was observed. The amide-III band analysis of the FTIR spectra showed an increase in the onset temperature of denaturation for the arteries from 57.0 ± 3.0^{o}C (fresh) to 63.4 ± 4.1 ^{o}C (frozen-thawed).
c. Freeze-thaw caused complete destruction of the SMCs. Following freeze-thaw, SMCs showed almost no response to norepinephrine and acetylcholine compared to control where a distinct contraction and relaxation was observed respectively.

Dehydration induced molecular changes to tropocollagen (Chapter 5)

In order to further investigate the molecular mechanisms underlying the dehydration induced increased thermal stability of the collagen matrix, molecular dynamics (MD) simulations were performed to understand the short time (ns) and high temperature (> 500 K) denaturation events within hydrated, partially dehydrated (thin watershell) and fully dehydrated (*in vacuo*) tropocollagen under constant pressure and constant volume conditions. Simulations suggested that increased thermal stability following dehydration, as induced by freeze-thaw (or other osmotic treatments), was observed at even at the molecular level, on a single tropocollagen molecule. Specific conclusions from the MD study are:

a. The tropocollagen triple helix is primarily stabilized by backbone-backbone hydrogen bonds. Under hydrated conditions, additional hydrogen bonds between the protein (mostly sidechain but some backbone as well) and water are formed that further stabilize the structure. Thermal denaturation at the molecular level is

characterized by breaking of the backbone-backbone hydrogen bonds that result in uncoiling of the triple helical structure.

b. Dehydration results in reduced protein-water hydrogen bonds due to absence of water molecules around tropocollagen. This leads to formation of new sidechain-backbone hydrogen bonds that are typically absent under hydrated conditions. It was also observed that dehydrated tropocollagen showed increased thermal stability and did not unfold when exposed to same thermal history as the hydrated case. This suggests that formation of new intra-protein hydrogen bonds in the absence of water molecules causes the increased thermal stability during dehydration.

Future Directions

1. Results from both uniaxial and indentation studies suggest that subjecting an artery section to freeze-thaw is similar to insertion of a vascular graft with significantly high stiffness. These results could be potentially (i.e. modulus of normal and diseased arteries as well as changes in them following cryoplasty) used in emerging computational models that account for solid-fluid coupling at the artery wall to provide initial insights on the hemodynamical changes in a cryoplasty treated artery. Significant variation in the hemodynamics of a cryoplasty treated artery might require the ability of potential chemical modifiers in mitigating the biomechanical effects be investigated.
2. Future work should be directed towards understanding the structural changes (at the level of fibers/fibril) in the collagen matrix using scanning/transmission electron microscopy. Future studies should also be directed towards understanding of the freeze-thaw effects on other arterial components such as elastin and glucosaminoglycans (GAGs) and incorporate these effects into the component based arterial model for thermobiomechanics. Such a model would significantly improve the understanding of underlying mechanisms of thermobiomechanics.

BIBLIOGRAPHY

(1) Ross, R., *Atherosclerosis- an Inflammatory Disease.* New England Journal of Medicine, 1999. **340**(2): p. 115-126.

(2) Ezekowitz, M.D., *Peripheral Vascular Diseases*, in *Heart Book*, B.L. Zaret, M. Moser., and L.S. Cohen, Editors. 1992, Yale University School of Medicine. p. 205-214.

(3) *Stent Procedure*, in *American Heart Association*. 2006.

(4) Altman, J.D., G.A. Bayes, and R.S. Schwartz, *Pathophysiology of Restenosis*, in *Restenosis: A Guide to Therapy*, D.P. Faxon, Editor. 2001, Martin Dunitz Ltd: London. p. 9-19.

(5) Shah, P.B. and C.M. Lilly, *Interventional Therapy for Coronary Artery Disease.* American Journal of Respiratory and Critical Care Medicine, 2002. **166**: p. 791-796.

(6) Santin, M., P. Colombo, and G. Bruschi, *Interfacial Biology of in-Stent Restenosis.* Expert Review of Medical Devices, 2005. **2**(4): p. 429-443.

(7) Barghava, B., G. Karthikeyan, A.S. Abizaid, and Roxana, *New Approaches to Preventing Restenosis.* British Medical Journal, 2003. **327**: p. 274-279.

(8) Diller, K.R. and T.P. Ryan, *Heat Transfer in Living Systems: Current Opportunities.* Journal of Heat Transfer, 1998. **120**: p. 810-829.

(9) Hoffmann, N.E. and J.C. Bischof, *Cryosurgery of Normal and Tumor Tissue in the Dorsal Skin Flap Chamber: Part 1 - Thermal Response.* Journal of Biomechanical Engineering, 2001. **123**(4): p. 301-309.

(10) Hoffmann, N.E. and J.C. Bischof, *Cryosurgery of Normal and Tumor Tissue in the Dorsal Skin Flap Chamber: Part 2 - Injury Response.* Journal of Biomechanical Engineering, 2001. **123**(4): p. 310-316.

(11) Jais, P., R. Weerasooriya, D.C. Shah, M. Hocini, L. Macle, K.-J. Choi, C. Scavee, M. Haissaguerre, and J. Clementy, *Ablation Therapy for Atrial Fibrillation (Af): Past, Present, and Future.* Cardiovascular Research, 2002. **54**: p. 337-346.

(12) Cheema, A.N., N. Nili, C.W. Li, H.A. Whittingham, J. Linde, R.J. van Suylen, M.R. Eskandrian, A.P. Wong, B. Qiang, J.-F. Tanguay, M. Lane, and B.H. Strauss, *Effects of Intravascular Cryotherapy on Vessel Wall Repair in a Balloon-Injured Rabbit Iliac Artery Model.* Cardiovascular Research, 2003. **59**: p. 222-233.

(13) Floren, M.G., R.W. Gunther, and T. Schmitz-Rode, *Noninvasive Inductive Stent Heating: Alternative Approach to Prevent Instent Restenosis?* Investigative radiology, 2004. **39**(5): p. 264-270.

(14) Karaca, I., E. Ilkay, M. Akbulut, and M. Yavuzkir, *Treatment of in-Stent Restenosis with Excimer Laser Coronary Angioplasty.* Japanese heart journal, 2003. **44**(2): p. 179-186.

(15) Kataoka, T., Y. Honda, H.N. Bonneau, P.G. Yock, and P.J. Fitzgerald, *New Catheter-Based Technology for the Treatment of Restenosis.* Journal of Interventional Cardiology, 2002. **15**: p. 371-380.

(16) Mudra, H., M. Hug, A. Knape, and C. Spes, *Intravascular Sonotherapy for Treatment of in-Stent Restenosis.* Zeitschrift fu̇r Kardiologie, 2002. **91**(3): p. 103-107.

(17) Terashima, M., Y. Honda, F.S. Goar, J.D. Joye, K. Tatsutani, M. Yoklavich, P.G. Yock, and P.J. Fitzgerald, *Feasibility and Safety of a Novel Cryoangioplasty System.* Journal of the American College of Cardiology, 2002. **39**(Suppl. A): p. 57.

(18) Laird, J., R.J. Michael, G. Biamino, T. McNamara, D. Scheinert, P. Zetterlund, E. Moen, and J.D. Joye, *Cryoplasty for the Treatment of Femoropopliteal Arterial Disease: Results of a Prospective, Multicenter Registry.* Journal of Vascular and Interventional Radiology, 2005. **16**(8): p. 1067-1073.

(19) Joye, J.D., *The Clinical Application of Cryoplasty for Infrainguinal Peripheral Arterial Disease.* Techniques in Vascular and Interventional Radiology, 2005. **8**(4): p. 160-164.

(20) Lafontaine, D., *Cryoplasty Device and Method*, S.L.S. Inc., Editor. 1999: United States.

(21) Li, A.K.C., H.P. Ehrlich, R.L. Trelstad, M.J. Koroly, M.E. Schattenkerk, and R.A. Malt, *Differences in Healing of Skin Wounds Caused by Burn and Freeze Injuries.* Annals of Surgery, 1980. **191**(2): p. 244-248.

(22) Baer, E., A. Hiltner, and D. Jarus, *Relationship of Hierarchical Structure to Mechanical Properties.* Macromolecular symposia, 1999. **147**: p. 37-61.

(23) Holzapfel, G.A., *Biomechanics of Soft Tissue.* Graz, 2000: p. No.7.

(24) Lee, T.C., R.J. Midura, V.C. Hascall, and I. Vesley, *The Effect of Elastin Damage on Mechanics of Aortic Valve.* Journal of biomechanics, 2001. **34**: p. 203-210.

(25) Spina, M., A. Friso, A.R. Ewins, K.H. Parker, and C.P. Winlove, *Physicochemical Properties of Arterial Elastin and Its Associated Glycoproteins.* Biopolymers, 1998. **49**: p. 255-265.

(26) Song, Y.C., S. Khirabadi, F. Lightfoot, K.G.M. Brockbank, and M.J. Taylor, *Vitreous Cryopreservation Maintains the Function of Vascular Grafts.* Nature Biotechnology, 2000. **18**: p. 296-299.

(27) Pegg, D.E., M.C. Wusteman, and S. Boylan, *Fractures in Cryopreserved Elastic Arteries.* Cryobiology, 1997. **34**: p. 183-192.

(28) Cui, Z.F., R.C. Dykhuizen, R.M. Nerem, and A. Sembanis, *Modeling of Cryopreservation of Engineered Tissues with One-Dimensional Geometry.* Biotechnology progress, 2002. **18**(2): p. 354-361.

(29) Nerem, R. and D. Seliktar, *Vascular Tissue Engineering.* Annu. Rev. Biomed. Eng., 2001. **3**: p. 225-243.

(30) Grassl, E.D., T.R. Oegema, and R.T. Tranquillo, *A Fibrin-Based Arterial Media-Equivalent.* Journal of Biomedical Materials Research, 2003. **66A**: p. 550-561.

(31) Taylor, C.A., T.J. Hughes, and C.K. Zarins, *Finite Element Modeling of Three-Dimensional Pulsatile Flow in the Abdominal Aorta: Relevance to Atherosclerosis.* Annals of Biomedical Engineering, 1998. **26**(6): p. 975-987.

(32) Stegemann, J.P., H. Hong, and R.M. Nerem, *Mechanical, Biochemical, and Extracellular Matrix Effects on Vascular Smooth Muscle Cell Phenotype.* Journal of Applied Physiology, 2005. **98**: p. 2321-2327.

(33) Durante, W., L. Liao, S.V. Reyna, K.J. Peyton, and A.I. Schafer, *Physiological Cyclic Stretch Directs L-Arginine Transport and Metabolism to Collagen Synthesis in Vascular Smooth Muscle.* The FASEB Journal, 2000. **14**: p. 1775-2783.

(34) Wilson, E., Q. Mai, K. Sudhir, R.H. Weiss, and H.E. Ives, *Mechanical Strain Induced Growth of Vascular Smooth Muscle Cells Via Autocrine Action of Pdgf.* Journnal of Cell Biology, 1993. **123**(741-747).

(35) Cunningham, K.S. and A. Gotlieb, *The Role of Shear Stress in the Pathogenesis of Atherosclerosis.* Laboratory investigation, 2005. **85**(1): p. 9-23.

(36) Humphrey, J.D. and C.A. Taylor, *Intracranial and Abdominal Aortic Aneurysms: Similarities, Differences, and Need for a New Class of Computational Models.* Annual Review of Biomedical Engineering, 2008. **10**(1).

(37) Cox, R., *Wave Propagation through a Newtonian Fluid Contained in Thick-Walled Viscoelastic Tube.* Biophysical Journal, 1968. **8**: p. 691-709.

(38) Fung, Y.C., *Wave Propagation in Blood Vessels*, in *Biodynamics Circulation*. 1984, Springer-Verlag: New York. p. 104-115.

(39) Gijsen, F.J.H., E. Allanic, F.N. van de Vosse, and J.D. Janssen, *The Influence of the Non-Newtonian Properties of Blood on the Flow in Large Arteries: Unsteady Flow in a 90° Curved Tube.* Journal of Biomechanics, 1999. **32**(7): p. 705-713.

(40) Nerem, R.M., *Tissue Engineering a Blood Vessel Substitute: The Role of Biomechanics.* Yonsei Medical Journal, 2000. **41**(6): p. 735-739.

(41) De Syo, D., B.D. Franjic, I. Lovricevic, M. Vukelic, and H. Palenkic, *Carotid Bifurcation Position and Branching Angle in Patients with Atherosclerotic Carotid Disease.* Collegium antropologicum., 2005. **29**(2): p. 627-639.

(42) Adham, M., J.-P. Gournier, J.-P. Favre, E. De La Roche, C. Ducerf, J. Baulieux, X. Barral, and M. Pouyet, *Mechanical Characteristics of Fresh and Frozen Human Descending Thoracic Aorta.* Journal of Surgical Research, 1996. **64**: p. 32-34.

(43) Fung, Y.C., *Elasticity of Connective Tissue in Simple Elongation.* American Journal of Physiology, 1967. **213**(6): p. 1532-1544.

(44) Mohan, D., *Failure Properties of Passive Human Aortic Tissue.I—Uniaxial Tension Tests.* Journal of Biomechanical Engineering, 1982. **15**: p. 887-902.

(45) Oyen, M.L., S.E. Calvin, and R.F. Cook, *Uniaxial Stress-Relaxation and Stress-Strain Responses of Human Amnion.* Journal of Materials Science: Materials in Medicine, 2004. **15**: p. 619-624.

(46) Cox, R., *Comparison of Mechanical and Chemical Properties of Extra- and Intralobular Canine Pulmonary Arteries.* American Journal of Physiology, 1982. **242**: p. H245-H253.

(47) Cox, R., *Comparison of Arterial Wall Mechanics Using Ring and Cylindrical Segments.* American Journal of Physiology, 1983. **244**: p. H298-H303.

(48) Guinea, G.V., J.M. Atienza, M. Elices, P. Aragoncillo, and K. Hayashi, *Thermomechanical Behavior of Human Carotid Arteries in the Passive State.* American journal of physiology. Heart and circulatory physiology, 2005. **288**(6): p. H2940-2945.

(49) Hayashi, K., H. Handa, S. Nagasawa, A. Okumura, and K. Moritake, *Stiffness and Elastic Behavior of Human Intracranial and Extracranial Arteries.* J Biomech, 1980. **13**(2): p. 175-84.

(50) Simha, N.K., C.S. Carlson, and J.L. Lewis, *Evaluation of Fracture Toughness of Cartilage by Micropenetration.* Journal of materials science, 2003. **14**: p. 631-639.

(51) Chin-Purcell, M.V. and J.L. Lewis, *Fracture of Articular Cartilage.* Journal of biomechanical engineering, 1996. **118**: p. 545-556.

(52) Ebenstein, D.M. and L.A. Pruitt, *Nanoindentation of Soft Hydrated Materials for Application to Vascular Tissues.* Mater Res, 2004. **69**: p. 222-232.

(53) Schulze-Bauer, C.A.J., C. Mörth, and G. Asme, *Passive Biaxial Mechanical Response of Aged Human Iliac Arteries.* Journal of Biomechanical Engineering, 2003. **125**: p. 395.

(54) De Korte, C.L. and A.F.W. Van der Steen, *Intravascular Ultrasound Elastography: An Overview*. Ultrasonics, 2002. **40**(1-8): p. 859-865.

(55) Yabushita, H., B.E. Bouma, S.L. Houser, H.T. Aretz, I.K. Jang, K.H. Schlendorf, C.R. Kauffman, M. Shishkov, D.H. Kang, and E.F. Halpern, *Characterization of Human Atherosclerosis by Optical Coherence Tomography*, in *Circulation*. 2002, Am Heart Assoc. p. 1640-1645.

(56) Busse, R., R.D. Bauer, A. Schabert, Y. Summa, P. Bumm, and E. Wetterer, *The Mechanical Properties of Exposed Human Common Carotid Arteries in Vivo.* Basic research in cardiology, 1979. **74**(5): p. 545-554.

(57) Cox, R., *Viscoelastic Properties of Canine Pulmonary Arteries.* American Journal of Physiology, 1984. **246**: p. H90-H96.

(58) Holzapfel, G.A., *A Continuum Approach for Engineering*. 2000, Chichester: John Wiley & Sons.

(59) Humphrey, J.D., *Cardiovascular Solid Mechanics: Cells, Tissues and Organs*. 2002, New York: Springer-Verlag.

(60) Fung, Y.C., *Biomechanics: Mechanical Properties of Living Tissues*. 2nd ed. 1993, New York: Springer-Verlag.

(61) Cao, L., I. Youn, F. Guilak, and L.A. Setton, *Compressive Properties of Mouse Articular Cartilage Determined in a Novel Micro-Indentation Test Method and Biphasic Finite Element Model.* Journal of Biomechanical Engineering, 2006. **128**: p. 766.

(62) Viidik, A. and T. Lewin, *Changes in Tensile Strength Characteristics and Histology of Rabbit Ligaments Induced by Different Modes of Postmortal Storage.* Acta Orthop Scandinav, 1966. **37**: p. 141-155.

(63) Oegema, T.R., L.B. Deloria, M.M. Fedewa, J.C. Bischof, and J.L. Lewis, *A Simple Cryopreservation Method for the Maintenance of Cell Viability and Mechanical Integrity of a Cultured Cartilage Analog.* Cryobiology, 2000. **40**: p. 370-375.

(64) Clavert, P., J.F. Kempf, F. Bonnomet, P. Boutemy, L. Marcelin, and J.L. Kahn, *Effects of Freezing/Thawing on the Biomechanical Properties of Human Tendons.* Surgical and Radiologic Anatomy, 2001. **23**(4): p. 259-62.

(65) Woo, S.L.-Y., C.A. Orlando, J.F. Camp, and W.H. Akeson, *Effects of Postmortem Storage by Freezing on Ligament Tensile Behavior.* Journal of Biomechanics, 1986. **19**(5): p. 399-404.

(66) Moon, D.K., S.L. Woo, Y. Takakura, M.T. Gabriel, and S.D. Abramowitch, *The Effects of Refreezing on the Viscoelastic and Tensile Properties of Ligaments.* Journal of Biomechanics, 2006. **39**(6): p. 1153-1157.

(67) Blondel, W.C.P.M., B. Lehalle, G. Maurice, X. Wang, and J.-F. Stoltz, *Rheological Properties of Fresh and Cryopreserved Human Arteries Tested in Vitro.* Rheol Acta, 2000. **39**: p. 461-468.

(68) Litwin, S.B., J. Cohen, and S. Fine, *Effects of Sterilization and Preservation on the Rupture Force and Tensile Strength of Canine Aortic Tissue.* Journal of Surgical Research, 1973. **15**: p. 198-206.

(69) Pukacki, F., T. Jankowski, M. Gabriel, G. Oszkinis, Z. Krasinski, and S. Zapalski, *The Mechanical Properties of Fresh and Cryopreserved Arterial Homografts.* European Journal of Vascular and Endovascular Surgery, 2000. **20**: p. 21-24.

(70) Rosset, E., A. Friggi, G. Novakovitch, P.-H. Rolland, R. Rieu, J.-F. Pellisier, P.-E. Magnan, and A. Branchereau, *Effects of Cryopreservation on the Viscoelastic Properties of Human Arteries.* Annals of Vascular Surgery, 1996. **10**: p. 262-272.

(71) Wang, P., Z. Shu, L. He, Y. Wang, X. Cui, J. Yu, J. Lu, and D. Gao, *The Viability, Structure, and Mechanical Properties of Cryopreserved Rabbit Carotid Artery.* Cell Preservation Technology, 2005. **3**(2): p. 85-95.

(72) Kang, T., J. Resar, and J.D. Humphrey, *Heat-Induced Changes in the Mechanical Behavior of Passive Coronary Arteries.* Journal of biomechanical engineering, 1995. **117**(1): p. 86-93.

(73) Baek, S., P.B. Wells, K.R. Rajagopal, and J.D. Humphrey, *Heat-Induced Changes in the Finite Strain Viscoelastic Behavioir of a Collaagenous Tissue.* Journal of Biomechanical Engineering, 2005. **127**: p. 580-586.

(74) Chae, Y., G. Aguilar, E.J. Lavernia., and B.J. Wong, *Characterization of Temperature Dependent Mechanical Behavior of Cartilage.* Lasers in surgery and medicine, 2003. **32**: p. 271-278.

(75) Silver, F.H., Y.P. Kato, M. Ohno, and A.J. Wasserman, *Analysis of Mammalian Connective Tissue: Relationship between Hierarchical Structures and Mechanical Properties.* Journal of long-term effects of medical implants, 1992. **2**(2,3): p. 165-198.

(76) Humphrey, J.D., *Cardiovascular Solid Mechanics: Cells, Tissues, and Organs*. 2002: Springer.

(77) Fischer, G.M. and J.G. Llaurado, *Collagen and Elastin Content in Canine Arteries Selected from Functionally Different Vascular Beds.* Circulation Research, 1966. **19**(2): p. 394-399.

(78) Fischer, G.M. and J.G. Llaurado, *Collagen and Elastin Concen in Canine Arteries Selected from Functionally Different Vascular Beds.* Circulation Research, 1966. **19**: p. 394-399.

(79) Stevens, F.S., R.J. Minns, and H. Thomas, *The Isolation of Chemically Pure Elastins in a Form Suitable for Mechanical Testing.* Connective Tissue Research, 1974. **2**(85-90).

(80) Wright, N.T. and J.D. Humphrey, *Denaturation of Collagen Via Heating: An Irreversible Rate Process.* Annual review of biomedical engineering, 2002. **4**: p. 109-128.

(81) Humphrey, J.D., *Continuum Thermomechanics and the Clinical Treatment of Disease and Injury.* Applied Mechanics Reviews, 2003. **56**: p. 231.

(82) Neidert, M.R., R.V. Devireddy, R.T. Tranquillo, and J.C. Bischof, *Cryopreservation of Collagen-Based Tissue Equivalents.Ii Effect of Freezing in the Presence of Cryoprotective Agents.* Tissue Engineering, 2004. **10**(1/2): p. 23-32.

(83) Aksan, A. and J.J. McGrath, *Thermomechanical Analysis of Soft-Tissue Thermotherapy.* Journal of Biomechanical Engineering, 2003. **125**: p. 700-708.

(84) Chen, S.S., N.T. Wright, and J.D. Humphrey, *Phenomenological Evolution for Heat-Induced Shrinkage of a Collagenous Tissue.* IEEE Transactions on Biomedical engineering, 1998. **45**(10): p. 1234-1240.

(85) Chen, S.S., N.T. Wright, and J.D. Humphrey, *Heat Induced Changes in Mechanics of a Collagenous Tissue: Isothermal Isotonic-Shrinkage.* ASME Journal of Biomechanical Engineering, 1998. **120**: p. 382-388.

(86) Miles, C.A., N.C. Avery, V.V. Rodin, and A.J. Bailey, *The Increase in Denaturation Temperature Following Cross-Linking of Collagen Is Caused by Dehydration of Fibers.* Journal of Molecular Biology, 2005. **346**: p. 551-556.

(87) Miller, J.D., *Freezing-Induced Microstructural Changes of Collagen Scaffolds.*, in *Mechanical Engineering*. 2006, University of Texas: Arlington.

(88) Pearce, J. and S. Thomsen, *Rate Process Analysis of Thermal Damage.* Optical-Thermal Response of Laser-Irradiated Tissue, 1995: p. 561–606.

(89) Kong, J. and S. Yu, *Fourier Transform Infrared Spectroscopic Analysis of Protein Secondary Structures.* Acta Biochimica et Biophysica Sinica, 2007. **39**(8): p. 549-559.

(90) Johnson Jr, W.C., *Protein Secondary Structure and Circular Dichroism: A Practical Guide.* Proteins, 1990. **7**(3): p. 205-214.

(91) Kelly, S.M. and N.C. Price, *The Application of Circular Dichroism to Studies of Protein Folding and Unfolding.* Biochimica et Biophysica Acta (BBA)/Protein Structure and Molecular Enzymology, 1997. **1338**(2): p. 161-185.

(92) Eggers, D.K. and J.S. Valentine, *Molecular Confinement Influences Protein Structure and Enhances Thermal Protein Stability.* Protein Science, 2001. **10**(2): p. 250.

(93) Gekko, K. and S. Koga, *Increased Thermal Stability of Collagen in the Presence of Sugars and Polyols.* Journal of Biochemistry, 1983. **94**(1): p. 199.

(94) Hayashi, T., S. Curran-Patel, and D.J. Prockop, *Thermal Stability of the Triple Helix of Type I Procollagen and Collagen. Precautions for Minimizing Ultraviolet Damage to Proteins During Circular Dichroism Studies.* Biochemistry, 1979. **18**(19): p. 4182-4187.

(95) Leikina, E., M.V. Mertts, N. Kuznetsova, and S. Leikin, *Type I Collagen Is Thermally Unstable at Body Temperature.* Proceedings of the National Academy of Sciences, 2002: p. 32307099.

(96) Sreerama, N. and R.W. Woody, *Estimation of Protein Secondary Structure from Circular Dichroism Spectra: Comparison of Contin, Selcon, and Cdsstr Methods with an Expanded Reference Set.* Analytical Biochemistry, 2000. **287**(2): p. 252-260.

(97) Cai, S. and B.R. Singh, *Identification of ß-Turn and Random Coil Amide Iii Infrared Bands for Secondary Structure Estimation of Proteins.* Biophysical Chemistry, 1999. **80**(1): p. 7-20.

(98) Cai, S. and B.R. Singh, *A Distinct Utility of the Amide Iii Infrared Band for Secondary Structure Estimation of Aqueous Protein Solutions Using Partial Least-Squares Methods.* Biochemistry, 2004. **43**(9): p. 2541-2549.

(99) Shah, N., W. Wolkers, W. Sun, and J.C. Bischof. *Effect of Gamma Irradiation on Protein Structure and Stability in Alloderm™ Skin Tissue Matrix*. in *Annual Biomedical Engineering Society Fall Meeting*. 2007. Hollywood, CA, USA.

(100) Gopinath, D., M.R. Ahmed, K. Gomathi, K. Chitra, P.K. Sehgal, and R. Jayakumar, *Dermal Wound Healing Processes with Curcumin Incorporated Collagen Films.* Biomaterials, 2004. **25**(10): p. 1911-1917.

(101) Pouliot, R., L. Germain, F.A. Auger, N. Tremblay, and J. Juhasz, *Physical Characterization of the Stratum Corneum of an in Vitro Human Skin Equivalent Produced by Tissue Engineering and Its Comparison with Normal Human Skin by Atr-Ftir Spectroscopy and Thermal Analysis (Dsc).* BBA-Molecular and Cell Biology of Lipids, 1999. **1439**(3): p. 341-352.

(102) Sturtevant, J.M., *Biochemical Applications of Differential Scanning Calorimetry.* Annual Reviews in Physical Chemistry, 1987. **38**(1): p. 463-488.

(103) Miles, C.A., T.V. Burjanadze, and A.J. Bailey, *The Kinetics of the Thermal Denaturation of Collagen in Unrestrained Rat Tail Tendon Determined by Differential Scanning Calorimetry.* Journal of molecular biology, 1995. **245**(4): p. 437-446.

(104) Miles, C.A. and M. Ghelashvili, *Polymer-in-a-Box Mechanism for Thermal Stabilization of Collagen Molecules in Fibers.* Biophysical Journal, 1999. **76**: p. 3243-3252.

(105) Bischof, J.C. and X. He, *Thermal Stability of Proteins.* Annals of the New York Academy of Sciences, 2005. **1066**: p. 12-33.

(106) Daggett, V., *Molecular Dynamics Simulations of the Protein Unfolding/Folding Reaction.* Acc. Chem. Res, 2002. **35**(6): p. 422-429.

(107) Fersht, A.R. and V. Daggett, *Protein Folding and Unfolding at Atomic Resolution.* Cell, 2002. **108**(4): p. 573-582.

(108) Daggett, V. and M. Levitt, *Molecular Dynamics Simulations of Helix Denaturation.* J. Mol. Biol, 1992. **223**: p. 1121-1138.

(109) Day, R., B.J. Bennion, S. Ham, and V. Daggett, *Increasing Temperature Accelerates Protein Unfolding without Changing the Pathway of Unfolding.* Journal of Molecular Biology, 2002. **322**(1): p. 189-203.

(110) Mayor, U., C.M. Johnson, V. Daggett, and A.R. Fersht, *Protein Folding and Unfolding in Microseconds to Nanoseconds by Experiment and Simulation.* Proceedings of the National Academy of Sciences, 2000. **97**(25): p. 13518.

(111) Ferguson, N., J.R. Pires, F. Toepert, C.M. Johnson, Y.P. Pan, R. Volkmer-Engert, J. Schneider-Mergener, V. Daggett, H. Oschkinat, and A. Fersht, *Using Flexible Loop Mimetics to Extend Phi-Value Analysis to Secondary Structure Interactions.* Proceedings of the National Academy of Sciences, 2001: p. 221467398.

(112) Vogel, A. and V. Venugopalan, *Mechanisms of Pulsed Laser Ablation of Biological Tissues.* CHEMICAL REVIEWS, 2003. **103**(2): p. 577-644.

(113) Hong, J., D.C. Sigg, J.A. Coles Jr, P.R. Oeltgen, H.J. Harlow, C.L. Soule, and P.A. Iaizzo, *Hibernation Induction Trigger Reduces Hypoxic Damage of Swine Skeletal Muscle.* Muscle Nerve, 2005.

(114) Bateson, E.A.J. and D.E. Pegg, *Cryopreservation of Arteries.* Cryo-Letters, 1994. **15**: p. 15–20.

(115) Zhu, C., G. Bao, and N. Wang, *C Ell M Echanics: Mechanical Response, Cell Adhesion, and Molecular Deformation.* Annual Reviews in Biomedical Engineering, 2000. **2**(1): p. 189-226.

(116) Suresh, S., *Biomechanics and Biophysics of Cancer Cells.* Acta Biomaterialia, 2007. **3**(4): p. 413-438.

(117) Balasubramanian, S.K., R.T. Venkatasubramanian, A. Menon, and J.C. Bischof, *Thermal Injury Prediction During Cryoplasty through in Vitro Characterization of Smooth Muscle Cell Biophysics and Viability.* Annals of Biomedical Engineering, 2008. **36**(1): p. 86-101.

(118) Grassl, E.D. and J.C. Bischof, *In Vitro Model Systems for Evaluation of Smooth Muscle Cell Response to Cryoplasty.* Cryobiology, 2005. **50**(2): p. 162-173.

(119) Arnoczky, S.P. and A. Aksan, *Thermal Modification of Connective Tissues: Basic Science Considerations and Clinical Implications.* Journal of the American Academy of Orthopaedic Surgeons, 2000. **8**(5): p. 305-313.

(120) Thomsen, S., J.A. Pearce, and W.F. Cheong, *Changes in Birefringence as Markers of Thermal Damage in Tissues.* IEEE Transactions on Biomedical engineering, 1989. **36**(12): p. 1174-1179.

(121) Orihara, K., S. Biro, S. Hamasaki, H. Eto, M. Miyata, Y. Ikeda, and C. Tei, *Hyperthermia at 43c for 2hrs Inhibits the Proliferation of Vascular Smooth Muscle Cells,but Not Endothelial Cells.* Journal of Mol Cell Cardiol, 2002. **34**: p. 1205-1215.

(122) Hayashi, K., *Experimental Approaches on Measuring the Mechanical Properties and Constitutive Laws of Arterial Walls.* ASME Journal of Biomechanical Engineering, 1993. **115**: p. 481-488.

(123) He, C.M. and M.R. Roach, *The Composition and Mechanical Properties of Abdominal Aortic Aneurysms.* Journal of Vascular Surgery, 1994. **20**: p. 6-13.

(124) Castier, Y., F. Francis, P. Cerceau, M. Besnard, J. Albertin, L. Fouilhe, O. Cerceau, P. Albaladejo, and G. Leseche, *Cryopreserved Arterial Allograft Reconstruction for Peripheral Graft Infection.* Journal of vascular surgery, 2005. **41**(1): p. 30-37.

(125) Desgranges, P., F. Beaujan, S. Brunet, A. Cavillon, P. Qvarfordt, D. Mellière, and J.-P. Becquemin, *Cryopreserved Arterial Allografts Used for the Treatment of Infected Vascular Grafts.* Annals of Vascular Surgery, 1998. **12**(6): p. 583-588.

(126) Song, Y.C., D.E. Pegg, and C.J. Hunt, *Cryopreservation of the Common Carotid Artery of the Rabbit: Optimization of Dimethyl Sulfoxide Concentration and Cooling Rate.* Cryobiology, 1995. **32**: p. 405-421.

(127) Rupp, C.C., N.E. Hoffman, F.R. Schmidlin, D.J. Swanlund, J.C. Bischof, and J.E. Coad, *Cryosurgical Changes in the Porcine Kidney: Histologic Analysis with Thermal History Correlation.* Cryobiology, 2002. **45**: p. 167-182.

(128) Tranquillo, R.T., T.S. Girton, B.A. Bromberek, T.G. Triebes, and D.L. Mooradian, *Magnetically Oriented Tissue-Equivalent Tubes: Application to a Circumferentially Orientated Media-Equivalent.* Biomaterials, 1996. **17**: p. 349-357.

(129) Okamoto, R.J., J. Wagenseil, W.R. DeLong, S.J. Peterson, N.T. Kouchoukos, and T.M. Sundt, *Mechanical Properties of Dilated Human Ascending Aorta.* Annals of Biomedical Engineering, 2002. **30**: p. 624-635.

(130) Girton, T.S., T.R. Oegema, E.D. Grassl, B.C. Isenberg, and R.T. Tranquillo, *Mechanisms of Stiffening and Strengthening in Media-Equivalents Fabricated Using Glycation.* Journal of Biomechanical Engineering, 2000. **122**(3): p. 216-223.

(131) Isenberg, B.C. and R.T. Tranquillo, *Long-Term Cyclic Distention Enhances the Mechanical Properties of Collagen-Based Media-Equivalents.* Annals of Biomedical Engineering, 2003. **31**: p. 937-949.

(132) Lanir, Y., *A Microstructural Model for the Rheology of Mammalian Tendon.* Journal of Biomechanical Engineering, 1980. **102**: p. 332.

(133) Girton, T.S., V.H. Barocas, and R.T. Tranquillo, *Confined Compression of a Tissue-Equivalent:Collagen Fibril and Cell Alignment in Response to Anisotropic Strain.* Journal of Biomechanical Engineering, 2002. **124**(5): p. 568-575.

(134) Tower, T.T. and R.T. Tranquillo, *Alignment Maps of Tissues: I. Microscopic Elliptical Polarimetry.* Biophysical Journal, 2001. **81**(5): p. 2954-2963.

(135) Tower, T.T. and R.T. Tranquillo, *Alignment Maps of Tissues: Ii. Fast Harmonic Analysis for Imaging.* Biophysical Journal, 2001. **81**(5): p. 2964-2971.

(136) Lewis, J.L., S.L. Johnson, and T.R. Oegema, *Interfibrillar Collagen Bonding Exists in Matrix Produced by Chondrocytes in Culture: Evidence by Electron Microscopy.* Tissue Engineering, 2002. **8**(6): p. 989-995.

(137) Nerem, R.M., *Hemodynamics and the Vascular Endothelium.* Journal of Biomechanical Engineering, 1993. **115**: p. 510-514.

(138) Taylor, C.A., T.J. Hughes, and C.K. Zarins, *Effect of Excercise on Hemodynamic Conditions in the Abdominal Aorta.* Journal of vascular surgery, 1999. **29**(6): p. 1077-1089.

(139) Schaar.J.A., d. Korte.C.L., M. F., and v.d.A.F.W. Steen, *Effect of Temperature Increase and Freezing on Intravascular Elastorgraphy.* Ultrasonics, 2002. **40**: p. 879-881.

(140) Krag, S. and T.T. Andreassen, *Effect of Freezing on Lens Capsule Mechanical Behavior.* Ophthalmic Research, 1998. **30**: p. 280-285.

(141) Devireddy, R.V., M.R. Neidert, J.C. Bischof, and R.T. Tranquillo, *Cryopreservation of Collagen-Based Tissue Equivalents.I Effect of Freezing in the Absence of Cryoprotective Agents.* Tissue Engineering, 2003. **9**(6): p. 1089-1100.

(142) Soloff, B.L., W.A. Nagle, A.J. Moss Jr, K.J. Henle, and J.T. Crawford, *Apoptosis Induced by Cold Shock in Vitro Is Dependent on Cell Growth Phase.* Biochem Biophys Res Commun, 1987. **145**(2): p. 876-83.

(143) Tatsutani, K.N., J.D. Joye, V. Renu, and M.J. Taylor, *In Vitro Evaluation of Vascular Endothelial and Smooth Muscle Cell Survival and Apoptosis in Response to Hypothermia and Freezing.* Cryoletters, 2005. **26**(1): p. 55-64.

(144) Salacinski, H.J., S. Goldner, A. Giudiceandrea, G. Hamilton, A.M. Seifalian, A. Edwards, and R.J. Carson, *The Mechanical Behavior of Vascular Grafts: A Review.* Journal of Biomaterials Applications, 2001. **15**(3): p. 241.

(145) Iaffaldano, R.A., *Patency of Cryopreserved Saphenous Vein Grafts as Conduits for Coronary Artery Bypass Surgery.* Chest, 1995. **108**(3): p. 725-729.

(146) Zhao, S.Z., X.Y. Xu, A.D. Hughes, S.A. Thom, A.V. Stanton, B. Ariff, and Q. Long, *Blood Flow and Vessel Mechanics in a Physiologically Realistic Model of a Human Carotid Arterial Bifurcation.* Journal of Biomechanics, 2000. **33**(8): p. 975-984.

(147) Leuprecht, A., K. Perktold, M. Prosi, T. Berk, W. Trubel, and H. Schima, *Numerical Study of Hemodynamics and Wall Mechanics in Distal End-to-Side Anastomoses of Bypass Grafts.* Journal of Biomechanics, 2002. **35**(2): p. 225-236.

(148) Gray, H., *The Arteries of the Lower Extremity*, in *Anatomy of the Human Body*. 1918, Lea & Febiger. p. 623.

(149) Hayes, W.C. and L.F. Mockros, *Viscoelastic Properties of Articular Cartilage.* Journal of applied physiology, 1971. **31**(4): p. 562-568.

(150) Carew, T.E., R.N. Vaishnav, and D.J. Patel, *Compressibility of the Arterial Wall.* Circulation Research, 1968. **23**(1): p. 61-68.

(151) Perktold, K., M. Hofer, G. Rappitsch, M. Loew, B.D. Kuban, and M.H. Friedman, *Validated Computation of Physiologic Flow in a Realistic Coronary Artery Branch.* Journal of Biomechanics, 1997. **31**(3): p. 217-228.

(152) Shen, Y.L., J.J. Williams, G. Piotrowski, N. Chawla, and Y.L. Guo, *Correlation between Tensile and Indentation Behavior of Particle-Reinforced Metal Matrix Composites: An Experimental and Numerical Study.* Acta Materialia, 2001. **49**(16): p. 3219-3229.

(153) Kozola, B.D. and Y.L. Shen, *A Mechanistic Analysis of the Correlation between Overall Strength and Indentation Hardness in Discontinuously Reinforced Aluminum.* Journal of Materials Science, 2003. **38**(5): p. 901-907.

(154) Venkatasubramanian, R.T., W. Wolkers, V.H. Barocas, D. Lafontaine, C.L. Soule, P.A. Iaizzo, and J.C. Bischof, *Freeze-Thaw Induced Biomechanical Property Changes: Role of Collagen Matrix and Smooth Muscle Cells.* Annals of Biomedical Engineering, 2008. **Submitted**.

(155) Van Popele, N.M., D.E. Grobbee, M.L. Bots, R. Asmar, J. Topouchian, R.S. Reneman, A.P.G. Hoeks, D.A.M. van der Kuip, A. Hofman, and J.C.M. Witteman, *Association between Arterial Stiffness and Atherosclerosis the Rotterdam Study*, in *Stroke*. 2001, Am Heart Assoc. p. 454-460.

(156) Venkatasubramanian, R.T., E.D. Grassl, V.H. Barocas, D. Lafontaine, and J.C. Bischof, *Effects of Freezing and Cryopreservation on the Mechanical Properties of Arteries.* Annals of Biomedical Engineering, 2006. **34**(5): p. 823-832.

(157) Wu, J.Z. and W. Herzog, *Elastic Anisotropy of Articular Cartilage Is Associated with the Microstructures of Collagen Fibers and Chondrocytes.* Journal of Biomechanics, 2002. **35**(7): p. 931-942.

(158) Mow, V.C., S.C. Kuei, W.M. Lai, and C.G. Armstrong, *Biphasic Creep and Stress Relaxation of Articular Cartilage in Compression? Theory and Experiments.* J Biomech Eng, 1980. **102**(1): p. 73-84.

(159) Huang, C.Y., M.A. Soltz, M. Kopacz, V.C. Mow, and G.A. Ateshian, *Experimental Verification of the Roles of Intrinsic Matrix Viscoelasticity and Tension-Compression Nonlinearity in the Biphasic Response of Cartilage.* Journal of Biomechanical Engineering, 2003. **125**: p. 84.

(160) Song, Y.C., *Vitreous Cryopreservation Maintains the Function of Vascular Grafts.* Nature biotechnology, 2000. **18**: p. 296-299.

(161) Fava, M., S. Loyola, A. Polydorou, P. Papapavlou, A. Polydorou, O. Mendiz, and J.D. Joye, *Cryoplasty for Femoropopliteal Arterial Disease: Late Angiographic Results of Initial Human Experience.* Journal of Vascular and Interventional Radiology, 2004. **15**(11): p. 1239-1243.

(162) Rifkin, B.S., U.C. Brewster, J.E. Aruny, and M.A. Perazella, *Percutaneous Balloon Cryoplasty: A New Therapy for Rapidly Recurrent Anastomotic Venous Stenoses of Hemodialysis Grafts?* Am J Kidney Dis, 2005. **45**(2): p. e27-32.

(163) Rupp, C.C., T.C. Nagel, D.J. Swanlund, J.C. Bischof, and J.E. Coad, *Cryothermic and Hyperthermic Treatments of Human Leiomyomata and Adjacent Myometrium and Their Implications for Laparoscopic Surgery.* American Association of Gynecologic Laparoscopists, 2003. **10**(1): p. 90-98.

(164) Sigg, D.C. and P.A. Iaizzo, *Malignant Hyperthermia Phenotype. Hypotension Induced by Succinylcholine in Susceptible Swine.* Anesthesiology, 2000. **92**(6): p. 1777-1788.

(165) Sokolis, D.P., H. Boudoulas, and P.E. Karayannacos, *Assessment of the Aortic Stress-Strain Relation in Uniaxial Tension.* Journal of Biomechanics, 2002. **35**: p. 1213-1223.

(166) Fung, Y. and P. Tong, *Classical and Computational Solid Mechanics*. 2001: World Scientific.

(167) Schenke-Layland, K., O. Vasilevski, F. Opitz, K. Konig, I. Riemann, K.J. Halbhuber, T. Wahlers, and U.A. Stocka, *Impact of Decellularization of Xenogeneic Tissue on Extracellular Matrix Integrity for Tissue Engineering of Heart Valves.* Journal of Structural Biology, 2003. **143**: p. 201-208.

(168) Stylianopoulos, T., A. Aksan, and V.H. Barocas, *A Structural, Kinetic Model of Soft Tissue Thermomechanics.* Biophysical Journal, 2007.

(169) Meng, F.G., Y.K. Hong, H.W. He, A.E. Lyubarev, B.I. Kurganov, Y.B. Yan, and H.M. Zhou, *Osmophobic Effect of Glycerol on Irreversible Thermal Denaturation of Rabbit Creatine Kinase.* Biophysical Journal, 2004. **87**(4): p. 2247-2254.

(170) Ramachandran, G.N. and G. Kartha, *Structure of Collagen.* Nature, 1955. **176**(4482): p. 593-595.

(171) Rich, A. and F.H.C. Crick, *The Structure of Collagen.* Nature, 1955. **176**(4489): p. 915-916.

(172) Fraser, R.D., T.P. MacRae, and E. Suzuki, *Chain Conformation in the Collagen Molecule.* J Mol Biol, 1979. **129**(3): p. 463-81.

(173) Kastelic, J., A. Galeski, and E. Baer, *The Multicomposite Structure of Tendon.* Connective Tissue Research, 1978. **6**(1): p. 11-23.

(174) Pierce, M.C., R.L. Sheridan, B. Hyle Park, B. Cense, and J.F. de Boer, *Collagen Denaturation Can Be Quantified in Burned Human Skin Using Polarization-Sensitive Optical Coherence Tomography.* Burns, 2004. **30**(6): p. 511-517.

(175) Despa, F., D.P. Orgill, J. Neuwalder, and R.C. Lee, *The Relative Thermal Stability of Tissue Macromolecules and Cellular Structure in Burn Injury.* Burns, 2005. **31**(5): p. 568-577.

(176) Stylianopoulos, T., A. Aksan, and V.H. Barocas, *A Structural, Kinetic Model of Soft Tissue Thermomechanics.* Biophysical Journal, 2008. **94**(3): p. 717.

(177) Buehler, M.J. and F.F. Abraham, *Hyperelasticity Governs Dynamic Fracture at a Critical Length Scale.* Nature, 2003. **426**: p. 141-146.

(178) Buehler, M.J. and S.Y. Wong, *Entropic Elasticity Controls Nanomechanics of Single Tropocollagen Molecules.* Biophysical Journal, 2007. **93**(1): p. 37.

(179) Lorenzo, A.C. and E.R. Caffarena, *Elastic Properties, Young's Modulus Determination and Structural Stability of the Tropocollagen Molecule: A Computational Study by Steered Molecular Dynamics.* Journal of Biomechanics, 2005. **38**(7): p. 1527-1533.

(180) De Simone, A., L. Vitagliano, and R. Berisio, *Role of Hydration in Collagen Triple Helix Stabilization.* Biochemical and Biophysical Research Communications, 2008. **372**: p. 121-125.

(181) Daggett, V. and M. Levitt, *A Model of the Molten Globule State from Molecular Dynamics Simulations.* Proceedings of the National Academy of Sciences of the United States of America, 1992. **89**(11): p. 5142.

(182) Daggett, V., A. Li, L.S. Itzhaki, D.E. Otzen, and A.R. Fersht, *Structure of the Transition State for Folding of a Protein Derived from Experiment and Simulation.* Journal of Molecular Biology, 1996. **257**(2): p. 430-440.

(183) Daggett, V., *Molecular Dynamics Simulations of the Protein Unfolding/Folding Reaction.* ACCOUNTS OF CHEMICAL RESEARCH, 2002. **35**(6): p. 422-429.

(184) MacKerell, A.D., D. Bashford, M. Bellott, R.L. Dunbrack, J.D. Evanseck, M.J. Field, S. Fischer, J. Gao, H. Guo, and S. Ha, *All-Atom Empirical Potential for Molecular Modeling and Dynamics Studies of Proteins.* JOURNAL OF PHYSICAL CHEMISTRY B, 1998. **102**: p. 3586-3616.

(185) Phillips, J.C., R. Braun, W. Wang, J. Gumbart, E. Tajkhorshid, E. Villa, C. Chipot, R.D. Skeel, L. Kale, and K. Schulten, *Scalable Molecular Dynamics with Namd.* JOURNAL OF COMPUTATIONAL CHEMISTRY, 2005. **26**(16): p. 1781.

(186) Humphrey, W., A. Dalke, and K. Schulten, *Vmd: Visual Molecular Dynamics.* Journal of Molecular Graphics, 1996. **14**(1): p. 33-38.

(187) Kramer, R.Z., J. Bella, B. Brodsky, and H.M. Berman, *The Crystal and Molecular Structure of a Collagen-Like Peptide with a Biologically Relevant Sequence.* Journal of Molecular Biology, 2001. **311**(1): p. 131-147.

(188) de Souza, O.N. and R.L. Ornstein, *Effect of Periodic Box Size on Aqueous Molecular Dynamics Simulation of a DNA Dodecamer with Particle-Mesh Ewald Method.* Biophysical Journal, 1997. **72**(6): p. 2395-2397.

(189) Jo, S., T. Kim, V.G. Iyer, and W. Im, *Charmm-Gui: A Web-Based Graphical User Interface for Charmm.* Journal of computational chemistry, 2008.

(190) Berisio, R., L. Vitagliano, L. Mazzarella, and A. Zagari, *Crystal Structure of the Collagen Triple Helix Model [(Pro-Pro-Gly) 10] 3.* Protein Science, 2002. **11**(2): p. 262-270.

(191) Brooks, B.R., R.E. Bruccoleri, B.D. Olafson, D.J. States, S. Swaminathan, and M. Karplus, *Charmm: A Program for Macromolecular Energy, Minimization, and Dynamics Calculations.* Journal of computational chemistry, 1983. **4**(2): p. 187-217.

(192) Li, A. and V. Daggett, *Characterization of the Transition State of Protein Unfolding by Use of Molecular Dynamics: Chymotrypsin Inhibitor 2.* Proc Natl Acad Sci US A, 1994. **91**(22): p. 10430-10434.

(193) Li, A. and V. Daggett, *Investigation of the Solution Structure of Chymotrypsin Inhibitor 2 Using Molecular Dynamics: Comparison to X-Ray Crystallographic and Nmr Data.* Protein Engineering Design and Selection, 1995. **8**(11): p. 1117-1128.

(194) Li, A. and V. Daggett, *Identification and Characterization of the Unfolding Transition State of Chymotrypsin Inhibitor 2 by Molecular Dynamics Simulations.* Journal of Molecular Biology, 1996. **257**(2): p. 412-429.

(195) Laidig, K.E. and V. Daggett, *Molecular Dynamics Simulations of Apocytochrome B562–the Highly Ordered Limit of Molten Globules.* Folding and Design, 1996. **1**(5): p. 335-346.

(196) Storch, E.M. and V. Daggett, *Structural Consequences of Heme Removal: Molecular Dynamics Simulations of Rat and Bovine Apocytochrome B5.* Biochemistry, 1996. **35**(36): p. 11596-11604.

(197) Mogilner, I.G., G. Ruderman, and J.R. Grigera, *Collagen Stability, Hydration and Native State.* Journal of Molecular Graphics and Modelling, 2002. **21**(3): p. 209-213.

APPENDIX A- THERMAL MODELING OF CRYOPLASTY

This chapter describes the thermal model for predicting temperature distribution during cryoplasty. The present author performed all the computer simulations and data analysis for the thermal modeling. Saravana K. Balasubramanian and Arjun Menon performed the *in vitro* experiments to quantify the thermal effects on SMC viability. The results from this chapter were published in the following citation:

i. Balasubramanian, S.K., Venkatasubramanian, R.T., Menon, A. and Bischof, J.C. (2008) "Thermal injury prediction during cryoplasty through *in vitro* characterization of smooth muscle cell biophysics and viability" *Annals of Biomedical Engineering* **36**(1): p86-101.

Abstract

Cryoplasty, a novel technique involving simultaneous stretching and freezing of the peripheral arteries using a cryogen filled balloon catheter, has shown the potential to combat restenosis. A thermal model of cryoplasty is useful in predicting the temperature distribution during cryoplasty; which in turn would be ultimately beneficial for further optimization of the technique. In the current chapter, the thermal history in arteries was predicted for different balloon temperatures using a thermal model. Based on the predicted temperature distribution, conservative estimates of injury regimes in the artery during cryoplasty were predicted.

7.1 INTRODUCTION

The most common types of vascular disease in the peripheral arteries (i.e. PAD) are blocked arteries due to fatty deposits that affected about 8-12 million people in the United States in 2006[1]. Endovascular techniques such as percutaneous transluminal angioplasty (PTA) are used to treat PAD. However, typically 30-40% of angioplasties result in restenosis[2,3]. This occurs because PTA causes substantial injury to the vessel wall during dilation of the arterial blockage. This disrupts not only the plaque but also the endothelium, the internal elastic lamina and the media, which can lead to aggressive proliferation of SMCs resulting in neointimal hyperplasia or restenosis[4]. To offset these drawbacks, alternative treatment procedures for PAD are being actively investigated[5]. Drug coated stents have been introduced as an option over PTA. However, there are durability issues associated with the treatment (e.g. material sloughing, restenosis over time etc.)[6]. This suggests the need for continued research and development in restenosis treatments.

One new and promising method is the use of freezing to treat stenotic vessels (cryoplasty) involving controlled freezing of the affected artery using a cryogen filled balloon catheter. The choice of the cryogen includes liquid N_2, Freon, nitrous oxide, CO_2 gas and in certain cases saline solution mixed with ethanol[7]. Freezing of the stenotic vessel can help predict the survival of the proliferating SMCs and also prevent elastic recoil of the artery, which could result in restenosis[7]. Other advantages of freezing include maintenance of ECM structure[8], the minimally invasive approach and lack of coagulation effects, i.e. thermal fixation[9]. Recently, a thermal model analyzing the temperature distribution in arteries during cryoplasty was reported[10]. Though relevant, assumption of constant thermal properties for tissues during freezing will affect predicted temperatures and cooling rates. Though promising, there is still a lack of clear understanding of the extent and distribution of thermal injury during freezing in arteries that limits its informed use.

The aim of the current study is to quantify and predict the thermal injury in arteries during cryoplasty. A thermal model is used to predict temperature distribution in femoral and popliteal arteries (two common targets) during freezing. Results from the

thermal model along with thermal effects on SMC viability are then used to obtain conservative estimates of thermal injury regimes in the artery.

7.2 THERMAL MODEL

The energy equation, modified to account for phase change using the enthalpy method[11, 12], was used to predict the thermal history of the artery during freezing. Similar use of the model was reported for a variety of tissue systems as reviewed recently[13]. The governing partial differential equation is given by:

$$\frac{1}{r}\frac{\partial}{\partial r}\left(kr\frac{\partial T}{\partial r}\right)=\rho\frac{\partial H}{\partial t} \tag{7.1}$$

In Eqn. 7.1, H is the volumetric enthalpy, k the thermal conductivity (W/m.K) and ρ the density (kg/m^3). The tissue was considered frozen for all $T < T_s$, unfrozen for all $T > T_l$ and a mushy zone considered for $T_s < T < T_l$ where T_s = -40^{o}C and T_l = -0.53^{o}C. The thermal properties used in the model, outside the mushy zone, are listed in Table 7.1. Calculation of the thermal properties and enthalpy inside the mushy zone has been discussed elsewhere[12, 14]. Briefly, the thermal properties and the enthalpy in the mushy zone were calculated as follows:

$$X_i = X_s + f(T)*(X_l - X_s) \tag{7.2a}$$

$$f(T)=\frac{\left(\frac{T_s}{T}-1\right)}{\left(\frac{T_s}{T_l}-1\right)} \tag{7.2b}$$

where X_s and X_l are the thermal property or enthalpy at T_s and T_l respectively and f(T) the release pattern describing the relation between temperature and the unfrozen tissue within the mushy zone. An Euler forward one dimensional finite difference analysis with time step of 10^{-5}s and element size 0.025mm was constructed and run to solve the thermal

model[15]. The results were additionally verified using finite element analysis (ANSYS 10.0, Canonsburg, PA).

Property	Values	Units
k_l	0.6	W/m-K
k_s	$2.24+ 5.975 \times 10^{-3} \times (-T)^{1.156}$	W/m-K
C_l	4100	J/Kg-K
C_s	7.16(T-273.15)+138	J/Kg-K
ρ_l	999	kg/m³
ρ_s	921	kg/m³
L	210	kJ/kg

Table 7.1 Thermal properties used in the model. Tissue properties from previously reported studies were assumed to be true for arteries. The latent heat of artery was calculated based on the assumption that the 60-65% of the tissue was water and the non-water portion did not contribute to the latent heat.

The thermal model predicted the temperature distribution in geometries corresponding to femoral and popliteal arteries. Fig. 7.1 depicts the arterial geometry modeled and the boundary conditions imposed. A lumen radius of 3mm for popliteal and 5.5mm for femoral artery was used while the arterial thickness was assumed to be 2mm for both the arteries[16, 17]. The thermal properties described in Table 7.1 were used for both. The arteries were assumed to be perfectly cylindrical and the heat transfer was assumed to be radial. Cryoplasty involves freezing of the artery to approximately -15 to -20°C for about 60s[18]. Thus, a constant boundary temperature of -15°C and -20°C was separately applied for each case at the inner artery wall for a time of 60s. The entire artery was assumed to be at an initial temperature of 37°C.

Both femoral and popliteal arteries are surrounded by blood perfused muscle fibers. Assuming that the blood flow in the surrounding tissues would maintain the outer arterial wall temperature at 37°C, a constant temperature boundary condition was imposed at the outer wall. In another case, as an extreme situation, the surrounding

tissues were included in the model and a constant temperature (37^{o}C) boundary condition imposed at 15.5mm from the lumen center. The surrounding tissues were also assigned the same thermal properties as the arteries. It is expected that an *in vivo* situation would fall in between the two boundary conditions described.

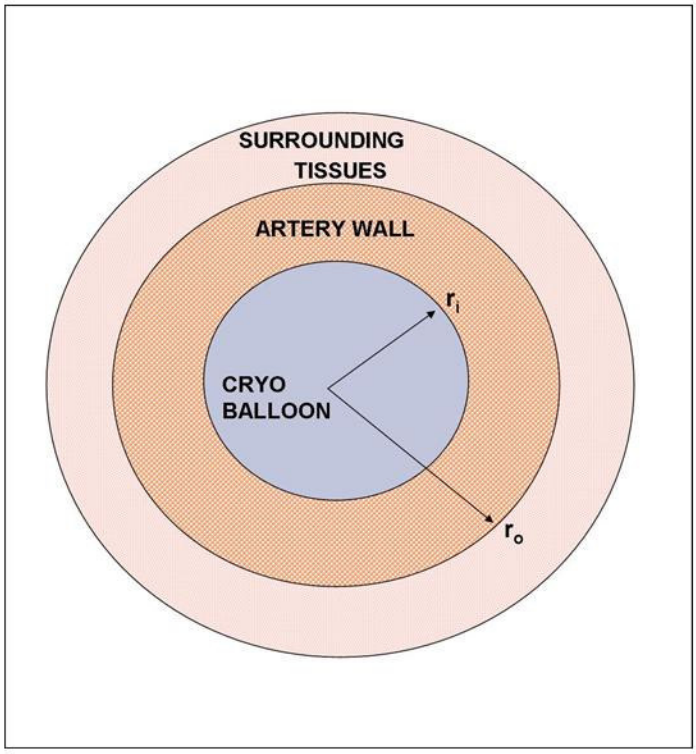

	r_i (mm)	r_o (mm)	T (r_i) (^{o}C)	T (r_o) (^{o}C)
Femoral Artery	5.5	7.5	-15 or -20	37
Popliteal Artery	3	5	-15 or -20	37
Extreme Case	5.5	15.5	-15 or -20	37

Figure 7.1 Artery geometry used in the thermal model for the prediction of temperature distribution during cryoplasty. The geometrical dimensions and the imposed boundary conditions for the thermal model are listed.

7. 3 RESULTS AND DISCUSSION

The temperature distribution in the artery vs. radial distance was estimated using the finite difference model. For a constant boundary temperature condition (Fig. 7.1), the ice ball edge grew up to approximately half the arterial thickness (~1mm) in each case. For

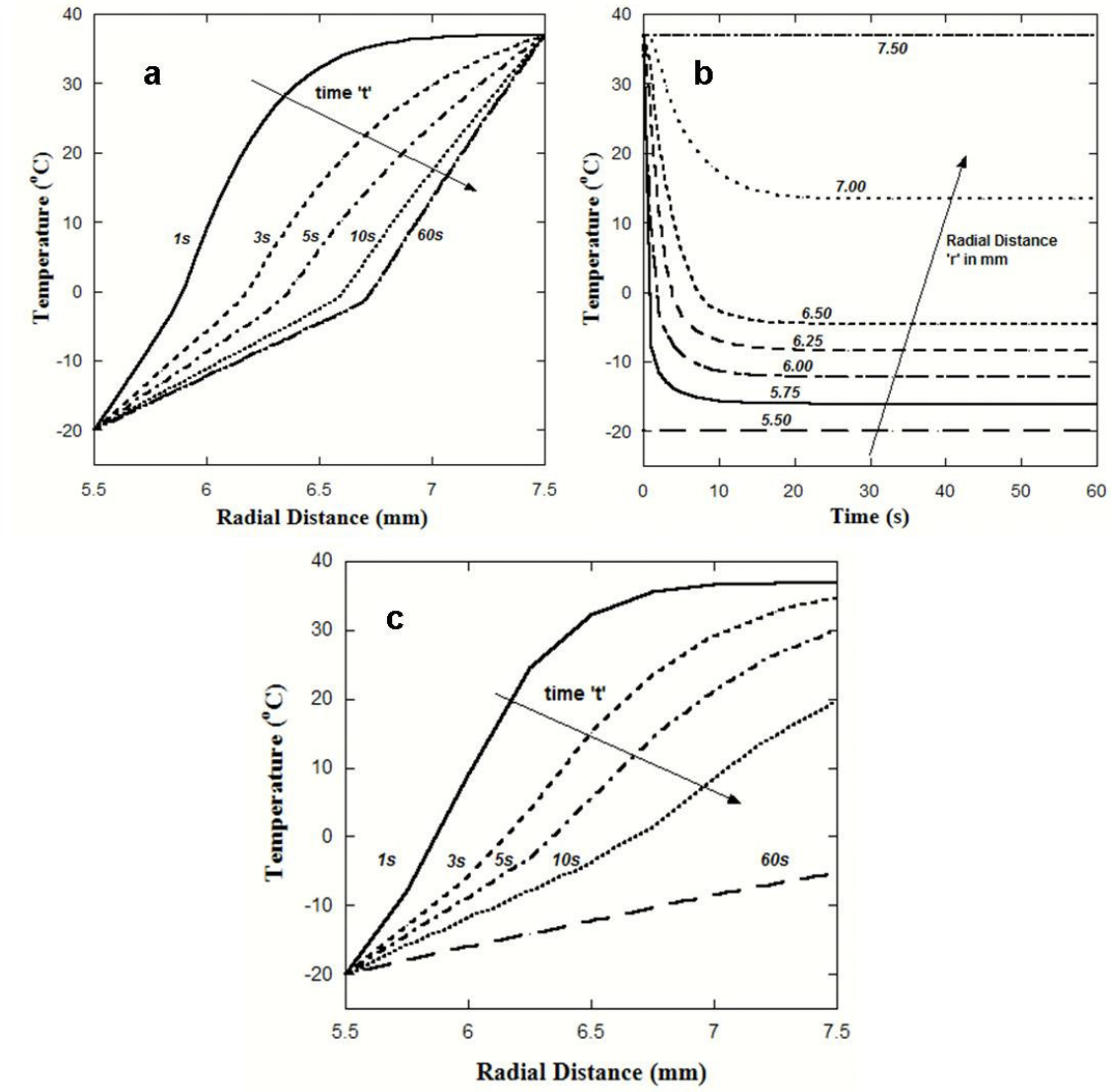

Figure 7.2 Thermal history of femoral artery (r = 5.5mm) wall during cryoplasty. (a) Temperature within the artery as a function of radial distance for different times (b) Temperature as a function of time at different locations (c) Temperature as a function of radial distance during the extreme case (i.e. constant boundary condition (37°C) at r_o = 15.5 mm)

e.g., in the femoral artery, for a constant boundary temperature of -20°C at the inner wall (r_i = 5.5mm), the iceball is predicted to grow to r = 6.7mm within 12s. Cooling rate at different radial locations in the artery is determined from the slope of the temperature variation over the first 15-20s as transients at any location reduces significantly after that time point (Fig. 7.2b). For the popliteal artery, the estimated cooling rates range from 2500 to 5°C/min at different radial locations. Table 7.2 provides information on end temperatures and cooling rates predicted at different locations within the artery for different initial balloon temperatures. In addition to the different conditions listed in Table 7.2, thermal response during constant boundary condition at r_o = 15.5mm (extreme case) is studied.

BT (°C) (@ r = 5.5 mm)	Femoral Artery								
	IBE (mm)	r (mm)						NZ (mm)	AZ (mm)
		5.9	6.3	6.6	5.9	6.3	6.6		
		CR (°C/min)			ET (°C)				
-15	6.6	530	100	-	-10	-5	0	5.5-5.9	5.8-6.6
-20	6.7	400	190	90	-14	-8	-3	5.5-6.2	6.2-6.7

BT (°C) (@ r = 5.5mm)	Popliteal Artery								
	IBE (mm)	r (mm)						NZ (mm)	AZ (mm)
		3.3	3.6	4.0	3.3	3.6	4.0		
		CR (°C/min)			ET (°C)				
-15	4.0	2300	220	-	-11	-7	0	3-3.3	3.3-4
-20	4.2	2500	380	80	-15	-10	-4	3-3.6	3.6-4.2

Table 7.2 Summary of the thermal injury following cryoplasty in the a) femoral and b) popliteal artery model. BT: Balloon temperature (°C), r: radius (mm), IBE: Ice ball edge (mm), NZ: Necrotic zone (mm), AZ: Apoptotic zone (mm), CR: Cooling Rate (°C/min) and ET: End Temperature (°C).

Figure 7.2c describes the temperature vs. radial distance at different times during the extreme case. *In vivo* thermal history is expected to be captured in between the two extreme cases considered in the thermal model. While the initial cooling rates did not change significantly, sub-zero temperatures are predicted in the entire artery and the ice ball edge grew beyond the artery wall. Based on the temperature predictions of the thermal model and results that quantify the thermal effects on SMC viability described elsewhere, conservative estimates of thermal injury during cryoplasty are presented.

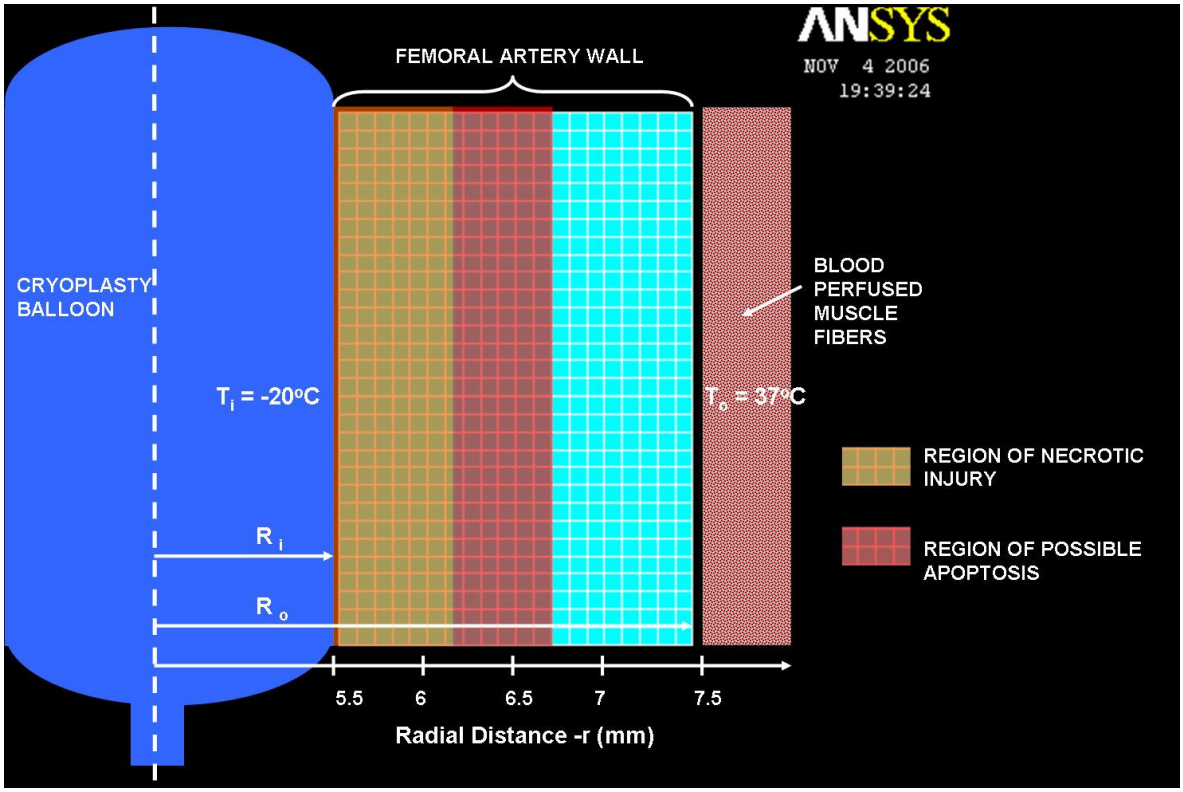

Figure 7.3 Thermal injury regimes during cryoplasty (with balloon temperature of -20°C) in a femoral artery as predicted using the thermal model and the *in vitro* studies on SMC biophysics and viability. Regions of both necrosis and apoptosis are predicted.

Based on the thermal history, the biophysical mechanisms and the viability outcomes presented elsewhere[19], conservative estimates of injury regimes within the artery are predicted (Table 7.2 and Fig. 7.3). We define temperature regimes and cooling rates that may result in necrotic or apoptotic cell injury. Necrotic injury is defined to occur in regimes experiencing a temperature less than -20°C and a cooling rate greater than 50°C/min (dominated by IIF). Apoptosis is defined to occur in regimes experiencing

temperatures between 0 and -10°C and a cooling rate less than 50°C/min. These estimates were based on *in vitro* studies performed to quantify the thermal effects on SMC injury. Regions close to the inner arterial wall or to the cryoplasty balloon experience a lower end temperature (~-20°C) and a high cooling rate (>130°C/min) and hence are presumed to have higher necrotic injury. The thermal injury was higher as expected when a lower balloon temperature (-20°C) was used. Figure 7.3 summarizes the different injury regimes, using the ANSYS model, in a femoral artery of 11mm lumen diameter when the balloon temperature was maintained at -20°C. Table 7.2 summarizes the predicted necrotic and apoptotic injury regimes for the femoral and popliteal artery due to freezing. When a constant temperature boundary condition was applied at radial distance of 15.5mm (Fig. 7.2c), the ice ball edge and the injury zones are expected to extend beyond the artery wall.

This study is useful in predicting possible temperature regimes that can yield higher necrotic or apoptotic cell injury by modifying the thermal conditions imposed. Arteries occlude when rapidly frozen to -80°C and apoptosis and necrosis are reported for balloon temperatures of -20°C and -10°C[20, 21] under *in vitro* conditions. Balloon temperatures in between -80°C and -20°C may be looked into as options to enhance cell injury post cryoplasty. The results of the study may be used in further optimization of the cryoplasty protocol and in designing *in vivo* studies.

Acknowledgements

The authors would like to acknowledge Boston Scientific for funding, Daniel Lafontaine and David Swanlund for technical assistance.

7.4 REFERENCES

(1) Association, A.H. *Peripheral Arterial Disease*. 2006.

(2) Altman, J.D., A. Bayes-Genis, and R.S. Schwartz, *Pathology of Restenosis*. Restenosis: A Guide to Therapy, ed. D.P. Faxon. 2001, London: Martin Dunitz. 9-19.

(3) Shah, P.B. and C.M. Lilly, *Interventional Therapy for Coronary Artery Disease.* American Journal of Respiratory and Critical Care Medicine, 2002. **166**: p. 791-796.

(4) Nakatani, M., Y. Takeyama, M. Shibata, M. Yorozuya, H. Suzuki, S. Koba, and T. Katagiri, *Mechanisms of Restenosis after Coronary Intervention: Difference between Plain Old Balloon Angioplasty and Stenting.* Cardiovascular Pathology, 2003. **12**(1): p. 40-48.

(5) Bhargava, B., G. Karthikeyan, A.S. Abizaid, and R. Mehran, *New Approaches to Preventing Restenosis.* British Medical Journal, 2003. **327**: p. 274-279.

(6) Stanik-Hutt, J.A., *Drug-Coated Stents: Preventing Restenosis in Coronary Artery Disease.* Journal of Cardiovascular Nursing, 2004. **19**(6): p. 404-408.

(7) Lafontaine, D.M., *Cryoplasty Device and Method*, in *United States Patent*. 1999, SciMed Life Systems Inc.: USA.

(8) Li, A.K.C., H.P. Ehrlich, R.L. Trelstad, M.J. Koroly, M.E. Schattenkerk, and R.A. Mali, *Differences in Healing of Skin Wounds Caused by Burn and Freeze Injuries.* Annals of Surgery, 1980. **191**: p. 244-248.

(9) Coad, J.E. and J.C. Bischof, *Histologic Differences between Cryothermic and Hyperthermic Therapies.* Proceedings of SPIE, 2003.

(10) Men-Chi, H. and T.S. Ravigururajan, *Biothermal Modeling of Post-Cryoplasty Atherosclerosis in Restenotic Patients.* Cardiovascular Engineering, 2007. **7**: p. 7-16.

(11) He, X. and J.C. Bischof, *Analysis of Thermal Stress in Cryosurgery of Kidneys.* Journal of Biomechanical Engineering, 2005. **127**(4): p. 656-661.

(12) Hoffmann, N.E. and J.C. Bischof, *Cryosurgery of Normal and Tumor Tissue in the Dorsal Skin Flap Chamber: Part I—Thermal Response.* Journal of Biomechanical Engineering, 2001. **123**: p. 301-309.

(13) He, X. and J.C. Bischof, *Quantification of Temperature and Injury Response in Thermal Therapy and Cryosurgery.* Critical Reviews in Biomedical Engineering, 2003. **31**(5 & 6): p. 355-422.

(14) Smith, D., W.M. Fahssi, D.J. Swanlund, and J.C. Bischof, *A Parametric Study of Freezing Injury in at-1 Prostate Tumor Cells.* Cryobiology, 1999. **39**(1): p. 13-28.

(15) Han, B. and J.C. Bischof, *Thermodynamic Nonequilibrium Phase Change Behavior and Thermal Properties of Biological Solutions for Cryobiology Applications.* Journal of Biomechanical Engineering, 2004. **126**(2): p. 196-203.

(16) Beach, K.W., C.A. Isaac, D.J. Phillips, and D.E.J. Strandness, *An Ultrasonic Measurement of Superficial Femoral Artery Wall Thickness.* Ultrasound Med Biol, 1989. **15**(8): p. 723-728.

(17) Sandgren, T., B. Sonesson, and L.T. Ryden-Ahlgren, *Arterial Dimensions in the Lower Extremities of Patients with Abdominal Aortic Aneurysms--No Indications of a Generalized Dilating Diathesis.* Journal of Vascular Surgery, 2001. **34**(6): p. 1079-1084.

(18) Venkatasubramanian, R.T., E.D. Grassl, V.H. Barocas, D. Lafontaine, and J.C. Bischof, *Effects of Freezing and Cryopreservation on the Mechanical Properties of Arteries.* Annals of Biomedical Engineering, 2006. **34**(5): p. 823-832.

(19) Balasubramanian, S.K., R.T. Venkatasubramanian, A. Menon, and J.C. Bischof, *Thermal Injury Prediction During Cryoplasty through in Vitro Characterization of Smooth Muscle Cell Biophysics and Viability.* Annals of Biomedical Engineering, 2008. **36**(1): p. 86-101.

(20) Cheema, A.N., N. Nili, C.W. Li, H.A. Whittingham, J. Linde, R.J. van Suylen, M.R. Eskandrian, A.P. Wong, B. Qiang, J.F. Tanguay, M. Lane, and B.H. Strauss, *Effects of Intravascular Cryotherapy on Vessel Wall Repair in a Balloon-Injured Rabbit Iliac Artery Model.* Cardiovascular Research, 2003. **59**: p. 222-233.

(21) Tatsutani, K.N., J.D. Joye, R. Virmani, and M.J. Taylor, *In Vitro Evaluation of Vascular Endothelial and Smooth Muscle Cell Survival and Apoptosis in Response to Hypothermia and Freezing.* CryoLetters, 2005. **26**(1): p. 55-64.